A STATISTICAL ASSESSMENT OF DROUGHT VARIABILITY AND CLIMATE PREDICTION FOR KANSAS

by

ZACHARY TODD ZAMBRESKI

B.S., Cornell University, 2014

A THESIS

submitted in partial fulfillment of the requirements for the degree

MASTER OF SCIENCE

Department of Agronomy
College of Agriculture

KANSAS STATE UNIVERSITY
Manhattan, Kansas

2016

Approved by:

Major Professor
Xiaomao Lin

Abstract

The high-quality climate data and high-resolution soil property data in Kansas and adjacent states were used to develop drought datasets for the monthly Palmer Drought Severity Index (PDSI), Standardized Precipitation Index (SPI), and the Standardized Precipitation-Evapotranspiration Index (SPEI) over 1900 to 2014. The statistical analysis of these multiple drought indices were conducted to assess drought occurrence, duration, severity, intensity, and return period. Results indicated that the PDSI exhibited a higher frequency for every category of drought in central and western Kansas than the SPEI by up to 10%. Severe and extreme drought frequency was the highest in southwest Kansas around the Arkansas River lowlands and lowest in the southeast. The mean total drought frequency for eastern, central, and western Kansas was 36%, 39%, and 44%, respectively. The regional mean correlations between the SPI and SPEI were greater than or equal to 0.95 for all regions, but due to statistically significant increases in potential evaporation in western Kansas, the PDSI and SPEI are recommended over the SPI for meteorological and hydrological drought analysis.

Drought variability of the last 115 years was analyzed through the Empirical Orthogonal Functions (EOFs) techniques and their Varimax rotations from 1900 to 2014 in Kansas. Large-scale synoptic patterns primarily dominated the Kansas spatial drought structures, especially during long-duration events. The EOFs indicated that the first principal components of drought explained approximately 70% of the drought variability across the state and demonstrated a statistically significant wetting trend over the last 115 years, oscillating at a period of about 14 years for all drought indices. The 99°W meridian line acted as the dominant transitional line demarcating the areas of Kansas' climate and vegetation relationship as spatial drought presented. The Multivariate El Nino Index (MEI) signal , which modulates global and regional

climate variabilities, provided a low-frequency indicator to couple with Kansas drought's leading modes by varying leads of 3 to 7 months depending on the use of drought index and time steps selected.

Large-scale predictors of surface temperature and precipitation are evaluated from the monthly forecasts in Climate Forecast System version 2.0 (CFSv2) from North Dakota down through central Texas (32.6 - 47.7 °N and 92.8 - 104.1 °W). By using singular value decomposition (SVD), the CFSv2 monthly forecasts of precipitation and 2-m temperature were statistically downscaled using ensemble mean predictions of reforecasts from 1982-2010. Precipitation skill was considerably less than temperature, and the highest skill occurred during the wintertime for 1-month lead time. Only the central and northern plains had statistically significant correlations between observed and modeled precipitation for 1-month lead time. Beyond a 1-month lead time, prediction skill was regionally and seasonally dependent. For the 3-month lead time, only the central plains demonstrated statistically significant mean anomaly correlation. After three-month lead times, the ensemble means of forecasts have shown limited reliable predictions which could make the forecast skill too low to be useful in practice for precipitation. However, temperature forecasts at lead times greater than five months showed some skill in predicting wintertime temperatures.

Table of Contents

List of Figures vi
List of Tables x
Acknowledgements xi
Chapter 1 - Spatiotemporal Characteristics of Drought Occurrence by Multiple Indices over 1900 to 2014 in Kansas 1
1. Introduction 2
2. Data and methods 4
2.1 Climate and soil property data 4
2.2 Drought indices and their algorithms 6
2.2.1 Palmer Drought Severity Index (PDSI) 6
2.2.2 Standardized Precipitation Index (SPI) and Standardized Precipitation Evapotranspiration Index (SPEI) 11
2.3 Statistical measures of drought characteristics 15
2.4 Spatial interpolation 19
3. Results 19
3.1 Empirical cumulative frequency distributions 19
3.2 PDSI relative frequency 21
3.3 Station and regional drought characteristics 23
3.4 PDSI severity return periods 31
4. Discussion 33
5. Conclusion 36
Chapter 2 - Space-Time Variability of Decadal Drought in Kansas 43
1. Introduction 44
2. Data and Methods 47
2.1 Data sources 47
2.2 Empirical Orthogonal Functions (EOFs) 49
2.3 Varimax Rotation 51
3. Results 52
3.1 Space-time variability of PDSI 52

3.2 Space-time variability of SPEI-n 58
3.3 El Nino Southern Oscillation (ENSO) and Drought in Kansas 60
4. Discussion 62
5. Conclusion 65
Chapter 3 - Seasonal Climate Prediction Downscaled in the U.S. Central Plains 71
1. Introduction 72
2. Data and Methods 75
2.1 Study Area 75
2.2 Forecasted data from NCEP CFSv2 76
2.3 Observed data from PRISM 78
2.4 Statistical Downscaling by Singular Value Decomposition (SVD) 78
2.5 Forecast Skill 82
3. Results 83
3.1 Precipitation 83
3.2 Two-Meter Temperature 89
4. Conclusions 95
Appendices 102
Appendix A - Available Water Capacity in Kansas Soils 102
Appendix B - Drought Tool Verification 108
Appendix C - Drought Characteristics by SPEI and SPI 110
Appendix D - SPEI-n EOF, REOF, and Spectral Analysis of PCs 115

List of Figures

Figure 1. Kansas climate stations (red stars) and surrounding climate stations (black squares). Station names are shown near to station sites. Background color was coded by available water capacity from 15.6 to 244 mm obtained from the 10m x 10m gSSURGO dataset for Kansas. The embedded histogram showed the frequency distribution of available water capacity in Kansas. Black vertical lines separate Kansas into eastern, central, and western regions. 5

Figure 2. An illustration of drought duration, severity, and interarrival time by using a PDSI time series observed for Manhattan, Kansas from 1950 to 1960. 17

Figure 3. The empirical cumulative frequency of the monthly PDSI and SPEI for western (top panel), central (middle panel), and eastern (bottom panel) Kansas. Vertical lines represent dry spell (red) and wet spell (green) thresholds classified in drought indices. 20

Figure 4. PDSI relative frequency of mild (a), moderate (b), severe (c), and extreme (d) drought over 1900 to 2014 in Kansas 22

Figure 5. The expected or mean interarrival time of (a) mild and (b) severe droughts in Kansas based on the PDSI. The average of expected interarrival time for each third of Kansas is shown at the bottom (y refers to the year). 26

Figure 6. The mean aggregated drought severities (histogram by left Y axis) and drought frequency (black dots by right Y axis) by decade for the PDSI (left panels) and SPEI-12 (right panels) for western (in red), central (blue), and eastern (green) KS. 27

Figure 7. Drought intensity time series over January 1900 to December 2014 for the SPEI- and SPI -3 (a), -6 (b), -12 (c), -24 (d) for western Kansas 28

Figure 8. Regional SPEI drought characteristics of (a) duration, |(b) severity|, and (c) intensity by SPEI-3, -6, -12, -18, and -24 for western (red), central (blue), and eastern (green) Kansas. 29

Figure 9. The regional mean relative frequency of droughts by indices persisting one or more years for (a) western, (b) central, and (c) eastern Kansas. For example, approximately 5% of all SPEI-3 droughts lasted between one and three years in eastern Kansas. 30

Figure 10. PDSI drought severity returns for 5, 10, 20, and 50 years (a, b, c, d). The return periods (years) of the 2010-2014 drought are shown (e) to provide context to a recent event within the scope of Kansas's recent drought history. 33

Figure 11. Annual PE (mm) for Lakin, KS between 1900 and 2014..... 35
Figure 12. The r-Pearson correlations for each decade between the SPEI and SPI at four time steps for (a) western, (b) central, and (c) eastern Kansas. 36
Figure 1. Map of Kansas and 0.5 °resolution grids used for temperature, precipitation, soil available water capacity, and drought data. 48
Figure 2. Spectrum of the variance explained by each eigenvalue (%) for first 10 principal components for the PDSI data set. 53
Figure 3. First three EOFs (a-c) and normalized PCs (d-f) of the PDSI. Contours of each EOF mode represent correlation with their corresponding PCs. There are statistically significant positive and negative trends for the PC1 and PC2 ($p < 0.001$), respectively. 54
Figure 4. Power spectral density of the PCs for the PDSI. Maximum peaks occur at periods of 14.22, 42.67, and 14.22 years for the PC1, 2, 3, respectively. 54
Figure 5. Three Varimax REOFs (a-c) and RPCs (d-f) of the PDSI. RPC1 and RPC2 showed statistically significant positive trends, and RPC3 had a negative trend but negative REOF3. 58
Figure 6. Temporal patterns of the first leading components of monthly PC1 (black) from (a) PDSI, (b) SPEI-3, (c) SPEI-6, and (d) SPEI-12 and Multivariate El Nino Index (MEI) (red). The time series were filtered by a 24-month low-pass filter. The drought index time series was shifted to correspond to the maximum cross-correlation with the MEI. 61
Figure 7. The same as Figure 6 but for monthly RPC2. 62
Figure 1. Resolution of CFSv2 (square) and the downscaling grid (triangle) used in this study. 76
Figure 2. (a) CFSv2 reforecast model run configuration and (b) reforecast climatology configuration. 77
Figure 3. Flow chart outlining the downscale procedures used in this study. Dashed line represents repeated cycles. 82
Figure 4. Cross-validated precipitation anomaly correlations 1-month lead across the study area for Jan-Dec (a-l). 84
Figure 5. Cross-validated mean anomaly correlation for precipitation predictions for north (a), central (b), and southern (c) plains in DJF (-) and JJA (--) between 1982 and 2010. Lead time is one month. 85

Figure 6. Precipitation anomaly correlations by lead time for Jan-Dec (a-l). Each line represents one of three regions in the study area. 87
Figure 7. Skill scores for 1-month lead precipitation anomalies. 88
Figure 8. Two-meter temperature anomaly correlations Jan-Dec (a-l) for a lead time of one month. 92
Figure 9. Cross-validated mean anomaly correlation between observed and predicted temperatures for north (a), central (b), and southern (c) plains in DJF(-) and JJA (--) between 1982-2010. Lead time is one month. 93
Figure 10. Two-meter temperature anomaly correlations by lead time for Jan-Dec (a-l). Each line represents one of three regions in the study area. 94
Figure 11. Skill scores for 1-month lead temperature anomalies. 95
Figure A1 PDSI relative frequencies of mild, moderate, severe, and extreme drought (top to bottom) for all stations and their available water capacity. 103
Figure A2. Relationship between total drought relative frequency (RF) (PDSI) and available water capacity (AWC) in western Kansas. 104
Figure A3. The same as Figure B2 except for extreme drought relative frequency. 105
Figure A4. Relationship between extreme drought relative frequency (RF) (PDSI) and available water capacity (AWC) for selected stations in eastern Kansas. 106
Figure A5. Available water capacity (AWC) less than 150 mm in Kansas (in purple). 107
Figure B1.One-to-one plot of Manhattan, KS PDSI calculated using Jacobi's tool and the tool developed at Kansas State University (Zambreski). 109
Figure C1. Drought intensity across time for the SPEI and SPI -3,-6,-12,-24 (top to bottom) for eastern Kansas 114
Figure D1. Spectrum of the variance explained by each eigenvalue (%) of the first 10 principal components for the SPEI-3. 115
Figure D2. The same as Fig. D1 but for the SPEI-6. 116
Figure D3. The same as Fig. D1 but for the SPEI-12. 117
Figure D4. The same as Fig. D1 but for the SPEI-24. 118
Figure D5. EOFs and PCs by using SPEI-3. 118
Figure D6. EOFs and PCs by using SPEI-6. 119
Figure D7. EOFs and PCs by using SPEI-12. 119

Figure D8. EOFs and PCs by using SPEI-24. 120
Figure D9. Power spectral density of the PCs for the SPEI-3. Maximum peaks occur at periods of 14.22, 1.29, and 21.33 years for the PC1, 2, 3, respectively. 120
Figure D10. Power spectral density of the unrotated PCs for the SPEI-6. Maximum peaks occur at periods of 14.22, 8.53, and 14.22 years for the PC1, 2, 3, respectively. 121
Figure D11. Power spectral density of the unrotated PCs for the SPEI-12. Maximum peaks occur at periods of 14.22, 8.53, and 14.22 years for the PC1, 2, 3, respectively. 122
Figure D12. Six REOFs of the SPEI-3. 123
Figure D13. Six RPCs of the SPEI-3. 123
Figure D14. The same as Fig. D12 but for the SPEI-6. 124
Figure D15. The same as Fig. D13 but for SPEI-6. 124
Figure D16. Three Varimax REOFs and RPCs of the SPEI-12. All rotated components have statistically significant positive trends. 125
Figure D17. The same as Fig D16 but for the SPEI-24. All rotated components have statistically significant positive trends. 125
Figure D18. The same as Fig. D16 but for the SPI-24. All rotated components have statistically significant positive trends. 126

List of Tables

Table 1. PDSI Drought Categories 11
Table 2. SPI Drought Categories 13
Table 3. Station PDSI drought characteristics, including available water capacity, minimum peak PDSI, and station's longest drought. 25
Table 1. Percentage of total variance explained for each rotated component. A dash indicates that the PC was not significant (evaluated by North's Rule of Thumb). 57
Table 1. Mean precipitation anomaly correlations for northern, central, and southern plains by lead time (***, **, * significant at the 0.01, 0.05, and 0.10 levels, respectively). 86
Table 2. Mean temperature anomaly correlations for northern, central, and southern plains by lead time (***, **, * significant at the 0.01, 0.05, and 0.10 levels, respectively). 93
Table C1. Station SPEI-3 drought characteristics, including minimum peak SPEI-3 and station's longest drought. 111
Table C2. Station SPEI-12 drought characteristics, including minimum peak SPEI-12 and station's longest drought. 112
Table C3. Station SPEI-24 drought characteristics, including minimum peak SPEI-24 and station's longest drought. 113

Acknowledgements

I would like to thank my major adviser and mentor Xiaomao Lin for his guidance throughout the entire research process. His assistance, critique, and high standards were essential to my improvement as researcher in the climate sciences. His foresight for my research in this field has been tremendously valuable. I cannot extend enough gratitude and am extremely thankful.

I would also like to extend thank the rest of my committee: Dr. Robert Aiken, Dr. Gerard Kluitenberg, and Dr. Daniel O'Brien. I have developed a newfound appreciation for the soil sciences from Dr. Kluitenberg, which has helped me have more insight and clarity in my work in the climate sciences.

I could not have been successful without my colleagues: Seth Kutikoff, Tianyi Zhang, and Guillermo Balboa. Tianyi's assistance was extremely beneficial through his time at Kansas State. Finally, I would like to acknowledge the Kansas Water Resource Institute and the USGS for the support for this project.

Chapter 1 - Spatiotemporal Characteristics of Drought Occurrence by Multiple Indices over 1900 to 2014 in Kansas

Abstract

High-quality climate data and high-resolution soil property data in Kansas and adjacent states were used to develop drought datasets for the monthly Palmer Drought Severity Index (PDSI), Standardized Precipitation Index (SPI), and Standardized Precipitation-Evapotranspiration Index (SPEI) over 1900 to 2014. Statistical analysis of these multiple drought indices were conducted to assess drought occurrence, duration, severity, intensity, and return period. Results indicated that the PDSI exhibited a higher frequency for every category of drought in central and western Kansas than the SPEI by up to 10%. Severe and extreme drought frequency was the highest in southwest Kansas around the Arkansas River lowlands and lowest in the southeast portion of the state and throughout the Flint Hills. The mean total drought frequency for eastern, central, and western Kansas was 36%, 39%, and 44%, respectively. Five-year return drought severity magnitudes were largest for northeast and western Kansas. Ten year returns were greatest for portions of central Kansas, while central and southwest Kansas have the largest magnitude droughts expected to return on the order of every 20 to 50 years. The regional mean correlations between the SPI and SPEI were greater than or equal to 0.95 for all regions, but due to statistically significant increases in potential evaporation in western Kansas, the PDSI and SPEI are recommended over the SPI for meteorological and hydrological drought analysis.

1. Introduction

Drought is a multi-faceted and complex climate-related issue, affecting more people than any other natural hazard (Sönmez et al. 2005). Definitions of drought vary depending on which activity related to water use is being studied. A general definition of drought is a condition of moisture deficit sufficient to have an adverse effect on vegetation, animals, and man over a sizeable area (Warwick 1975). These impacts can be partitioned into their own category: meteorological drought is usually defined as the degree of dryness relative to some "normal" or average of amount of precipitation and duration of the dry period; agricultural drought is closely associated with vegetation productivity; hydrological drought is related to the shortfalls on streamflow and surface and underground water supplies; and social-economic drought emphasizes impacts on communities and businesses (Heim 2002). Because drought generally has a slow onset and temperamental duration (McKee et al. 1993), it is difficult to quantify as it relates to these four impacts (Svoboda et al. 2002).

Drought in Kansas is one of the most costly natural disasters. Kansas has been ravaged by persistent, widespread severe droughts during the 1930s and 1950s, causing major economic damage and social disturbance (Clement 1989). From 2000 to 2006, stream flows in some parts of Kansas were recorded at their lowest levels, surpassing even the most devastating twentieth century droughts due to land use changes (Putnam et al. 2008). The Kansas Department of Agriculture estimated the cost of the 2012 drought at more than $3 billion in crop losses (Metzger 2013). Farmers and decision makers that have a better understanding of drought can opt to purchase the most appropriate insurance plan to protect against these serious losses. Continued food and water security requires identification of effective adaption practices to address the dual climate constraints of drought and excessive temperatures (Zhang et al. 2015).

Structured analysis of drought using historical climate data can provide tools that support a real-time drought assessment and forecasting system that can contribute to the Kansas Water Plan's goal of "…reducing our vulnerability to extreme events…" (Metzger 2013).

There are several drought indices available that have been developed in the last sixty years. These drought indices provide a means for quantifying the extent of dryness an area undergoes for a particular time scale. The best measures of drought are those related to drought impacts such as reduced water resources, economic losses, environmental damage and crop failures (Vicente-Serrano et al. 2011). Drought metrics can also explain the intrinsic nature of the process, which can have important implications for understanding the structure of drought. No single drought index has been able to adequately capture the intensity and severity of drought and its impacts on diverse group of users (Heim 2002). Wayne Palmer developed the Palmer Drought Severity index (PDSI) (Palmer 1965), a landmark of drought indices, which has long been widely used in drought monitoring and assessment in the United States and elsewhere. The PDSI was originally developed using western Kansas climate data with an extension to verify this index within nine climatic divisions in seven states in the United States. Due to PDSI's limitation of spatial comparison and autoregressive characteristic (conditioned up to four previous years in the drought index computation) (Guttman 1998), the Standardized Precipitation Index (SPI) was introduced, which considers statistical departures from climate normal using only a precipitation data but with a specific time scale (McKee et al. 1993). However, the SPI calculation doesn't consider air temperature, wind speed, soil moisture, and evapotranspiration (vegetation and soil) that could affect droughts. Therefore, the Standardized Precipitation-Evapotranspiration Index (SPEI) was developed by using precipitation and temperature to

calculate a statistical departure from normal conditions under different time scales (Vicente-Serrano et al. 2010).

Since these multiple drought indices have been widely used from years to decades, understanding spatiotemporal patterns of drought statistics in a specific region, like Kansas, is particularly important as it affects water resource management, crop yields, and energy consumption. In addition, each drought index might provide a somewhat different measure of drought, therefore, a statistical comparison of multiple drought indices could provide a more comprehensive assessment of drought in Kansas. In this study, our objectives are to i) construct complete drought index datasets that include the PDSI, SPI, and SPEI for Kansas from 1900 to 2014; and ii) perform statistical analysis on these multiple drought indices to assess drought occurrence, duration, severity, intensity, and return period in Kansas.

2. Data and methods

2.1 Climate and soil property data

Kansas is located in the interior Central Plains of the United States between 37 °and 40 ° N and 94° 30’ and 102° W. In order to robustly interpolate temperature and precipitation the bounds of climate station selection were extended to neighboring states including Oklahoma, Missouri, Nebraska, and Colorado (Fig. 1). Data from climate stations selected in this study were obtained from the monthly United States Historical Climatology Network (USHCN), which is a long-term high-quality data set commonly used for climate change detection and attribution (Menne et al. 2009). Sixty-three USHCN stations were selected in this study including 29 Kansas USHCN stations and 34 stations in surrounding states for monthly temperature and precipitation.

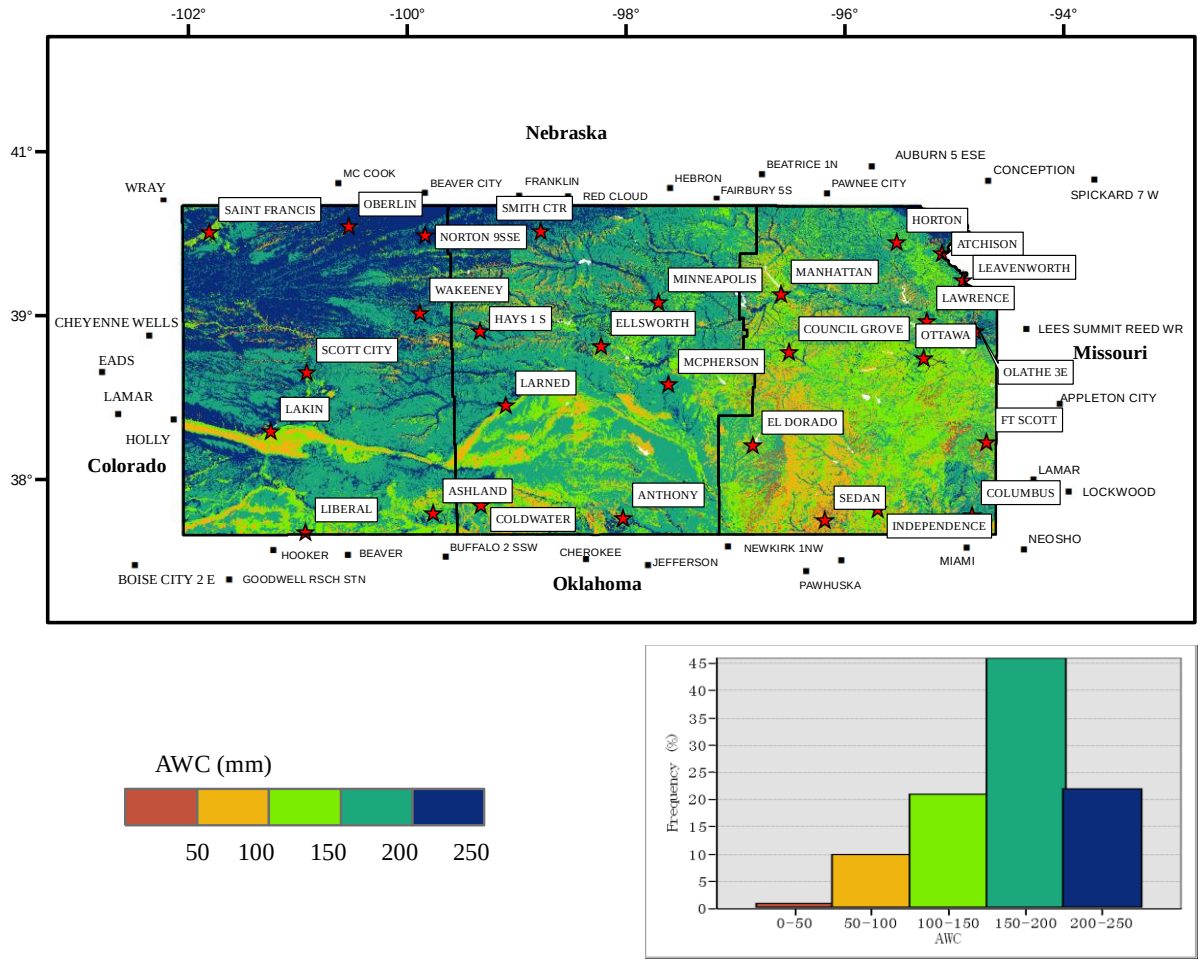

Figure 1. Kansas climate stations (red stars) and surrounding climate stations (black squares). Station names are shown near to station sites. Background color was coded by available water capacity from 15.6 to 244 mm obtained from the 10m x 10m gSSURGO dataset for Kansas. The embedded histogram showed the frequency distribution of available water capacity in Kansas. Black vertical lines separate Kansas into eastern, central, and western regions.

Available water capacity (AWC) in Kansas and surrounding states were obtained from the Gridded Soil Survey Geographic Database (gSSURGO) (Soil Survey Staff 2014). Unlike PDSI currently reported from the National Centers of Environmental Information (NCEI), the PDSI calculation in this study introduced soil AWC from the gSSURGO. A major source of criticism of the PDSI has been the lack of data on the complex field capacity variable (Ward 2013). The NCEI computes the PDSI for nine climate divisions across the state of Kansas and

assumes a discrete range of total available water capacities between 150 and 250 mm, but approximately 32% of the state has a lower AWC. The gSSURGO provided AWC at multiple soil levels at a resolution of 10m x 10m. Each station's geographic coordinates were used to obtain the corresponding grid values of AWC in the defined surface and underlying soil layers. The variables used in gSSURGO were AWC in the 0 to 25 cm layer and AWC 0 to 100 cm layer. Water is assumed to be evenly distributed in these layers.

2.2 Drought indices and their algorithms

2.2.1 Palmer Drought Severity Index (PDSI)

Palmer (1965) developed the PDSI to quantify the extent and severity of meteorological drought based on a soil-water balance model pertinent to agriculture. To compute the PDSI, monthly average temperature, monthly precipitation (P), and available water capacity (AWC) are required. The soil moisture storage is processed by dividing the soil into the surface (0-20 cm) and underlying (20-100 cm) layers. The underlying layer has an available capacity depending upon the soil characteristics of the site being taken. Soil moisture in the surface layer cannot be used to recharge the underlying layer until the surface layer has been completely replenished. Inside the PDSI, potential evapotranspiration (PE), a measure of water transfer to the atmosphere from a homogeneous parcel of vegetated land with saturated soils, is calculated using the original, empirical equation by Thornthwaite (1948). Evapotranspiration losses from the soil occur when the PE is larger than precipitation. The PE, monthly precipitation, and soil property data together are used to calculate the hydrologic budget, including total soil moisture, recharge, evapotranspiration, and runoff. The hydrologic parameters are calculated as follows:

If precipitation (P) is less than PE, evapotranspiration loss at a potential rate from the surface layer (L_s) is assumed to be:

$$L_s = \min (S_s', PE-P) \quad (1)$$

where S_s' is the amount of available moisture stored in the surface layer at the beginning of the month, and

$$L_u = (PE-P-L_s) \cdot \frac{S'_u}{AWC} \quad (2)$$

where L_u is the evapotranspiration (ET) loss from the underlying layer, S'_u is the storage of the underlying soil layer at the beginning of the month, and AWC is the total available water capacity of both soil layers; and,

$$ET = \min (L_s + L_u + P, PE) \quad (3)$$

When precipitation exceeds PE, loss equals zero, and recharge occurs. If both soil layers are at their AWC, remaining moisture is lost as runoff. Loss and recharge must deplete or refill completely the surface layer before the parameters can be calculated for the underlying soil layer.

Each component in the water balance has an associated potential value, that is, potential loss (PL), potential recharge (PR), and potential runoff (PRO) that represent the maximum conditions that could exist. Potential loss is the maximum loss of moisture that a soil layer could experience for one given month. Potential losses are calculated as:

$$PL_s = \min (S_s', PE) \quad (4)$$

and

$$PL_u = (PE-PL_s) \cdot \frac{S'_u}{AWC} \quad (5)$$

Potential recharge (PR) is the amount of moisture required to bring both layers to the AWC.

$$PR=AWC- S' \quad (6)$$

where S' is the total soil moisture in both layers at the beginning of the month. Potential runoff (PRO) is defined as:

$$PRO=AWC-PR \quad (7)$$

Thus, water balance coefficients for four potential values including potential evapotranspiration (PE) are then computed individually for each month's (i from 1 to 12):

$$\alpha_i=\frac{\overline{ET_i}}{\overline{PE_i}}\ (PE) \qquad \delta_i=\frac{\overline{L_i}}{\overline{PL_i}}\ (Loss) \qquad \gamma_i=\frac{\overline{RO_i}}{\overline{PRO_i}}\ (Runoff) \qquad \beta_i=\frac{\overline{R_i}}{\overline{PR_i}}\ (Recharge) \quad (8)$$

These coefficients, dependent on the climate of the area being addressed, are used to find the hydroclimatological reference value, which Palmer designates as the precipitation *Climatically Appropriate For Existing Conditions* (CAFEC). The CAFEC is computed for a calibration period by multiplying each month's potential hydrologic parameter by its corresponding water balance coefficient:

$$CAFEC_i= \alpha_i\ PE_i+ \beta_i\ PR_i+ \gamma_i\ PRO_i - \delta_i\ PL_i \quad (9)$$

The CAFEC values represent the precipitation expected to meet the hydrologic demands on average for that particular month. The departure (d) from normal conditions is the precipitation minus the CAFEC:

$$d=P_i-CAFEC_i \quad (10)$$

The NCEI calibration period for calculating the CAFEC coefficients is 1931-1990. Published literature supports longer calibration periods (50 or more years) when calculating the PDSI (Karl, 1986). Jacobi *et al.* (2013) reexamined two calibration periods: the NCEI calibration period and full record calibration period for datasets of varying lengths and found that results

from 1931-1990 calibration period were well consistent with full calibration. Therefore, the calibration period 1931-1990 was used in this study.

The departure (d) is multiplied by the climatic characteristic (K_i) to find the monthly weighted moisture anomaly index (z) for the month:

$$z_i = K_i \, d_i \tag{11}$$

where

$$K_i = \frac{17.67 \, k_i}{\sum_{i=1}^{12} Di \cdot k_i} \tag{12}$$

$$k_i = 1.5 \log_{10} \left(\frac{\left[\frac{\overline{PE_i} + \overline{R_i} + \overline{RO_i}}{\overline{P_i} + \overline{L_i}} \right] + 2.8}{D_i} \right) + 0.5, \tag{13}$$

where D_i= the mean of the absolute values of d for month i. The $\frac{\overline{PE_i} + \overline{R_i} + \overline{RO_i}}{\overline{P_i} + \overline{L_i}}$ is a measure of the ratio of "moisture demand" to "moisture supply" for a specific month (i) at a specific region.

The PDSI is a drought index designed for climatological evaluation, since it relies upon a complete time series being available with both "past" and future" values of the water-budget terms for each month in the time series (Ward 2013). Starting value transience can give unreliable values in the first 3 years of PDSI data given that the PDSI has long-term memory (Guttman 1991) and thus depends on previous soil conditions (Cook et al. 1999). The value for the PDSI (here it is X_i) is calculated using a first-autoregressive process (i.e., the previous month's PDSI (X_{i-1}) (excluding the first month) and the weighted moisture anomaly index:

$$X_i = 0.897 \cdot X_{i-1} + \frac{1}{3} z_i \tag{14}$$

If a drought is occurring ($X_i \leq -1$), the probability that the dry spell has ended is:

$$P_e = \frac{\sum_{j=0}^{j=j^*} U_{w,i-j}}{Z_e + \sum_{j=0}^{j=j^*} \left[U_{w,i-j} - U_{w,i} \right]} \tag{15}$$

Where,

Z_e= -2.691X_{i-1}-1.5, is a z-value to indicate the end of the drought in a single month,

j* = the first month in the dry spell, and

U_w= z_i+0.15 is the effective wetness during the month i. If a wet spell is occurring ($X_i \geq 1$), the probability equation is the same, but Z_e and U_w are replaced by, respectively:

Z_e= -2.691X_{i-1}+1.5 that indicates a z-value to end the wet spell in a single month and

U_d= z_i-0.15 which is the effective dryness during the month i.

The probability that the dry spell has ended is calculated for every month afterwards until P_e= 0 or P_e= 100% . If the probability becomes 100% or greater, dry-spell termination protocols are enacted, and the PDSI is retroactively changed for the previous months in which the probability was not equal to 0. The selection of appropriate value of X is not obvious and Palmer designed a set of operating rules that depend upon computation over several months and then backtracking based on the direction in which weather conditions appeared to be going (see details in Palmer, 1965). Alley (1984); Karl (1986), and Guttman (1991) described the rules thoroughly that can be referenced to replicate the procedure. The drought categories for the PDSI established by Palmer are presented in Table 1.

Table 1. PDSI Drought Categories

PDSI	Drought Categories
.49 to .-49	Near normal
-.50 to -.99	Incipient Drought
-1.00 to -1.99	Mild Drought
-2.00 to -2.99	Moderate Drought
-3.00 to -3.99	Severe Drought
≤-4.00	Extreme Drought

2.2.2 Standardized Precipitation Index (SPI) and Standardized Precipitation Evapotranspiration Index (SPEI)

McKee et al. (1993) developed the Standardized Precipitation Index (SPI) to analyze precipitation departures from the normal precipitation for a particular month or determined time scale. These time scales reflect the impact of drought on the availability of different water resources (Yang, 2010). To compute the SPI, precipitation is first aggregated according to the time scale chosen (m). The SPI-m is a multi-scalar index and is usually aggregated for 3, 6, 12, 24, and 36 months. If the time scale chosen is *m* months, the monthly aggregated time series will be:

$$x_i = \sum_{i}^{i+m-1} P_i \tag{16}$$

Each month's precipitation in the aggregated time series (x_i) depends on itself and the previous m-1 months. Shorter time scales (3 and 6 months) are used to detect agricultural drought while longer time scales determine hydrologic drought such as underground waters, river flows, and

dam levels (Batisani 2011). The time steps used in this study were 3, 6, 12, 18, and 24 months. Secondly, a two-parameter gamma probability density function is fitted to the aggregated precipitation data for each month of the year for obtaining a total of 12 distributions:

$$g(x)=\frac{1}{\beta^{\alpha}\Gamma(\alpha)}x^{\alpha-1}e^{-x/\beta} \quad (17)$$

where:

$\alpha > 0$ α is a shape parameter.

$\beta > 0$ β is a scale parameter.

$x > 0$ x is the accumulated precipitation total for the time scale.

$\Gamma(\alpha) = \int_0^{\infty} t^{\alpha-1}e^{-t}dt$ and $\Gamma(\alpha)$ is the gamma function of α. Letting $t= x/\beta$, for each x_i the cumulative density probability is calculated:

$$G(x)=\frac{1}{\Gamma(\alpha)}\int_0^{x} t^{\alpha-1}e^{t}dt. \quad (18)$$

Because the gamma function is undefined for x = 0, the cumulative probability becomes:

$$H(x)=q + (1-q)G(x) \quad (19)$$

Where q is the probability of a zero (Thom 1966). If *m* represents the number of zeros in the time series and *n* is the length of the time series, q can be estimated by *m*/*n*. H(x) is transformed to a standard normal random variable with mean zero and variance of one. This standardized variable is the value of the SPI. A length of monthly time series at least thirty years is recommended for the SPI (McKee et al. 1993). Drought categories for the SPI are given in Table 2.

Table 2. SPI Drought Categories

SPI Values	Drought Categories	Time in Category
0 to -0.99	Mild Drought	~24 %
-1.00 to -1.49	Moderate Drought	~9.2 %
-1.50 to -1.99	Severe Drought	~4.4 %
≤ -2.00	Extreme Drought	~2.3 %

The Standardized Precipitation-Evapotranspiration Index (SPEI) is a combined index recently developed as a drought measure with the capability of including the effects of temperature variability that the SPI lacks (Vincente-Serrano *et al., 2010).* Mathematically, the calculation procedure is similar to the SPI. Potential evapotranspiration (PE) is estimated based on the Thornthwaite procedure. The departures (d-series) are calculated as the precipitation for the month minus the PE, aggregated similarly to the SPI based on the time scale chosen (*m*):

$$d_i = \sum_{i}^{i+m-1} (P_i - PE_i) \tag{20}$$

The aggregated departures, d_i, are fitted to a three-parameter log-logistic probability distribution for each month. The log-logistic probability distribution shows a gradual decrease in the probability curve towards low values of d_i, corresponding to more coherent probabilities than other candidate distributions tested in the development of the index (Vicente-Serrano et al. 2010). Probability weighted moments (w_0, w_1, and w_2) are calculated for each month of the year by ordering all of the departures for a particular month (*N)* from least to greatest:

$$w_0 = \frac{1}{N} \sum_{i=1}^{N} d_{i,sort} \tag{21}$$

$$w_1=\frac{N-1}{N}\left[\sum_{i=1}^{N} d_{i,sort}\cdot(N-i)\right] \tag{22}$$

$$w_2=\frac{(N-1)(N-2)}{N}\left[\sum_{i=1}^{N} d_{i,sort}\cdot(N-i)\cdot(N-i-1)\right] \tag{23}$$

The probability weighted moments are used to calculate the shape (β), scale (α), and origin parameters (γ) for the log-logistic distributions for each month:

$$\beta=\frac{2w_1-w_0}{6w_1-w_0-6w_2} \tag{24}$$

$$\alpha=\frac{(w_0-2w_1)(\beta)}{\Gamma(1+\frac{1}{\beta})\Gamma(1-\frac{1}{\beta})} \tag{25}$$

$$\gamma=w_0-\left[\alpha\,\Gamma\left(1+\frac{1}{\beta}\right)\Gamma\left(1-\frac{1}{\beta}\right)\right] \tag{26}$$

The cumulative density function $F(d)$ for the d series is used to find standardized values of the SPEI:

$$F(d)=\left(1+\left[\frac{\alpha}{d-\gamma}\right]^{\beta}\right)^{-1} \tag{27}$$

Following the Abramowitz and Stegun (1964) classic approximation for finding the standardized values of a log-logistic distribution,

$$SPEI=W-\frac{C_0+C_1W+C_2W^2}{1+d_1W+d_2W^2+d_3W^3} \tag{28}$$

where

Px=1-F(d);

$W=\sqrt{-2\cdot \ln Px}$ for $Px \leq 0.5$; for $Px > 0.5$, Px is replaced by 1-Px and the sign of resulting SPEI is reversed; and

$C_0=2.515517$, $C_1=0.802853$, $C_2=0.010328$, $d_1=1.432788$, $d_2=0.189269$, and $d_3=0.001308$.

The mean SPEI is 0 with a standard deviation of one because of its standardized property. Similar to the SPI, the time steps used in this study were 3, 6, 12, 18, and 24 months for the SPEI-m (for example, SPEI-12 represents SPEI calculated by a 12-month scale).

The tools for calculating the indices were developed based on available literature and original methods in Python, which is a free and open-source programming language. These tools are available through the agronomy department at Kansas State University. Agreement between the Kansas State tools and other available tools is extremely high (see Appendix B).

2.3 Statistical measures of drought characteristics

Statistical methods used for this work have been adopted from Saravi et al. (2009), Sönmez et al. (2005), and Yang (2010). The time series data for the PDSI, SPI, and SPEI are analyzed at each station. Six statistical drought characteristics in this study are described as:

I. *Empirical Cumulative Frequency* ($F_N(t)$)

$$F_N(t)=\frac{1}{N}\sum_{i=1}^{N} 1(x_i \leq t) \tag{29}$$

where N is the number of months in observations and $(x_i \leq t)$ is the number of drought index values less than the value t (that is, if drought index is less than t the summation adds one, otherwise zero until the total length of monthly time series).

II. *Relative Frequency (RF)*

The number of months (n) that an index value meets a set drought criterion divided by the number months in the entire series (N) is the relative frequency (Saravi et al. 2009):

$$RF=\frac{n}{N}\cdot 100\% \quad (30)$$

Spatial relative frequency maps can be derived for each drought category for the PDSI. Relative frequency is less meaningful for the SPI and SPEI since the time each index spends in each drought category remains relatively constant because both are derived as standardized variables (see table 2) (McKee et al. 1993).

III. *Duration (L)*

The length of time (months) that the drought index is consecutively at or below a truncation level is the drought duration (Fig. 2). The total duration of the drought is considered one event. In this study, the threshold used for the PDSI was -1.0 and 0 for the SPEI and SPI, respectively.

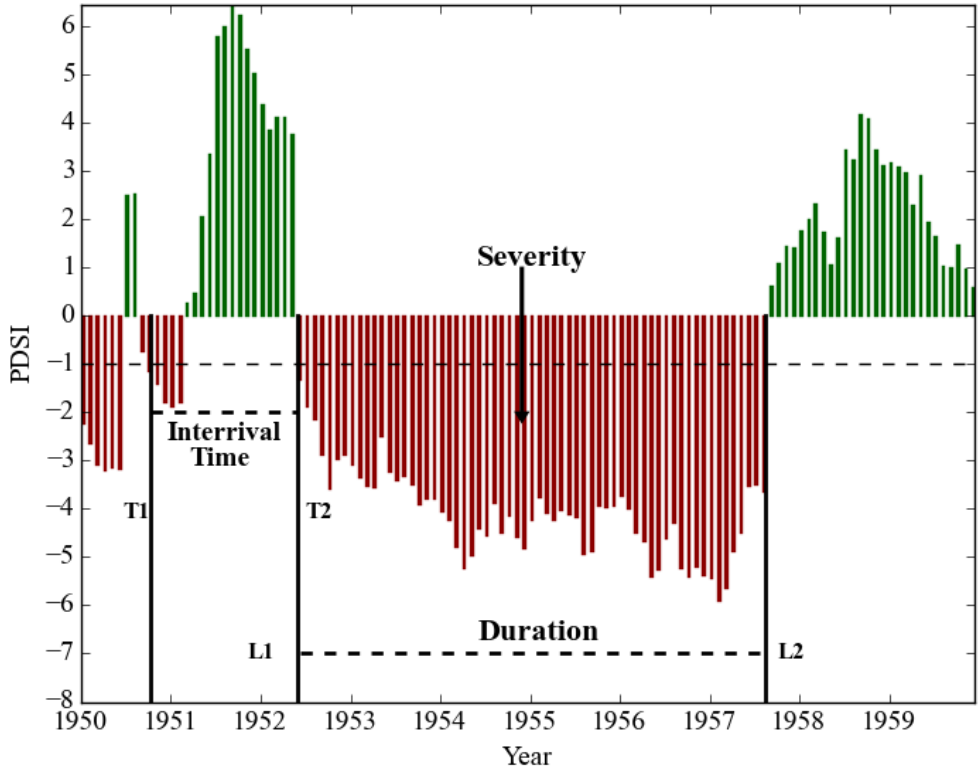

Figure 2. An illustration of drought duration, severity, and interarrival time by using a PDSI time series observed for Manhattan, Kansas from 1950 to 1960.

IV. *Severity (S)*

The severity is the cumulative sum of the index value based on the duration extent (Yang 2010):

$$S = \sum_{i=1}^{\text{Duration}} \text{Index} \tag{31}$$

V. *Intensity (I)*

The intensity of a drought is the severity divided by the duration. Droughts that have shorter durations and higher severities will have larger intensities:

$$I=\frac{\text{Severity}}{\text{Duration}} \tag{32}$$

VI. *Return Period of a Drought Event*

Drought events are stochastic in nature and usually assumed to independent and identically distributed (iid), therefore, the frequency analysis of the recurrence interval or return period of drought events shown in Fig. 2 is an attractive measure for drought and water resource assessments. The interarrival time (T) is the time between the start of one drought (T1) at a pre-set truncation level and the beginning of the next drought event with the same index threshold (T2) (Bonaccorso et al. 2003) (Fig. 2). In drought studies, the return period of a drought event is then defined as the mean interarrival time of droughts with a certain severity level or greater (Haan 1977; Shiau and Shen 2001). The severity return period was calculated from Shiau and Shen (2001):

$$T_s=\frac{E(L)}{1-F_s(s)} \tag{33}$$

where T_s is the return period in years, E (L) is the expected (or mean) interarrival time, and $F_s(s)$ is the cumulative probability density function at severity *s*. The expected interarrival time is calculated by fitting geometric distributions (Bonaccorso et al. 2003) to the drought and non-drought durations to find $p_{drought}$ and $p_{non\text{-}drought}$, the probability of drought and non-drought occurrence, respectively. Then from Shiau and Shen (2001),

$$E(L)=\frac{1}{p_{drought}}+\frac{1}{p_{non\text{-}drought}} \tag{34}$$

The density function at specific severity (s) chosen was obtained from a candidate list of distributions using the Kolmogorov-Smirnov test, which uses a null hypothesis that the index data is a good fit for the candidate distribution. The same density function was utilized across all stations for uniformity given that it was included as a good candidate at the 0.05 significance

level. All stations identified the two-parameter gamma function as a good fit for dry events. The scale and shape parameters for the distribution were fitted using the SCIPY statistical library (Jones et al. 2001).

2.4 Spatial interpolation

Spatial maps were generated using ArcGIS 10.1 software by the Environmental Systems Research Institute (ESRI). An interpolation approach was used to estimate the value of the indices and statistical measures at locations where no observed data exists. The interpolation method chosen was Inverse Distance Weighting (IDW) because it is not computationally intensive and has been used extensively in drought mapping (Saravi et al. 2009). During the spatial interpolation, the search radius is 150 km (Cook et al. 1999) with a total of five stations needed to interpolate at a single point, and the distance power was 4 to lessen the influence of distant points given the spatially sensitive nature of precipitation (Cook et al. 1999). The output grid size was 500m.

3. Results

3.1 Empirical cumulative frequency distributions

Figure 3 shows the cumulative frequency distribution for all regions for both PDSI and SPEI. Results for the SPI are not included in Figure 3 because the SPI cumulative frequency distributions are similar to those for the SPEI. Figure 1 shows that the distributions have a non-zero mean and gradually decrease in frequency towards the tails. It is difficult to differentiate between time steps of the SPEI except in western Kansas where the SPEI-12 has higher frequency of mild drought and lower frequencies for mild wet spells.

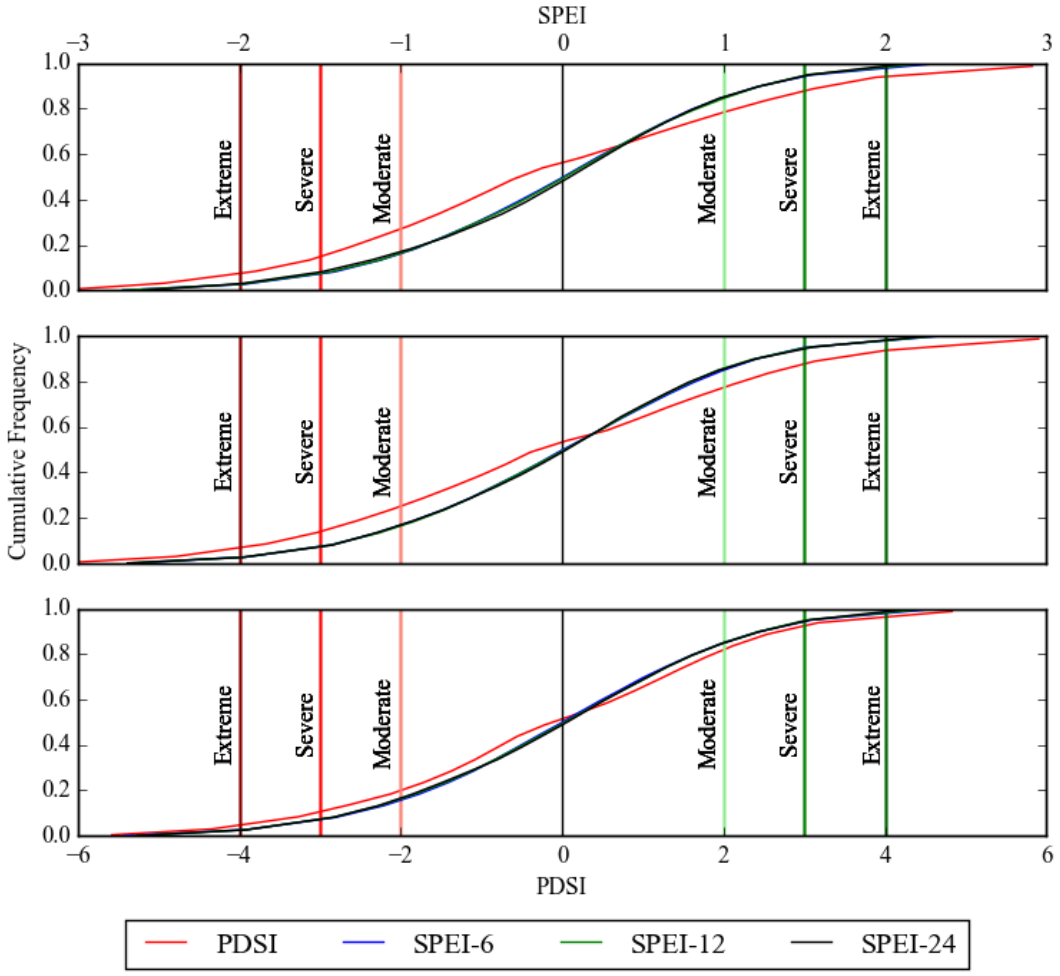

Figure 3. The empirical cumulative frequency of the monthly PDSI and SPEI for western (top panel), central (middle panel), and eastern (bottom panel) Kansas. Vertical lines represent dry spell (red) and wet spell (green) thresholds classified in drought indices.

In eastern Kansas the PDSI cumulative frequency ranges between 3-5% higher than the SPEI in moderate to extreme drought categories. In addition, the indices share similar frequencies of mild drought and moderate to extreme wet spells (Fig. 3). This results show that the bimodal distribution of the PDSI is evident with the decreasing slope at 0, which supports findings by Alley (1984). There is a higher frequency of incipient drought and wet spell values (-0.5 to -1.0 and 0.5 to 1.0) than purely neutral PDSI values (-0.5 to 0.5). This characteristic is

more pronounced in central and western Kansas (Fig. 3) where established drought or wet spells are more persistent, which enhances the bimodal structure of the PDSI distribution at more intense drought or wet spell categories.

Central and western Kansas have notably higher frequency of all drought categories by PDSI than the SPEI by up to 10% (Fig. 3). The extreme, severe, and moderate drought departures from the SPEI are similar for these two regions, but western Kansas experiences a higher frequency of incipient and mild drought. Conversely, there is a lower frequency of severe and extreme wet spells when using the PDSI in central and western Kansas than in eastern Kansas, which could indicate bias in the index due to a shift in the mean from 0 for all regions.

3.2 PDSI relative frequency

The empirical cumulative frequency distribution of the PDSI can be analyzed in a higher spatial resolution by examining the relative frequency for each drought category across Kansas. For the mild drought frequency, it was observed more frequently in the western and southeastern regions of Kansas (Fig. 4a). The global maximum (19%) occurred around Sedan and remains above 15% throughout the Flint Hills region of Kansas for mild droughts. South central and western Kansas experienced relative frequencies between 15 and 18%. Central and north central Kansas experienced the lowest frequency of mild drought (9 -15%). However, moderate drought frequency increased from east to west across the state (Fig. 4b). The frequency of moderate drought in eastern Kansas was about 10% and peaks to 22% along the southwestern Kansas-Colorado border (Fig. 4).

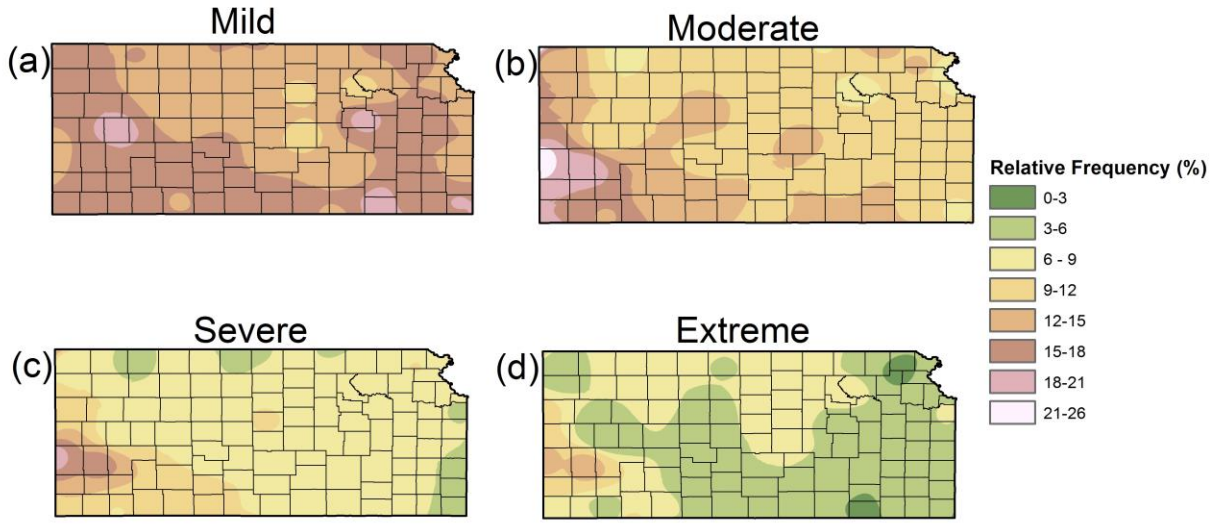

Figure 4. PDSI relative frequency of mild (a), moderate (b), severe (c), and extreme (d) drought over 1900 to 2014 in Kansas

Compared to mild and moderate drought frequencies, the southeast areas showed the lowest frequency across the state for both severe and extreme droughts. Severe drought frequency is less than 6 % in the southeast areas. It may be worthwhile to note that the highest frequency of severe drought (20%) occurs in southwest Kansas around the Arkansas River lowlands and extreme drought occurrence ranged from 1% near Sedan to 12% at the western Kansas border near Holly, Colorado. The Flint Hills in eastern Kansas typically experienced the least occurrence of extreme drought (3-6%) while extreme drought occurrence was between 6 and 10% in southwest Kansas and along the Nebraska border.

The average total drought frequencies in eastern, central, and western Kansas was 36%, 39%, and 44%, respectively. Areas in southeast Kansas with a relatively low AWC should expect to oscillate between wet and dry spells more frequently than the surrounding areas given

it receives more rainfall than the rest of the state. This lower AWC allows single precipitation events to have a major influence on PDSI, for example, flash drought (Mo and Lettenmaier 2016). Lakin, possessing a drought frequency of 64%, was the only station to deviate more than 12% above the mean total drought frequency, indicative of its likelihood to be experiencing drought conditions. Lakin has an AWC less than 110 mm from the gSSURGO. When the PDSI was manually calculated for a set range of AWCs (50 to 305mm) at each station, drought characteristics of stations in far western Kansas were different from those in the rest of the state (details in Appendix A). Locations at risk of higher frequency of severe and extreme drought occur along the Arkansas and Cimarron Rivers in southwest Kansas.

3.3 Station and regional drought characteristics

Stations located within central Kansas had the longest PDSI drought duration during the 1930s. McPherson and Ellsworth had droughts during the 1930s that lasted longer than 100 months (Table 1). The dry period during the 1930s was typically the longest duration drought during the last century using the PDSI as the drought indicator (Table 1). Two sample t-tests between the 1930s and 1950s drought events demonstrated statistical differences for drought duration but not severity or intensity at the 0.05 significance level. Atchison in eastern Kansas had the least number of consecutive drought months (27), occurring between 1936 and 1938. The average drought length of Kansas' longest duration droughts is 6 years (Table 1).

Severe drought occurrence (PDSI < -3) has an expected interarrival time of 5.57 years in western Kansas and 5.68 years in eastern Kansas (Fig. 5). The average accumulated severity for each decade between 1900 and 2010 shows that the 1930s and 1950s were the anomalies of the twentieth century for all regions (Fig. 6). Only in eastern Kansas was the 1950s drought on

average just as severe as the 1930s drought due to precipitation distribution between 1934 and 1936 isolated to eastern Kansas (Fig. 6). The frequency or number of drought events per decade ranged between 3 and 9. The 1930s droughts in eastern Kansas had an overall high severity accumulation and large number of events, indicating that it experienced a recurrence of intense droughts. The most recent drought to affect Kansas occurred between 2011 and 2014. The peak of the drought occurred in November 2012 when 68% of the state was experiencing severe or extreme drought. The median rank in severity for this drought event was 7^{th}, 10^{th}, and 3^{rd} over 1900 to 2014 in eastern, central, and western Kansas, respectively. It ranked in the top 3 of most intense droughts for 35% of Kansas stations, underscoring the severity of the drought reached in a short amount of time.

Table 3. Station PDSI drought characteristics, including available water capacity, minimum peak PDSI, and station's longest drought.

	Station	AWC (mm)	Peak PDSI Intensity			Longest Duration (PDSI≤-1)			
			PDSI	Year	Mo	Duration (mo)	Years	Severity	Intensity
Eastern Kansas	Atchison	198.5	-6.78	1956	6	27	1936-1938	-63.67	2.36
	Columbus	161.6	-6.35	1902	3	57	1952-1957	-201.30	3.53
	Council Grove	103.9	-5.93	1934	8	57	1936-1940	-198.14	3.48
	El Dorado	195.7	-7.17	1956	9	57	1952-1957	-242.27	4.25
	Ft Scott	210.0	-7.75	2012	7	45	1929-1933	-121.62	2.70
	Horton	176.1	-7.67	1934	8	67	1936-1941	-196.96	2.93
	Independence	140.4	-5.37	1956	10	62	1962-1967	-206.25	3.33
	Lawrence	132.4	-6.06	1956	10	57	1952-1957	-214.66	3.75
	Leavenworth	198.4	-5.87	1902	4	54	1952-1957	-190.62	3.53
	Manhattan	200.8	-8.67	1934	8	63	1936-1941	-190.58	3.02
	Olathe 3E	208.8	-7.11	1934	8	63	1952-1957	-249.36	3.96
	Ottawa	132.4	-5.75	1940	2	44	1911-1914	-133.70	3.04
	Sedan	88.4	-5.06	1911	1	56	1953-1956	-164.04	2.53
Central Kansas	Anthony	200.0	-6.67	1954	9	64	1932-1938	-198.21	3.09
	Coldwater	177.5	-6.92	1956	10	64	1932-1938	-228.57	3.57
	Ellsworth	180.0	-6.95	1939	10	110	1931-1940	-429.32	3.90
	Hays 1 S	222.2	-5.62	1956	10	58	1933-1938	-179.74	3.10
	Larned	202.8	-6.23	1956	9	64	1932-1938	-215.72	3.37
	McPherson	171.8	-8.08	1956	9	132	1930-1941	-427.38	3.24
	Minneapolis	171.8	-7.60	1934	8	95	1932-1940	-397.93	4.19
	Smith Center	192.7	-6.85	1940	7	89	1933-1940	-381.21	4.28
Western Kansas	Ashland	167.5	-7.21	1934	8	65	1932-1938	-243.51	3.75
	Lakin	106.4	-6.98	1939	10	103	1960-1969	-379.47	3.68
	Liberal	178.9	-5.45	1956	9	58	1952-1957	-206.00	3.55
	Norton 9SSE	203.2	-6.60	2002	9	102	1932-1940	-436.28	4.28
	Oberlin	220.0	-7.06	1936	8	100	1932-1940	-447.50	4.46
	Saint Francis	180.0	-6.23	1911	7	106	1996-2005	-285.11	2.70
	Scott City	191.9	-5.71	1956	10	77	1952-1957	-247.94	3.22
	Wakeeney	191.5	-6.38	2012	9	92	1933-1940	-327.04	3.55

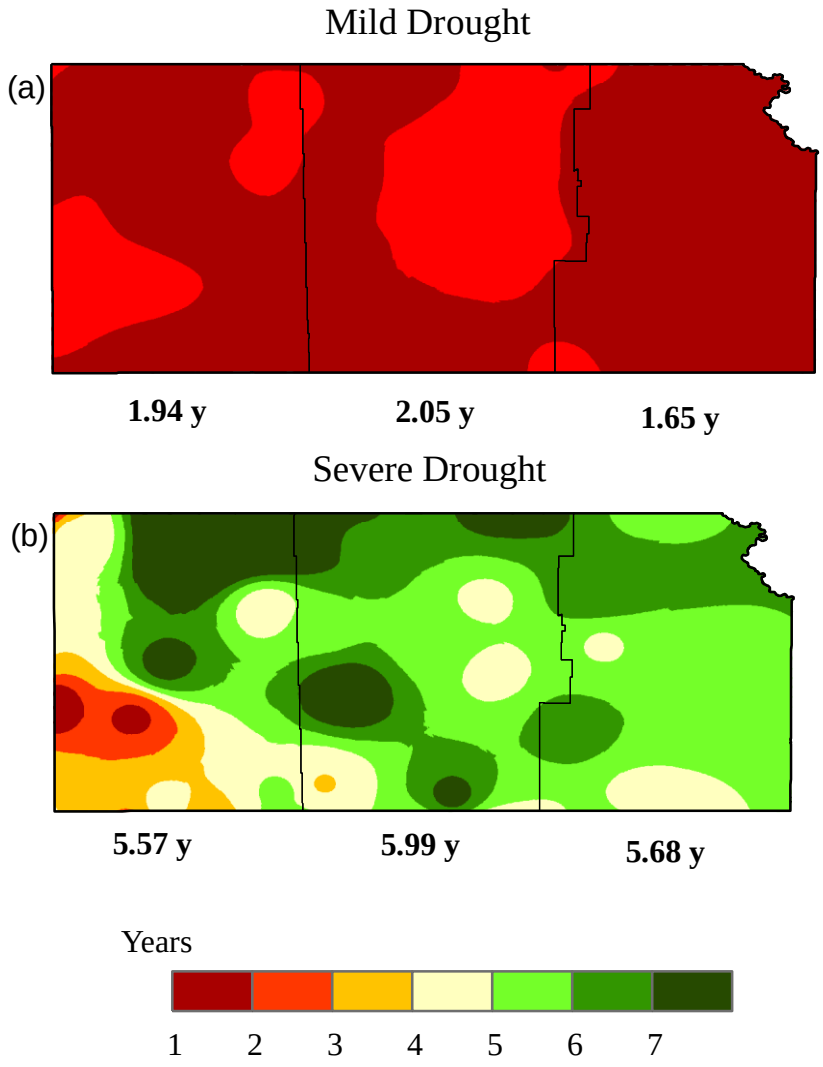

Figure 5. The expected or mean interarrival time of (a) mild and (b) severe droughts in Kansas based on the PDSI. The average of expected interarrival time for each third of Kansas is shown at the bottom (y refers to the year).

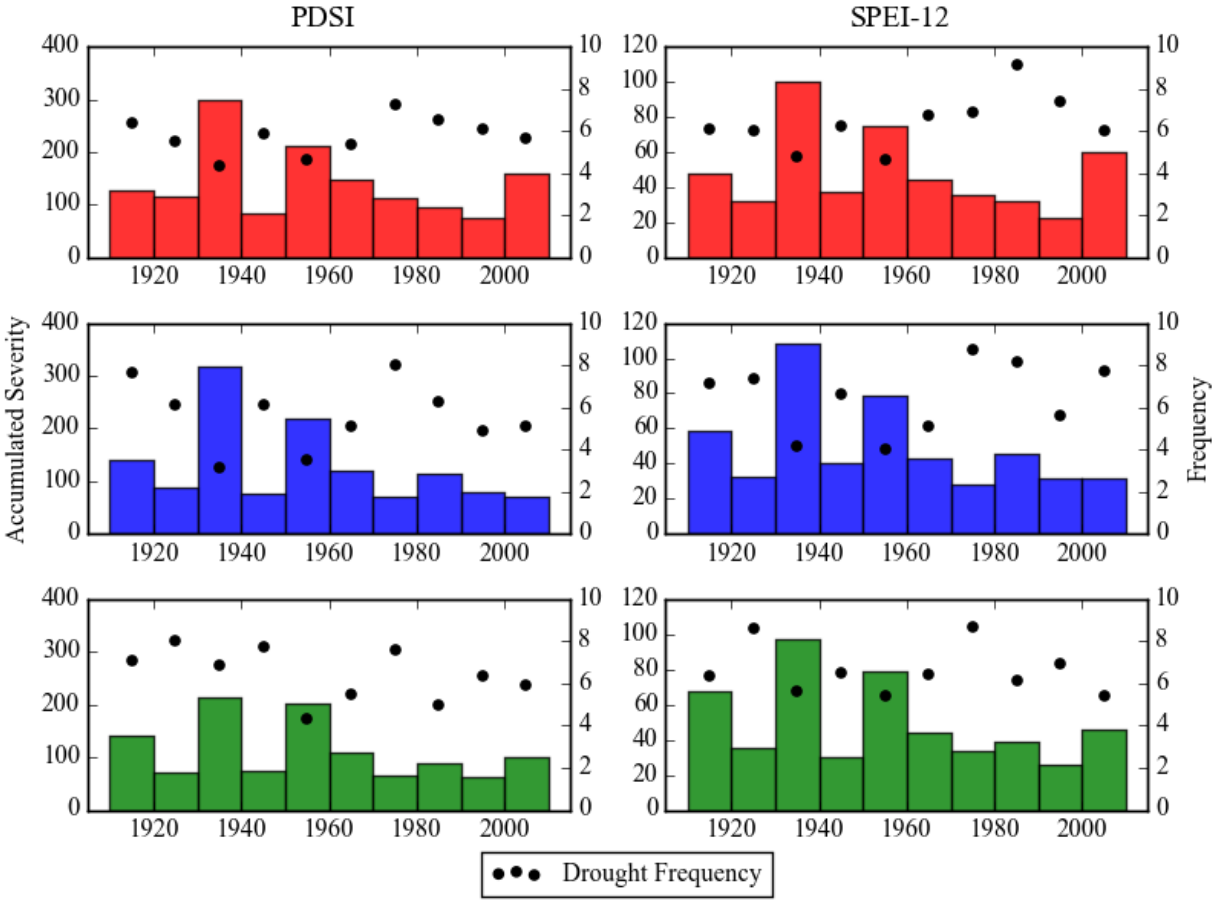

Figure 6. The mean aggregated drought severities (histogram by left Y axis) and drought frequency (black dots by right Y axis) by decade for the PDSI (left panels) and SPEI-12 (right panels) for western (in red), central (blue), and eastern (green) KS.

Both SPI and SPEI allow drought to be assessed at multiple time steps. For this study, the 3, 6, 12, 18, and 24 months of SPI and SPEI were used for individual stations. Detailed individual station SPI and SPEI results can be found in Appendix C. Proceeding from short-term to long-term drought, the SPI-3 and SPEI-3 both had the highest frequencies between droughts and wet spells as expected. The mean interarrival time for three-month drought across Kansas was 8 months. The highest intensity drought occurred in 1910 for the SPEI-3 and 2012 for the SPEI-6 in western Kansas (Fig. 7). The maximum durations at a single station for the SPEI-3 and

SPI-3 were 37 and 31 months, respectively (see Appendix C). Most stations did not have SPEI-3 droughts lasting longer than two years. Less than 7% of agricultural droughts at the 3-month time step lasted longer than one year across all regions of the state (Fig. 7)**.** Notice that the peak intensity of Kansas's most recent hydrologic drought occurred in 2014 in western Kansas by SPEI-24, which was two years (24 months) later than the peaks of the SPEI-3 and SPEI-6 (i.e., 2012 drought) (Fig. 7).

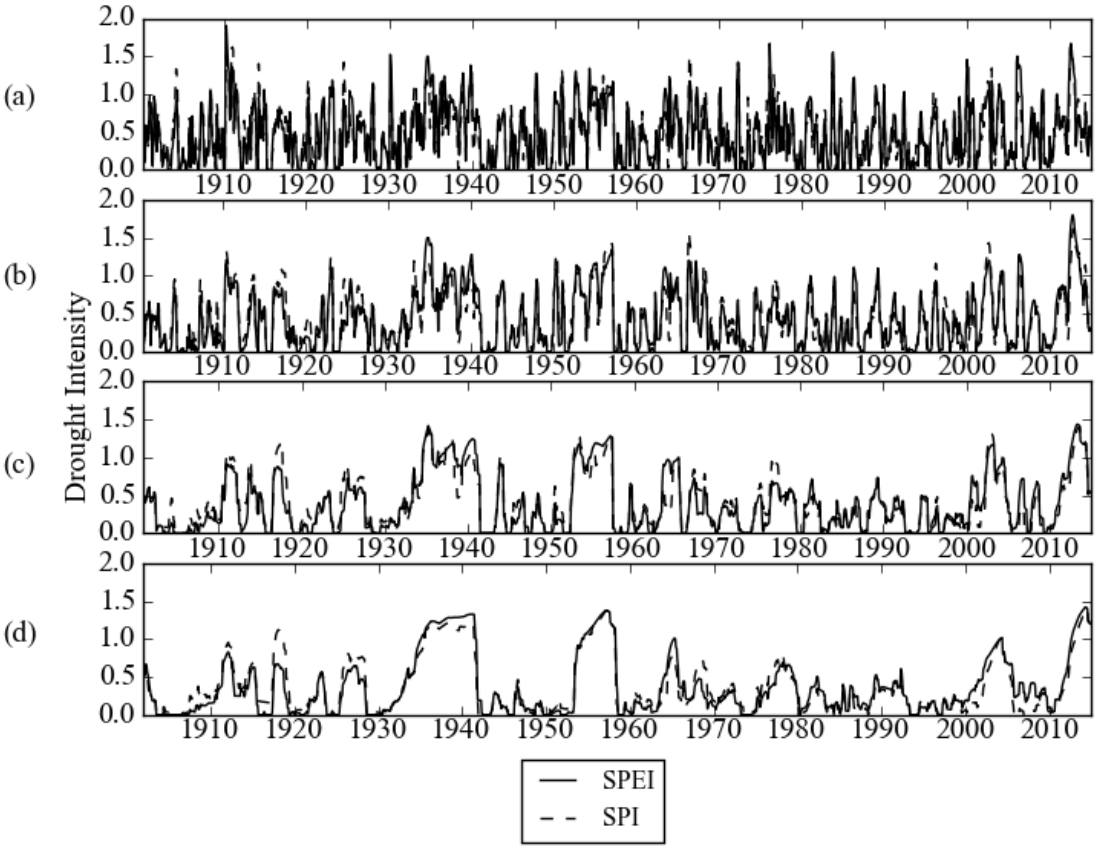

Figure 7. Drought intensity time series over January 1900 to December 2014 for the SPEI- and SPI -3 (a), -6 (b), -12 (c), -24 (d) for western Kansas

The SPI-12 and SPEI-12 showed a large increase in the maximum drought duration across all stations (appendix C). Both the SPEI-12 and SPI-12 had a maximum drought duration

of 128 months at Ashland. Categorized as an intermediate to long-term drought indicator, the SPEI-12 produced mean maximum durations of 58, 74, and 83 months across eastern, central, and western Kansas, respectively (Fig. 8). Between 25 - 30% of all droughts at this time step last longer than one year, and less than 5% persist longer than 3 years. Only eastern Kansas SPEI-18 had statistically lower drought durations and severities than the rest of the state (Fig. 8). It should be noted that the SPEI at different time steps could result in different drought statistical characteristics in Kansas especially when the drought duration and severity were evaluated (Fig. 8).

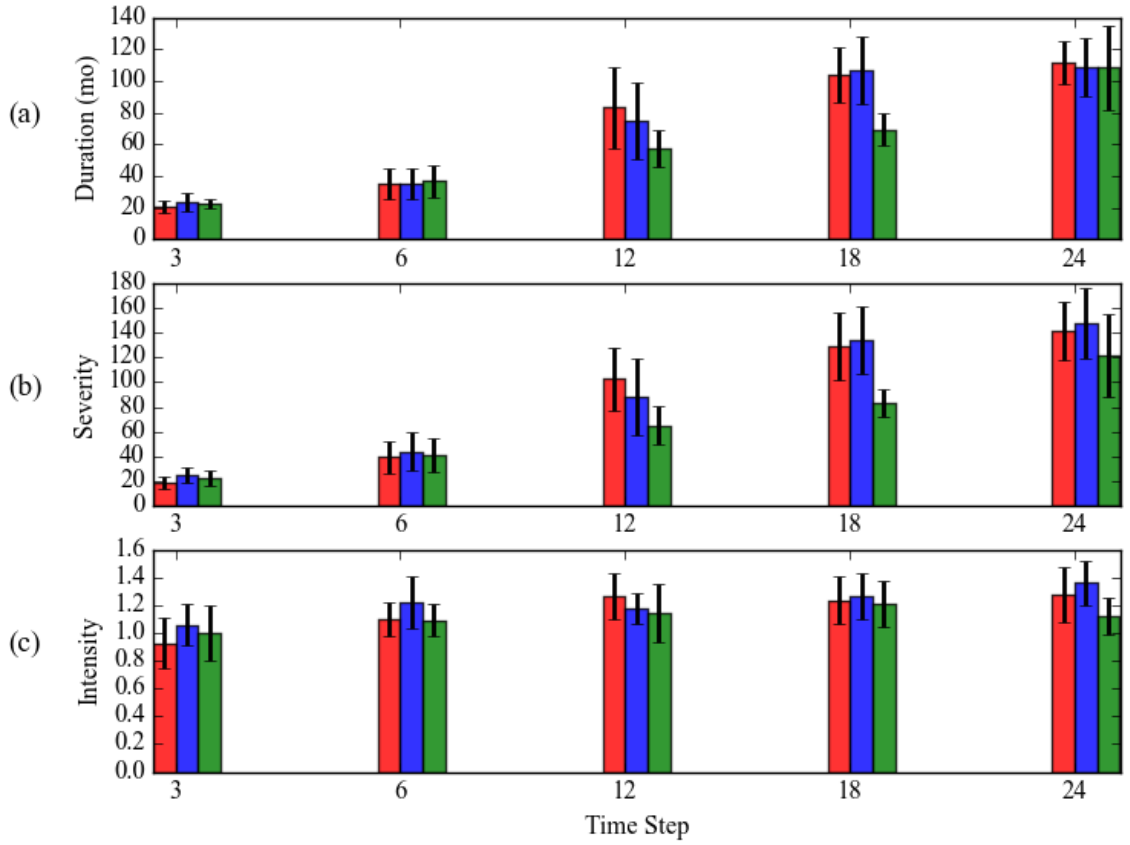

Figure 8. Regional SPEI drought characteristics of (a) duration, |(b) severity|, and (c) intensity by SPEI-3, -6, -12, -18, and -24 for western (red), central (blue), and eastern (green) Kansas.

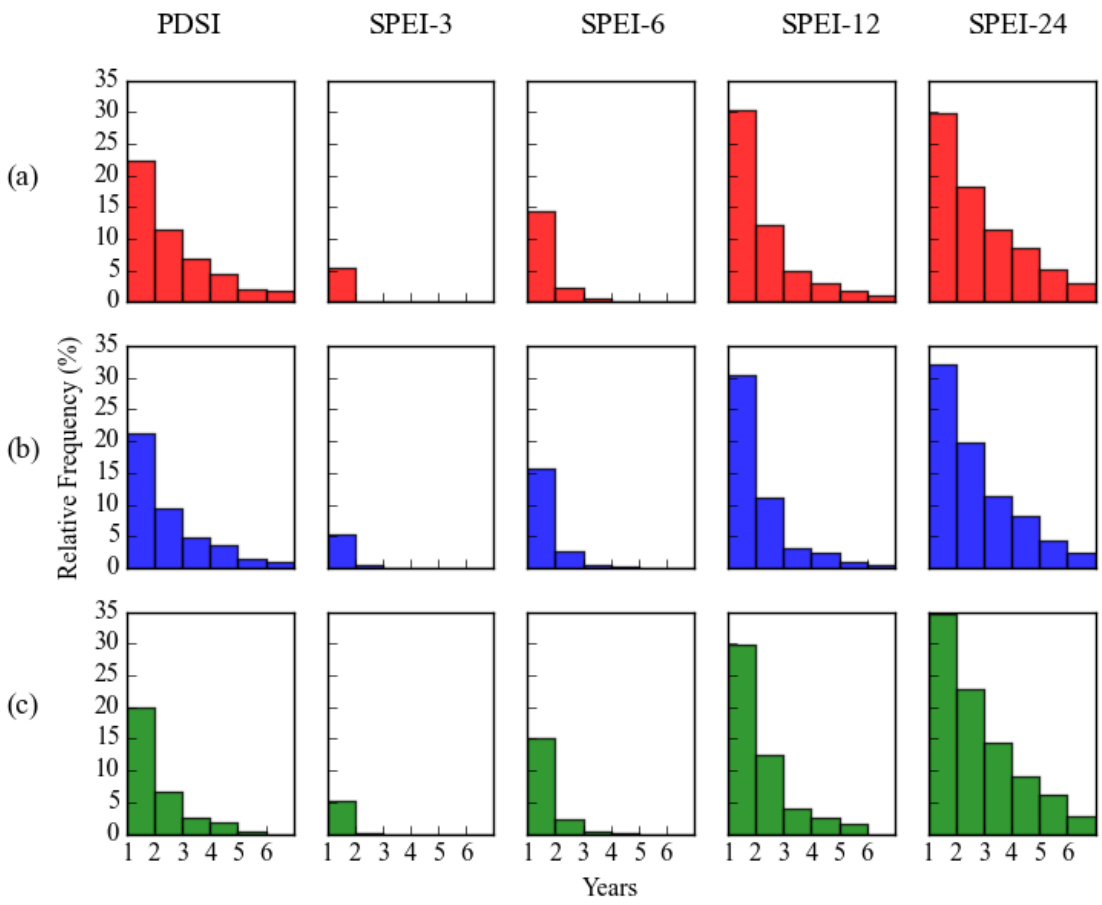

Figure 9. The regional mean relative frequency of droughts by indices persisting one or more years for (a) western, (b) central, and (c) eastern Kansas. For example, approximately 5% of all SPEI-3 droughts lasted between one and three years in eastern Kansas.

The longest SPEI-24 drought that occurred persisted approximately 12 years during the 1930s and early 1940s at Horton, KS (see Appendix C). These long-term droughts in Kansas can persist between 5 and 12 years across the state, underscoring the devastating hydrologic effects on the state's rivers and reservoirs. Maximum drought durations, severities, and intensities for all three regions in Kansas were not statistically different by SPEI-24 using multiple tests and bonferroni procedures; thus, eastern Kansas is equally as vulnerable to extreme hydrologic drought as western Kansas (Figs. 8 and 9). In eastern Kansas, SPEI-24 drought intensity during

the 1950s was far greater than any other drought events in the record (see Appendix C). The 2011-2014 SPEI-12 drought is ranked as the 5th, 3rd, and 3rd most severe drought in recent history for eastern, central, and western Kansas, respectively. Both SPEI-6 and SPEI-12 drought intensities rivaled that of the 1930s and 1950s for western Kansas (Fig. 7) but were less in eastern Kansas (shown in Appendix C). Using the SPEI-24 as the drought indicator, it was on average the most intense hydrologic drought on record in western Kansas (Figs. 7 to 9).

3.4 PDSI severity return periods

PDSI drought severities ranged from -6 to -53 for five year returns and -18 to -70 for ten year returns (Figs. 10a and 10b). These are the magnitudes of the drought severities expected to occur on average for a five and ten year period, respectively. In northeast Kansas and western Kansas, there was the highest risk of more severe five year droughts. On a ten year return cycle, a region from Hays extending to the Oklahoma border has the highest risk of drought with accumulated severities greater than -47. Stations such as McPherson, Oberlin, and Minneapolis with extreme outlying severities from the 1930s drought tended to produce isolated "bulls-eye" spatial return patterns at twenty and fifty year return periods (Figs. 10c and 10d). The twenty year and fifty year return severities were less in eastern and south central Kansas. Severities greater than -125 at the twenty year return period occurred from Manhattan all the way into southwest Kansas. Fifty-year return severities showed the same spatial structure as the twenty-year returns but demonstrated drought severities approaching the magnitude of the 1930s and 1950s drought.

The most recent drought event between 2011 and 2014 ranged from a small to relatively severe drought in the context of Kansas's recent drought history. Eastern Kansas had the smallest

return periods between 3 and 16 years, excluding a region in northeast Kansas which experienced higher drought severities (Fig. 10e). A drought event of this nature would likely occur once every decade. Northwestern and parts of southwestern Kansas were the hardest hit in Kansas with return periods ranging from 33 to 95 years, indicating this event would return on a half to almost full century cycle.

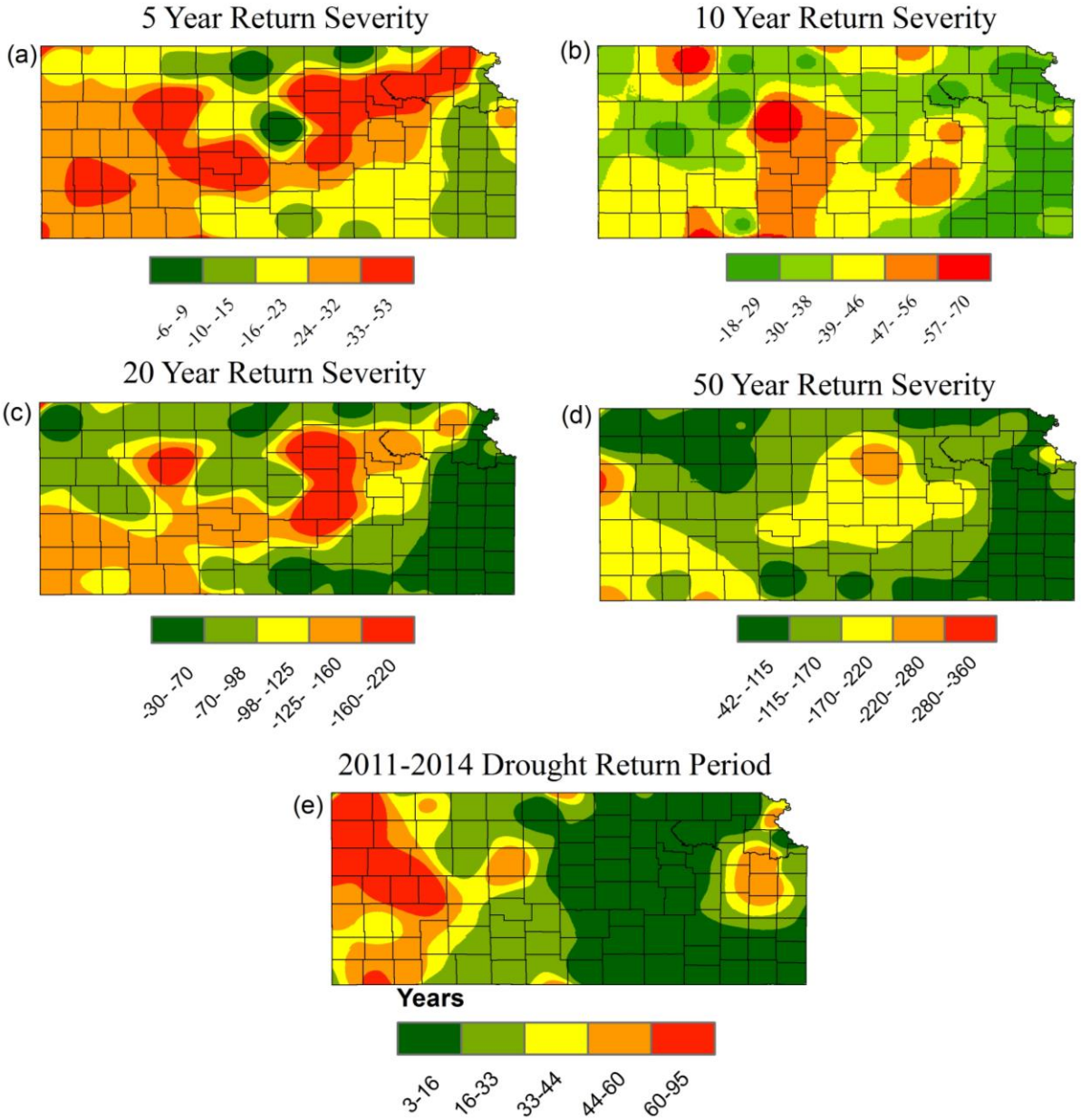

Figure 10. PDSI drought severity returns for 5, 10, 20, and 50 years (a, b, c, d). The return periods (years) of the 2010-2014 drought are shown (e) to provide context to a recent event within the scope of Kansas's recent drought history.

4. Discussion

Palmer briefly addresses the effects of available water on the PDSI (Palmer 1965). Low values of AWC limit the method's ability to show large departures from normal in humid climates. Estimates of the amount of rain needed to recharge the soil lie close to monthly normal precipitation amounts, regardless of the previous wetness or dryness (Palmer 1965). This eliminates large departures from normal and extreme values of the PDSI. Karl (1983) found that larger AWCs tended to increase the duration of the most severe droughts in the interior United States and that higher values of AWC in similar climates result in more extreme drought. Sandy soils with low AWC that lie in far western Kansas experience the highest frequency of severe and extreme soil moisture drought based on the PDSI.

Mean durations for each region between the SPEI and SPI of Kansas exhibited statistically significant different results only for western Kansas for the SPI (SPEI)-3 and central Kansas for the SPI (SPEI)-6. More variation between the two indices is exhibited in the drought onset and termination of 3 and 6-month droughts outside of eastern Kansas. No significant differences in severities were found at any time interval, and the maximum drought durations and severities were not statistically different in any region. The additional role of temperature introduced in the SPEI calculation does not appear to change the duration and severities of the most severe droughts in Kansas as compared to the SPI. The PDSI had the strongest correlation ($r = 0.83$) with the SPEI-12 in central Kansas. The lowest correlation ($r= 0.62$) with the PDSI occurred for the SPEI-24 in eastern Kansas. Maximum drought durations for all regions between

the PDSI and SPEI (SPI)-12 were not statistically significant, further underscoring the similarity between the two drought indices.

The regional mean r-Pearson correlation coefficients for all time steps between the SPI and SPEI were 0.98, 0.97, and 0.95 for eastern, central, and western Kansas, respectively. The PE term in SPEI plays a slightly more influential role in the drought calculations for western Kansas. All stations in western KS (excluding Ashland and Saint Francis) and Hays and Larned in central Kansas had statistically significant increases (α=0.05) in annual sum of PE (Fig. 11). Given that no station displayed a temporal trend with PE in eastern KS, either index is appropriate for future drought analysis for this region. Climates with low interannual variability of temperature respond mainly to variability in precipitation (Vicente-Serrano et al. 2010), which has been the case for eastern Kansas. However, the SPEI has an advantage over the SPI in western and central Kansas due to the significant increases in PE. Although the drought characteristics (severity, duration, and intensity) between the two indices were similar across Kansas, continued increases in temperature suggest that this might not hold true through the end of the 21st century (Rosenberg et al. 1999).

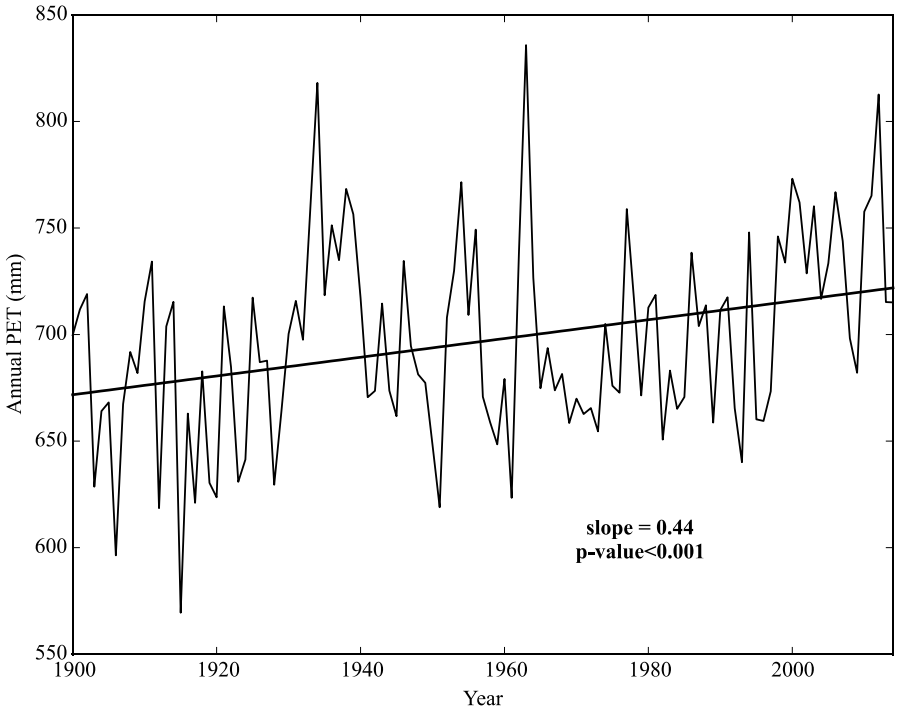

Figure 11. Annual PE (mm) for Lakin, KS between 1900 and 2014.

In order to examine the difference between SPEI and SPI, the correlation coefficients by each decade for each region were analyzed and they showed their consistency among time steps in eastern Kansas but relatively more variations observed in central and western Kansas (Fig. 12). The 3-month time step produced the most drastic departures from the other time steps in central and western Kansas as it was expected. The minimum correlation coefficient is 0.93 for the 24-month time step in the 1960s for western Kansas. This feature was caused by a spike in PE in 1963 (Fig. 11), followed by relatively steady PE for the remaining years in the decade. The shorter time steps were less consistent in the 1930s, 1940s, and 1950s, which contained the longest duration and most severe droughts in the period of record.

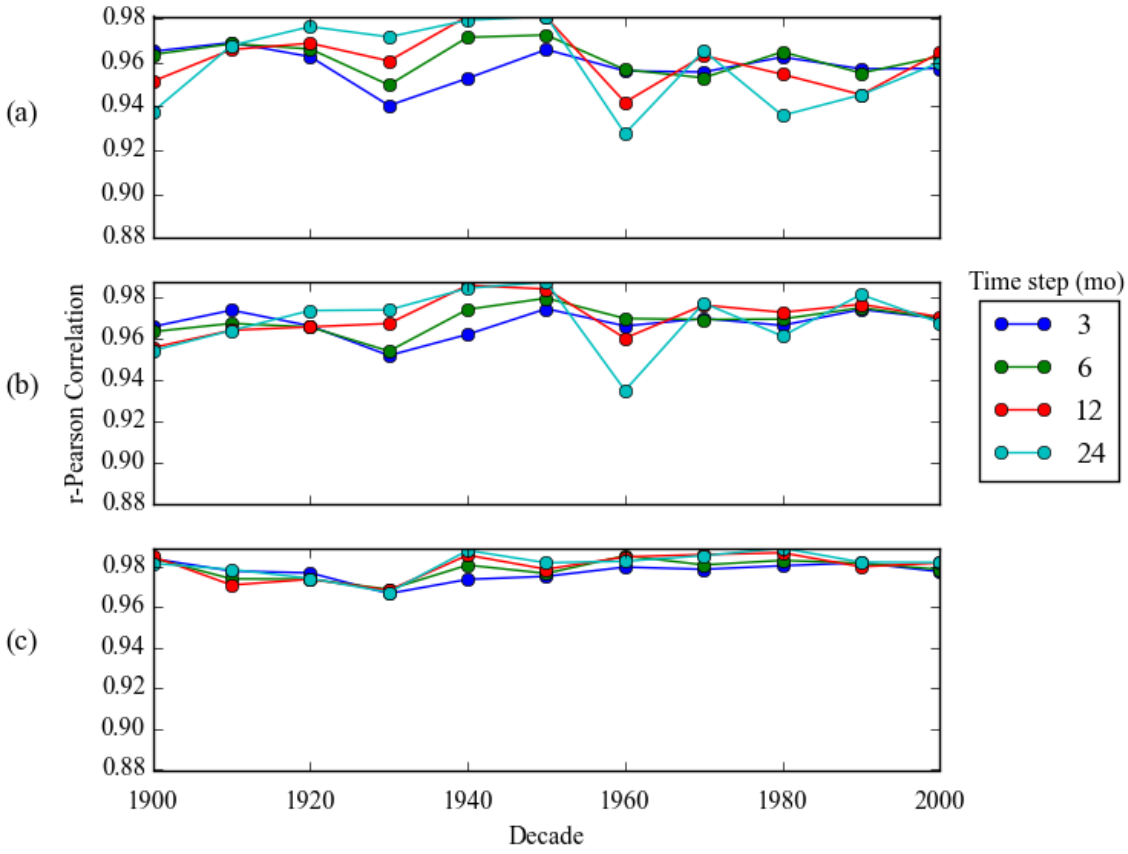

Figure 12. The r-Pearson correlations for each decade between the SPEI and SPI at four time steps for (a) western, (b) central, and (c) eastern Kansas.

5. Conclusion

In this study, drought assessment was conducted for Kansas through the use of three indices: the PDSI, SPI, and SPEI. The PDSI exhibited a higher frequency for every category of drought in central and western Kansas than the SPEI by up to 10%. Severe and extreme drought frequency was the highest in southwest Kansas around the Arkansas River lowlands and lowest in the southeast portion of the state and throughout the Flint Hills. The mean total drought frequency for eastern, central, and western Kansas was 36%, 39%, and 44%, respectively.

The drought of the 1930s had the longest duration for all of central Kansas. The 1952-1957 drought had overall severities less than the 1930s but a faster onset given its fast ascent to intensity levels that rivaled the 1930s drought. The accumulated severity of all 1930s and 1950s droughts showed that these decades were the anomalies of the twentieth century for the state. The average drought length of the longest duration droughts in the state is 6 years, and the number of drought events per decade ranged from 3 to 9. Severe drought occurrence can be expected to occur on average of 5.57 years in western Kansas and 5.68 years in eastern Kansas. Hydrologic drought across Kansas can persist between 5 and 12 years across the state, underscoring the devastating hydrologic effects on the state's rivers and reservoirs. The most recent drought between 2011 and 2014 peaked in coverage in November 2012 and reached intensity levels that rivaled the droughts that occurred in the 1930s and 1950s in western Kansas.

Five-year return drought severity magnitudes were the largest for northeast and western Kansas. Ten-year severity returns were the greatest for portions of central Kansas, while central and southwest Kansas have the largest magnitude droughts expected to return on the order of every 20 to 50 years. The regional mean correlations between the SPI and SPEI were greater than or equal to 0.95 for all regions, but due to statistically significant increases in potential evaporation in western Kansas, the SPEI is recommended over the SPI for meteorological and hydrological drought analysis in this region. Land use changes in the last thirty years towards a reliance on surface water reservoirs and ground water irrigation will diminish stream flow in moderate to severe drought, particularly if PE continues to increase in western Kansas. It is prudent for planners to have conservation strategies than can keep irrigation and municipal water supplies adequate for an increase growth in population. Knowledge of the specific

spatiotemporal characteristics of drought occurrence provides the foundation for the development of forecast products particular to Kansas's drought history.

References

Abramowitz, M., and I. A. Stegun, 1964: *Handbook of Mathematical Functions: With Formulas, Graphs, and Mathematical Tables.* Dover Publications.

Alley, W. M., 1984: The Palmer Drought Severity Index: limitations and assumptions. *Journal of Climate and Applied Meteorology*, **23,** 1100-1109.

Batisani, N., 2011: Spatio-temporal ephemeral streamflow as influenced by climate variability in Botswana. *Journal of Geographical Sciences*, **21,** 417-428.

Bonaccorso, B., A. Cancelliere, and G. Rossi, 2003: An analytical formulation of return period of drought severity. *Stochastic Environmental Research and Risk Assessment (SERRA)*, **17,** 157-174.

Clement, R., 1989: National Water Summary 1988-89 Floods and Droughts: KANSAS.

Cook, E., D. Meko, D. Stahle, and M. Cleavland, 1999: Drought Reconstructions for the Continental United States. *Journal of Climate*, **12,** 1145-1162.

Guttman, N., 1998: Comparing the Palmer Drought Index and the Standardized Precipitation Index. *Journal of the American Water Resources Association*, **34**.

Guttman, N. B., 1991: A Sensitivity Analysis of the Palmer Hydrologic Drought Index. *JAWRA Journal of the American Water Resources Association*, **27,** 797-807.

Haan, C. T., 1977: *Statistical Methods in Hydrology*. Iowa State University Press.

Heim, R. R., 2002: A Review of Twentieth-Century Drought Indices Used in the United States. *Bulletin of the American Meteorological Society*, **83,** 1149-1165.

Jones, E., T. Oliphant, and P. Peterson, 2001: SciPy: Open Source Scientific Tools for Python.

Karl, T., 1986: The Sensitivity of the Palmer Drought Severity Index and Palmer's Z-Index to their Calibration Coefficients Including Potential Evapotranspiration *Journal of Climate and Applied Meteorology* **25**.

Karl, T. R., 1983: Some Spatial Characteristics of Drought Duration in the United States. *Journal of Climate and Applied Meteorology*, **22,** 1356-1366.

McKee, T. B., N. J. Doeskin, and J. Kleist, 1993: The relationship of drought frequency and duration to time scales. *8th Conf. on Applied Climatology*, Anaheim, Canada, 179-184.

Menne, M., C. Williams, and R. Vose, 2009: The United States Historical Climatology Network monthly temperature data Version 2.5. *Bulletin of the American Meteorological Society , 90, 993-1007*.

Metzger, S., 2013: Kansas Water Plan Update.

Mo, K. C., and D. P. Lettenmaier, 2016: Precipitation Deficit Flash Droughts over the United States. *Journal of Hydrometeorology*, **17,** 1169-1184.

Palmer, W. C., 1965: *Meteorological drought.* vi, 58 pages pp.

Putnam, J. E., C. A. Perry, and D. M. Wolock, 2008: Hydrologic droughts in Kansas—Are they becoming worse?: U.S. Geological Survey Fact Sheet 2008–3034, 6 pp.

Rosenberg, N., D. Epstein, D. Wang, L. Vail, R. Srinivasan, and J. Arnold, 1999: Possible Impacts of Global Warming on the Hydrology of the Ogallala Aquifer Region. *Climatic Change*, **42,** 677-692.

Saravi, M., A. A. Safdari, and A. Malekian, 2009: Intensity-Duration-Frequency and spatial analysis of droughts using the Standardized Precipitation Index. *Hydrology and Earth System Sciences Discussions*, **6,** 1347-1383.

Shiau, J.-T., and H. W. Shen, 2001: Recurrence Analysis of Hydrologic Droughts of Differing Severity. *Journal of Water Resources Planning and Management*, **127,** 30-40.

Soil Survey Staff, 2014: Gridded Soil Survey Geographic (SSURGO) Database for KS, CO, OK, NE, and MO. N. R. C. S. United States Department of Agriculture, Ed.

Sönmez, F. K., A. L. I. Ü. Kömüscü, A. Erkan, and E. Turgu, 2005: An Analysis of Spatial and Temporal Dimension of Drought Vulnerability in Turkey Using the Standardized Precipitation Index. *Natural Hazards*, **35,** 243-264.

Svoboda, M., and Coauthors, 2002: The Drought Monitor. *Bulletin of the American Meteorological Society*, **83,** 1181-1190.

Thom, H. C. S., 1966: *Some Methods of Climatological Analysis.* Secretariat of the World Meteorological Organization.

Thornthwaite, C. W., 1948: An Approach Toward a Rational Classification of Climate. *Soil Science*, **66,** 77.

Vicente-Serrano, S. M., S. Beguería, and J. I. López-Moreno, 2010: A Multiscalar Drought Index Sensitive to Global Warming: The Standardized Precipitation Evapotranspiration Index. *Journal of Climate*, **23,** 1696-1718.

——, 2011: Comment on "Characteristics and trends in various forms of the Palmer Drought Severity Index (PDSI) during 1900–2008" by Aiguo Dai. *Journal of Geophysical Research*, **116**.

Ward, G. H., 2013: Hydrological indices and triggers, and their application to hydrometeorological monitoring and water management in Texas.

Warwick, R. A., 1975: Drought hazard in the United States: A research assessment: Boulder, Colorado. I. o. B. S. University of Colorado, Ed.

Yang, W., 2010: Drought Analysis under Climate Change by Application of Drought Indices and Copulas, Civil and Environmental Engineering, Portland State University, 82 pp.

Zhang, T., X. Lin, and G. F. Sassenrath, 2015: Current irrigation practices in the central United States reduce drought and extreme heat impacts for maize and soybean, but not for wheat. *Sci Total Environ*, **508,** 331-342.

Chapter 2 - Space-Time Variability of Decadal Drought in Kansas

Abstract

Drought variability of the last 115 years was analyzed through the Empirical Orthogonal Functions (EOFs) techniques and their Varimax rotations from 1900 to 2014 in Kansas. Large-scale synoptic patterns primarily dominated the Kansas spatial drought structures, especially during long-term wet and drought conditions in central and eastern Kansas. The EOFs analysis indicated that the first principal components of drought explained approximately 70% of the drought variability across the state and demonstrated a statistically significant wetting trend for the state over the last 115 years, oscillating at a dominant period of about 14 years for all drought indices used in the study. The 99°W meridian line acted as the dominant transitional line demarcating the areas of Kansas' climate and vegetation (crop and grassland) relationship as spatial drought presented. The Multivariate El Nino Index (MEI) signal as it modulates global and regional climate variabilities provided a low-frequency indicator to couple with Kansas drought's leading modes by varying leads of 3 to 7 months depending on the use of drought index and time steps selected.

1. Introduction

Drought is a complex and natural phenomenon of climate that costs the state of Kansas billions of dollars during its most extreme events (Metzger 2013). Reducing Kansas' vulnerability to extreme drought and flooding events is an essential goal to mitigating economic, social, and environmental impacts. Hayes et al. (2004) describe a risk-based approach that includes assessment of drought risk and risk management. As drought develops from a slow onset, its characteristics such as inception, termination, frequency, and severity are difficult to assess, which makes it a hazardous phenomenon to most socioeconomic systems in any region of the world. Drought can be driven by major meteorological processes and soil properties, and it is assumed that this structure can be decomposed into orthogonal sub-climate regimes through Empirical Orthogonal Functions (EOFs). These functions were first used for applications in meteorology and climatology by Lorenz and Project (1956) as tools for examining the spatial and temporal patterns of variability of a single variable (Bjornsson and Venegas 1997). The goal of EOFs analysis is to seek field structures that explain the maximum amount of variance in a two dimensional dataset. One dimension represents the dimension that the analyst is examining for structure, and the other dimension represents the sample realizations of this structure (Hartmann 2014). In the atmospheric sciences, the structure dimension is generally space (points or grids), and the sampling dimension is time.

Large and small-scale studies of drought EOFs have been conducted across the globe in regions including China (Cai et al. 2015), Romania(Cheval et al. 2014), Croatia (Bojariu et al. 2012), Portugal (Martins et al. 2012), Turkey (Tatli and Türkeş 2011), and Sicily (Bonaccorso et al. 2003). For example, Raziei et al. (2010) regionalized drought across Iran into four sub regions based on the variability of the Standardized Precipitation Index (SPI-24) at a scale of 24 months.

Applications of EOFs in these studies included but were not limited to: assessment of the similarities and differences amongst drought indices, identification of strong and weak temporal signals in the drought index time series, and the separation of a region into sub-climate regimes. Studies on drought variability are valuable for the design and management of water resource systems (Bonaccorso et al. 2003).

Drought variability studies that focus on areas in the central plains emphasize the paleoclimatic record over instrumental (1900-present) records. Early studies documented that the 1930s drought had significant impacts on the true prairies in Nebraska, Kansas, and western Iowa, where the death of prairie plants due to droughts ranged from 20 to 50% in the eastern portions and 80-95% in the western portions (Weaver and Albertson 1936). Native American annual pictographic accounts have been used to corroborate extended periods of drought in the Great Plains between 1777 and 1869 (Gallo and Wood 2015). Woodhouse and Overpeck (1998) used tree rings, lake sediments, geomorphic data, and historical documents to demonstrate that multidecadal, severe droughts occurred in the central Plains before 1600. Layzell (2012) performed a similar analysis specifically for the state of Kansas. He determined through tree ring records (Cook et al. 1999) that drought variability of the instrumental record (1900-present) is just a subset of the potential variability in the context of the last thousand years. Droughts in the last millennium have surpassed the severity and duration of the 1930s and 1950s droughts in the Great Plains region and Kansas (Cook et al. 2007). It is important to note that water systems are commonly designed to handle the "drought of record," identified as the most severe hydrological event from the instrumental record. In Kansas the 1950s drought (1952-57) remains the planning benchmark and is used to calculate reservoir yield through droughts with a 2% chance of occurrence in any one year (K.A.R. 98-5-8).

Logan et al. (2010) conducted a study on the spatiotemporal variability of drought in the Kansas River basin using the slope of the SPI-6,-12, and -24 over the instrumental records. They showed an increase in SPI over time for most of central and eastern Kansas, excluding portions of far western Kansas and eastern Colorado. Broader studies of drought trends using the different forms of the Palmer Drought Severity Index (PDSI) over the contiguous United States have shown an increase in precipitation during the latter half of the 20th century with an increase in the percentage of wet area and decrease in dry area from the 1950s to 1990s (Dai 2011); thereafter, the United States has been experiencing fairly dry conditions. Studies on the state level have the advantage of greater applicability to agricultural and municipal managements that require local-scale information to effectively implement mitigation strategies. An increase in the understanding and prediction of climatic variability based on the El Nino Southern Oscillation has added substantial value to the United States agricultural industry (Solow et al. 1998).

The objectives of this study were to i) investigate the spatial and temporal variability of drought and wetting episodes in Kansas during the instrumental period 1900-2014 by application of EOFs and Varimax rotation and ii) examine drought variability's relationship to the El Nino Southern Oscillation (ENSO). Multiple drought indices (PDSI, SPI, and Standardized Precipitation Evapotranspiration Index (SPEI)) were used to distinguish changes in drought type such as agricultural (vegetation productivity), meteorological (precipitation deficits), and hydrologic (streamflow and surface and underground water supplies) drought (Heim 2002).

2. Data and Methods

2.1 Data sources

Monthly precipitation and average temperature were obtained from Oregon State's Parameter-elevation Regressions on Independent Slopes Model (Prism 2016). These datasets at an original 4 kilometer resolution were re-gridded by zonal averaging to 0.5 °latitude by 0.5 ° longitude for a total of 90 grids across the state of Kansas (Fig. 1). High-resolution (10 m) Gridded Soil Survey data (Soil Survey Staff 2014) was utilized to calculate available water capacity for the PDSI calculation. The PDSI, SPI, and SPEI were calculated at each grid point from 1900-2014 using tools developed at Kansas State University. Time steps chosen for the SPI and SPEI were 3, 6, 12, and 24 months. Each drought dataset was converted into *n x p* matrices for EOF analysis:

$$\begin{bmatrix} x_{11} & x_{12} & \cdots & x_{1p} \\ x_{21} & x_{22} & \cdots & x_{2p} \\ \vdots & \vdots & \vdots & \vdots \\ x_{n1} & x_{n2} & \dots & x_{np} \end{bmatrix} \quad (1)$$

where each row represents a map (or field) of drought index at time t = 1…n and each column represents a time series of drought index at given locations (or measurements) from 1 to p.

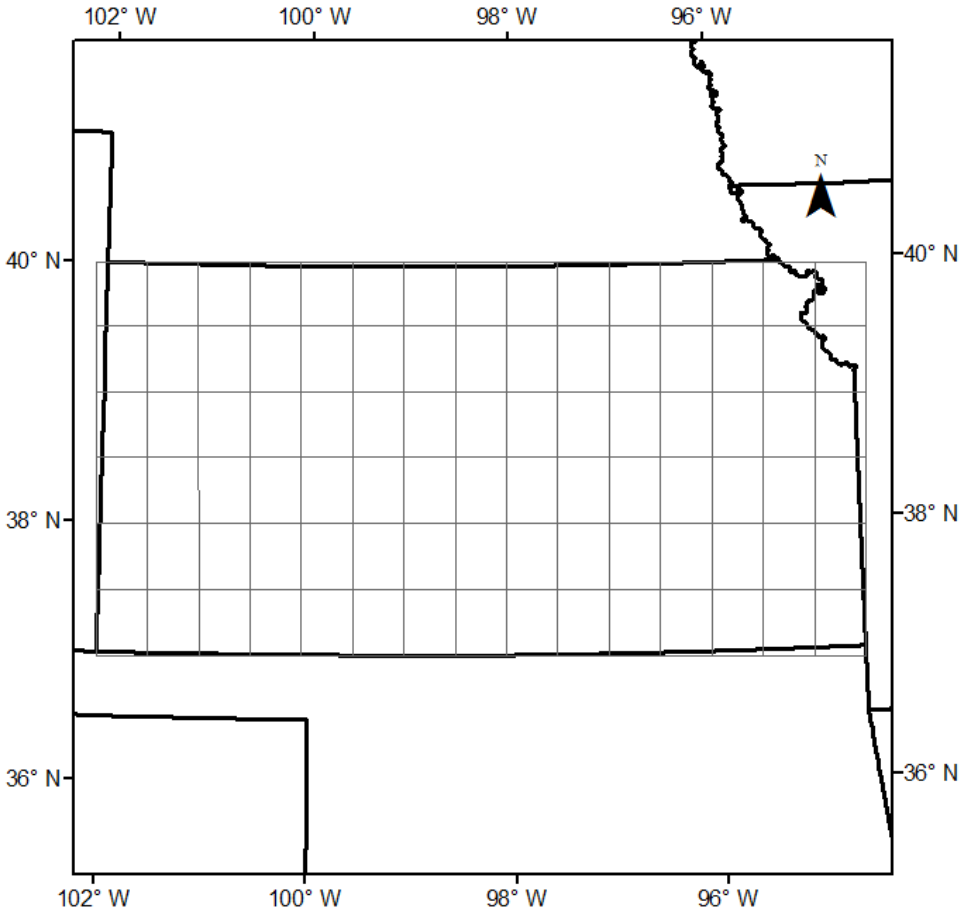

Figure 1. Map of Kansas and 0.5 °resolution grids used for temperature, precipitation, soil available water capacity, and drought data.

The Multivariate El Nino Index (MEI) retains the most important coupled ocean-atmosphere phenomenon to cause global climate variability on seasonal to inter-annual time series. There is a long-term time series of MEI starting from 1871 (Wolter and Timlin 2011) but when considering the data quality issues, the latest available data from 1950 to 2014 was utilized in this study from the Earth System Research Laboratory as a metric of the strength of the El Nino Southern Oscillation (Wolter and Timlin 1998). Large positive MEI values indicate the occurrence of El Nino conditions, while large negative MEI values indicate the occurrence of La Nino conditions.

2.2 Empirical Orthogonal Functions (EOFs)

The anomaly of drought index time series was calculated by subtracting the mean of each column in Eq. (1). These anomalies were weighted by the cosine of each grid's latitude (Bjornsson and Venegas 1997). These weighted anomalies were standardized to form a new data matrix F in Eq. (2). Then the covariance matrix (*p x p*) is defined by:

$$C = F^T F \tag{2}$$

which contains the covariances between the time series of the field at any pair of grid points. The covariance matrix C is symmetric, and positive semi-definite, which means all eigenvalues of C are greater than or equal to zero. The goal of EOFs analysis is to detect uncorrelated linear combinations of the different spatial variables that explain the maximum variance. The EOFs are obtained as the solution to the eigenvalue problem:

$$CU = U\mathbf{\Lambda}. \tag{3}$$

The *n x n* diagonal matrix $\mathbf{\Lambda}$ contains the eigenvalues λ_i of C. The columns (c_i) of U *(p x p)* are the eigenvectors of C corresponding to the eigenvalues λ_i (Bjornsson and Venegas 1997). These eigenvectors are commonly referred to as the EOFs. Eigenvectors, properly normalized (i.e., divided by their Euclidean norm and multiplied by the square root of their corresponding eigenvalue), represent the correlation between the original data and the corresponding principal component time series. The k^{th} principal component (time series; expansion coefficients, commonly named as PC_k) are obtained by projecting the E_k eigenvector onto the original standardized data whose elements a_{jk}, t = 1, … n, are given by:

$$a_{tk} = \sum_{j=1}^{p} x_{tj} U_{kj} \,. \tag{4}$$

There are *p* principal components of length *n*. The first principal component (PC1) is the time series corresponding to the spatial pattern of eigenvectors (EOF1), the PC2 is corresponding to EOF2, and etc.

The percentage of the total variance explained by each eigenvector (loading) can be obtained by dividing each individual eigenvalue by the sum of all eigenvalues λ_i

$$\frac{\lambda_i}{\sum_i^p \lambda_i} \cdot 100\% \tag{5}$$

Generally, the first few leading modes should be able to explain most of the variance exhibited by the drought's spatial and temporal variations. The remaining modes do not significantly contribute to the overall variance. In order to assess how many modes are adequate, it is helpful to use North's Rule of Thumb (North et al. 1982) to determine the sampling error (σ_λ) of a particular eigenvalue λ_i as,

$$\sigma_{\lambda i} \sim \lambda_i \left(\sqrt{\frac{2}{N}} \right) \tag{6}$$

If its value is comparable or larger than the spacing between the eigenvalue and the nearest eigenvalue, then the sampling error of the associated EOF is comparable to its closest neighboring EOFs, where the N is the number of realizations. Pearson's correlation and cross-correlation measures were used for evaluating correlations at the 95% confidence level. Trend analysis was based the least-square linear regression at the 95% confidence level with its p values.

2.3 Varimax Rotation

Unrotated EOFs often exhibit some characteristics which hamper their utility to isolate individual modes of variation. These characteristics are: domain shape dependence, subdomain instability, sampling problems, and inaccurate portrayal of the physical relationships in the data (Richman 1986). These issues can sometimes be resolved through the rotation of eigenvectors. The main objective of rotation is to alleviate the orthogonality/uncorrelation of EOFs and domain dependence of EOF patterns, obtain simple structures, and ease the interpretation of obtained patterns (Hannachi et al. 2007). It allows the corresponding retained modes to be more spatially localized (the rotated loadings have high correlation with a smaller set of spatial variables). The number of leading EOFs and principal components to retain for rotation (*m*) was evaluated using the North's rule of thumb. EOFs were weighted (multiplied) by the square root of their corresponding eigenvalue, U_m, before applying rotation. Expansion coefficients were normalized by dividing by the square root of their associated eigenvalue. The rotation is formally achieved by obtaining an *m x m* rotation matrix *R* to construct the rotated EOFs, *B*, according to:

$$B=U_mR \tag{7}$$

where R is the rotation matrix and U_m are the weighted EOFs assuming m leading EOFs are selected.

The goal of rotation is expressed as the maximization problem:

$$\max f(U_m R) \tag{8}$$

The functional $f()$ represents the rotation criterion chosen. Varimax orthogonal rotation (Kaiser 1958) was applied to identify and interpret the physical modes of spatial variability (Preisendorfer and Mobley 1988) of drought in Kansas. Because Varimax rotation is orthogonal, R is subject to the constraint:

$$RR^T=R^TR=I_m \tag{9}$$

where I_m is the identity matrix. It seeks to maximize (5) according to the simplicity criterion:

$$\max\left(f(U_mR)=\sum_{k=1}^{m}\left[p\sum_{j=1}^{p}b_{jk}^4-\left(\sum_{j=1}^{p}b_{jk}^2\right)^2\right]\right) \tag{10}$$

where *m* is the number of EOFs retained, *p* the number of observations (rows), and b_{jk}, j = 1,…p, and k = 1,…m, the elements of the B in Eq. (7) (Hannachi et al. 2007). It attempts to simplify the structure of the patterns by pushing loading coefficients toward zero or ±1.

3. Results

3.1 Space-time variability of PDSI

Figure 2 shows the variance explained by each principal component for the PDSI. Three components (*m*) were retained for analysis as indicated by the error bars from the North's rule of thumb. These three leading eigenvalues were nondegenerate and separated from the rest of eigenvalues (Fig. 2). The spatial and temporal patterns for the first three PDSI EOFs are shown in Figure 3. The percentage of variance explained by the first three EOFs are 69.01%, 9.73%, 5.45%, respectively for a total of 84.19% (Fig. 2). The spatial extent of the first EOF, a mono-pole pattern, demonstrates that the climate across most of Kansas explains most of the variation in drought across the state. Central Kansas is strongly correlated (r > 0.9) with the first primary component while the four corners of the state are moderately correlated (0.75) (Fig. 3a). The overall high correlation across the state demonstrates that large-scale weather patterns typically dominate Kansas climate. The fraction of local variance explained decreases towards the eastern and western Kansas (Fig. 3a). Areas that behave the most climatically independent are in the southwest, northwest, northeast, and southeast corners. The 1930s and 1950s droughts from PC1

are the most easily identifiable, indicating that the severity, duration, and extent across the state was appreciable compared to the other intermittent droughts (Fig. 3d). The trend of PC1 (PC2) is increasing (decreasing) and they are statistically significant at the alpha level 0.05. No linear trend was found for PC3. Based on the high spatial correlation of the EOF1 with the PC1, Kansas as a whole showed a slight increase towards wetter PDSI in PC1 between 1900 and 2014 (Fig. 3d).

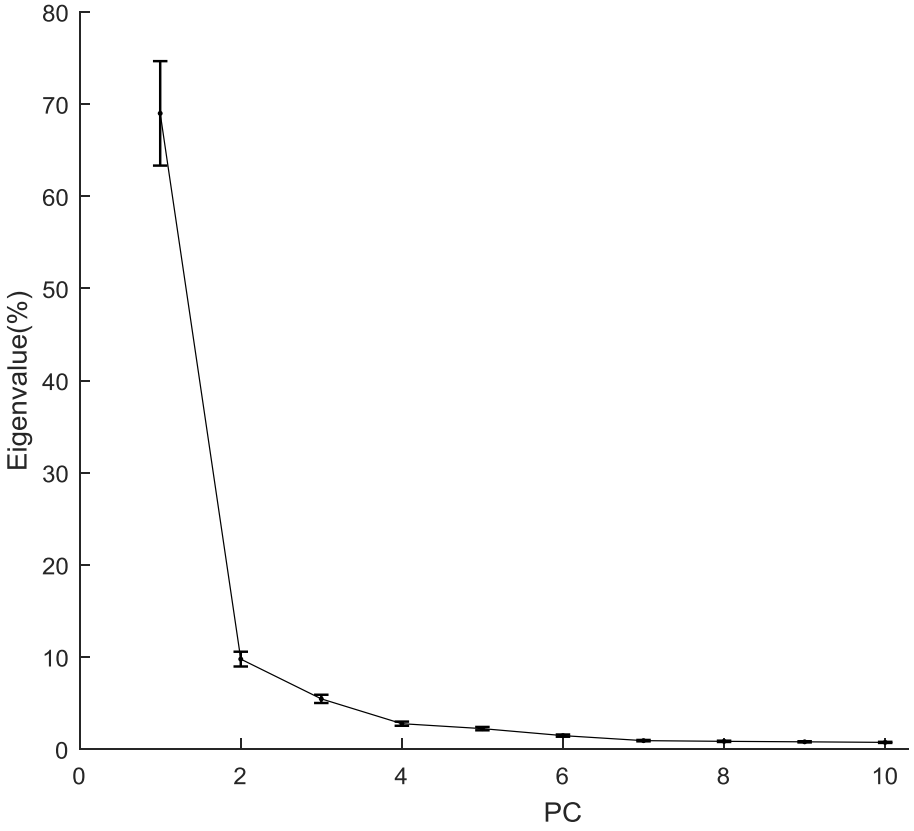

Figure 2. Spectrum of the variance explained by each eigenvalue (%) for first 10 principal components for the PDSI data set.

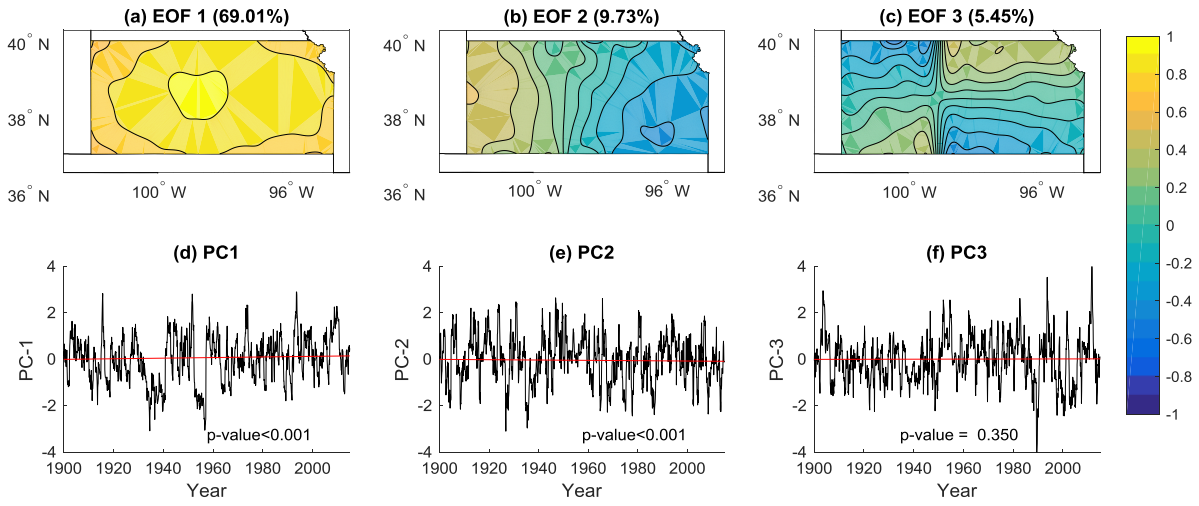

Figure 3. First three EOFs (a-c) and normalized PCs (d-f) of the PDSI. Contours of each EOF mode represent correlation with their corresponding PCs. There are statistically significant positive and negative trends for the PC1 and PC2 (p < 0.001), respectively.

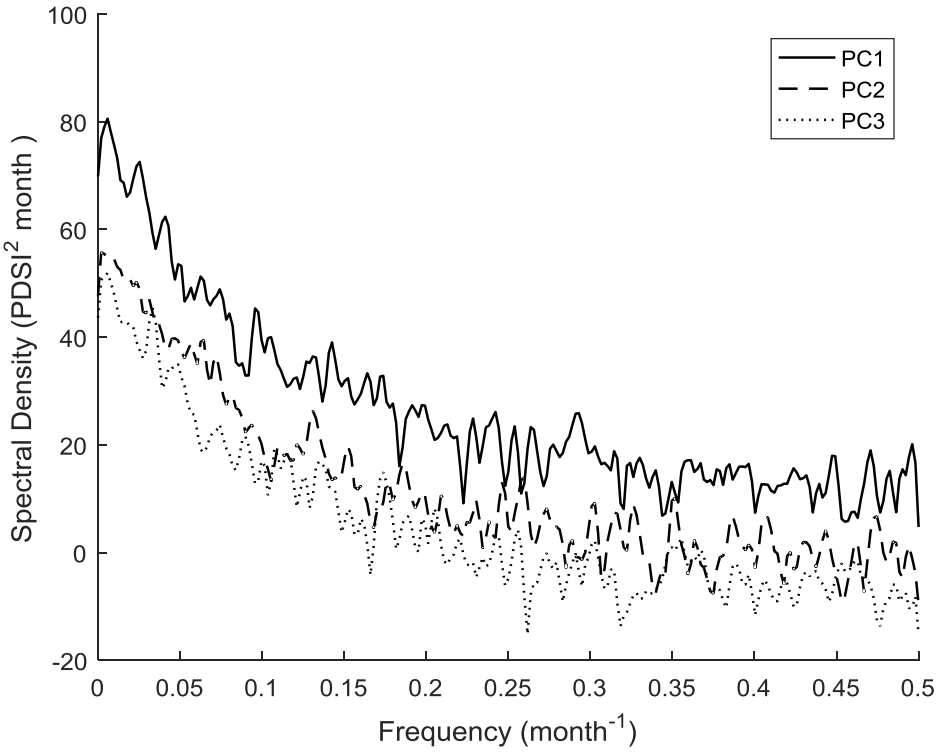

Figure 4. Power spectral density of the PCs for the PDSI. Maximum peaks occur at periods of 14.22, 42.67, and 14.22 years for the PC1, 2, 3, respectively.

The 2nd EOF was meridional in the direction of Kansas's average precipitation gradient (Fig. 3b). Precipitation decreases dramatically from southeastern to western Kansas, which is a synoptic result of the flow of moisture north and east from the Gulf of Mexico across eastern Kansas. Because the indices in this study are considered to be their normalization for both regionality and seasonality (a particular area's climate), it is not surprising that the stronger gradient in precipitation is only secondarily influential with a 9.73% variance explained (Fig. 3b and 3e). Western Kansas is moderately positively correlated (0.5) while eastern Kansas is negatively correlated (-0.4). The PC2 time series trend is decreasing and statistically significant. Although the amount of variance explained by this component is small (9.73%), it does reveal a drying trend of a much weaker signal in western Kansas ($R^2 = 0.008$) (Figs. 3b and 3e).

The 3rd principal component (EOF3) explains the least of the 3 retained principal components (5.47%) and does not show any statistically significant linear trend (Figs.3c and 3f). However, it does exhibit a heteroscedastic shape with an increase in variance after 1980 if we set 1980 as a change point, which may indicate its lack of stationarity due to non-constant variance over time. The Kwiatkowski-Phillips-Schmidt-Shin (KPSS) test for stationarity demonstrated that the principle component is not stationary at the 0.1 significance level. The minimum peak in 1989 and the maximum peaks in 1993 and 2011 correspond to relatively higher intensity drought and flooding events, respectively, observed in Kansas. As the intensity of a drought event represents its severity divided by its duration, the higher intensity droughts and floods have larger severities and shorter durations. Although weaker than the previous two components, this EOF3 signal indicates an increase in short-term but severe extreme precipitation and drought events in the last three decades for areas in northeast and southwest Kansas (Figs. 3c and 3f).

To further examine drought patterns in a temporal domain of each principal component, three previous PC time series were decomposed into the time-frequency space (Torrence and Webster 1998). The power spectral density function using a Fourier transform with a Hamming window showed the frequencies of drought and wetting that contribute substantially to the overall variance of time series (Fig. 4). The fundamental harmonic frequency occurred 0.0059 cycles per month or a period of 14.22 years in PC1 time series (Fig. 4). Most of the power intensity of the PC1 signal occurred between one and two decades, underscoring the region's natural oscillation cycle between significant wet and dry periods (Fig. 4). These are the higher intensity and longer duration droughts that can create significant impacts on the Kansas economy. The next strongest period occurred at 3.28 years, which are the small scale, high-frequency fluctuations between wet and dry periods that are short duration and lower severity. The dominant oscillation cycle or period in the PC2 signal was 42.67 years, and it is interesting to note that the amplitude of the signal was decayed after 1980. The overall wetting trend as demonstrated by PC1 is thus underlined by subtle drying in western Kansas.

Rotation of the first three modes resulted in changes of the variance explained by each mode to 22.81%, 30.88%, and 30.51%, respectively (Table 1). The spatial distribution of the first rotated component (REOF1) identified two sub regions: one dominant in the northeast and a smaller zone in southwest Kansas (Fig. 5a), which is similar to the spatial pattern of the third unrotated EOF3 (Fig. 3c). The correlation between RPC1 and unrotated PC1 is 0.90. Thus, rotation of PDSI only subtly changed the temporal drought signal component to correspond with the drought characteristics of northeast and southwest Kansas. The 2nd rotated pattern (REOF2) demonstrated the same structure as the unrotated component (EOF2) and explained a higher proportion of variance than the 1st rotated score (Fig. 5b). The RPC2 was also identical to PC2

with a correlation of 0.91, suggesting only subtle distinctions in western and eastern Kansas drought variability of the dominant drought signal. The main differences were seen in the increase in intensity and duration of the 1988-1989 drought in northeast Kansas, drought relief in eastern and southwest Kansas during the 1930s drought, and an increase in intensity of flooding episodes in western Kansas between 1900 and 1930.

The third rotated pattern showed a dipole between southwest and southeast Kansas and underscores a strong wetting trend in southeast Kansas. The north-south asymptotic behavior of the spatial patterns of REOF1 and REOF3 occurs approximately at 99 °W, passing near the population centers of Great Bend and Hays. The 99 °W meridian and four quadrants of similar drought variability in Kansas are consistent with the transitional boundary of Kansas shortgrass prairie (to the west) and tallgrass prairie (to the east) as well as agricultural activities between sub humid (rainfed crops) and semiarid (cattle, irrigated, and dryland crops) areas (Tomanek 1995).

Table 1. Percentage of total variance explained for each rotated component. A dash indicates that the PC was not significant (evaluated by North's Rule of Thumb).

	Varimax (%)				
n.PCs	PDSI	SPEI-3	SPEI-6	SPEI-12	SPEI-24
1	22.81	14.12	13.25	26.73	26.82
2	30.88	32.41	32.93	34.08	30.79
3	30.51	22.21	3.70	28.87	32.78
4	-	18.89	19.51	-	-
5	-	5.13	23.40	-	-
6	-	1.64	1.62	-	-

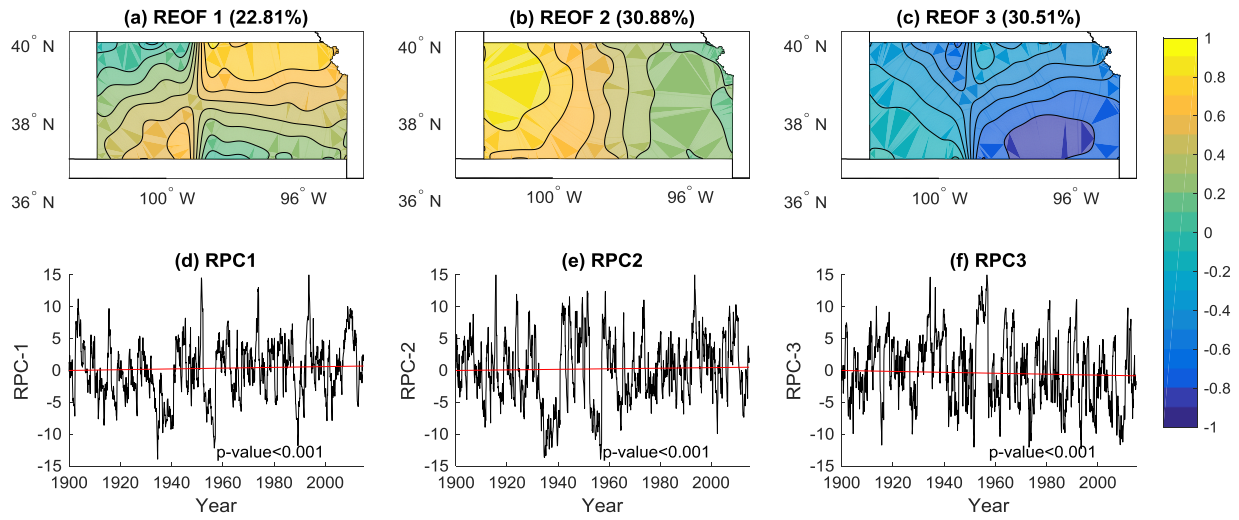

Figure 5. Three Varimax REOFs (a-c) and RPCs (d-f) of the PDSI. RPC1 and RPC2 showed statistically significant positive trends, and RPC3 had a negative trend but negative REOF3.

3.2 Space-time variability of SPEI-n

Results of the SPI are not shown given they are nearly identical to the SPEI. Differences will be discussed in Section 4. The number of significant components to retain for analysis based on North's rule of thumb for the SPEI-3 and -6 was six, and the number to retain for the SPEI-12 and -24 were three (see Appendix D). The total variance (%) explained by the unrotated modes four through six for the SPEI-3, -6 were 6.16% and 5.71%, respectively. These lower modes will only be analyzed after Varimax rotation for SPEI. The structure of the normalized eigenvectors is remarkably similar to the PDSI for the first three modes (see Appendix D). With each increase in time step, higher correlation ($r > 0.9$) in the EOF1 was moved towards central and eastern Kansas. At the longer time steps, southwest and northwest Kansas retained some climatic variability different from the rest of the state. The proportion of variance explained by PC1 increased from 72.35% for the SPEI-3 to 77.38% for the SPEI-24 (Appendix D). Thus,

hydrologic drought (SPEI-24) has higher spatial and temporal coherence than meteorological (SPEI-6, 12) and agricultural drought (SPEI-3) given its long-term memory.

PC1 of all SPEI time steps had their dominant period at 14.22 years, which is the same as the PDSI (see Appendix D). PC2 had a dominant period of one year for the SPEI-3 and eight years for longer time steps, oscillating at much high frequencies than the PC2 of the PDSI. The SPEI-24 shows the strongest linear relationships among all drought indices in PC1 and PC2 (increase and decrease, respectively) based on R^2. This statistically significant decrease in the PC2 was the strongest in western Kansas ($R^2 = 0.028$), confirming the subtle long-term drying in the region that was also shown by the PDSI. The linear relationships of shorter time steps were also decreasing but weaker. The long-term effects of drought on ground recharge and water levels will be more noticeable than short term impacts in the future in western Kansas.

The spatial patterns of the first three rotated modes were similar to the rotated patterns of the PDSI for the SPEI-12, 24 but different from the SPEI-3, 6. The retained six modes of the SPEI-3, 6 are distinctly different, excluding mode 2 (see Appendix D for rotated SPEI EOFs). Analysis of time steps less than 12 months were included for rotated EOFs that each explained more than 15% of the total variance. The second rotated EOF for the SPEI-3 and -6 was similar to the rotated and unrotated second EOFs and explained the largest percentage of variance (32%). All three EOFs showed weak linear trends towards wetter conditions. EOFs three and four (four and five) isolate regions of maximize correlation to southeast and northeast Kansas for the SPEI-3 (-6).

All three rotated PCs of the SPEI-12 showed statistically significant increases over the instrumental records. The strongest increases were in eastern Kansas (RPC1 and RPC3), and the weakest increase was in western Kansas (RPC2). The rotated SPEI-24 patterns were similar to

the SPEI-12; however, the 3rd REOF exhibited the largest explained variance of the three modes (32.78%) and had the strongest linear relationship among all drought index primary component series in this study (R^2 = 0.044). As an index for identifying long term hydrologic drought as it relates to underground water, river flow, and dam levels (Batisani 2011), the third rotated component of the SPEI-24 indicates a strong increase in long term wetting covering a broad area of southeast Kansas. In addition, although the first REOFs explained a smaller proportion of the variance (26.82%), it showed a similar wetting trend for northeast Kansas and a small area along the 99 ºW meridian line close to the Oklahoma border (R^2 = 0.040).

3.3 El Nino Southern Oscillation (ENSO) and Drought in Kansas

The Multivariate El Nino Index (MEI) takes into account six important fields (sea level pressure, zonal and meridional surface wind components, sea-surface temperature, near-surface temperature, and total cloudiness) across the tropical Pacific and is the first unrotated principal component of all six observed fields (Wolter and Timlin 2011). A low-pass (24 months) filter was applied to the MEI and each of the drought index time series to observe low-frequency relationships between the MEI and drought indices in Kansas. The PC1 has the highest cross-correlation with the MEI of all unrotated drought indices (Fig. 6). Among the drought indices, the PDSI has a maximum cross-correlation coefficient (0.367) with the MEI at a lag of six months (i.e. MEI arrives 6-month earlier than PDSI, hereafter, a positive lag means the drought index is behind the MEI), which indicates that there is a semi-annual delay in response to drought and wet episodes in Kansas (Fig. 6). On the other hand, from first three leading RPCs, the cross-correlation of the RPC2 for all drought indices were increased ($r > 0.4$), highlighting a stronger regional correlation in western Kansas given the EOFs pattern (Figs. 7, 5b and 5e). The

result indicated that decadal variability of agricultural drought (SPEI-3) shows a distinctly strong relationship with ENSO in western Kansas (r = 0.5) (Fig 7b and Fig. D12b in Appendix D). All correlations were statistically significant at the 0.05 level.

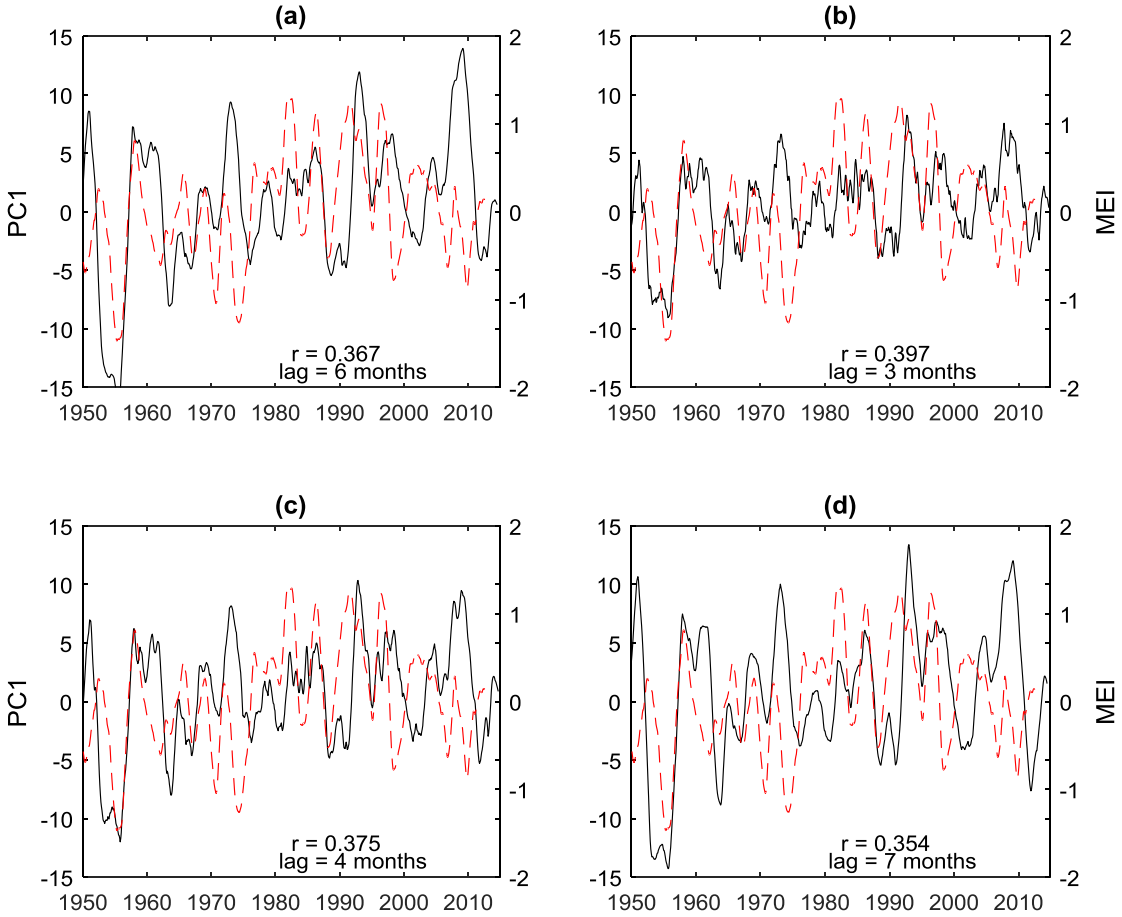

Figure 6. Temporal patterns of the first leading components of monthly PC1 (black) from (a) PDSI, (b) SPEI-3, (c) SPEI-6, and (d) SPEI-12 and Multivariate El Nino Index (MEI) (red). The time series were filtered by a 24-month low-pass filter. The drought index time series was shifted to correspond to the maximum cross-correlation with the MEI.

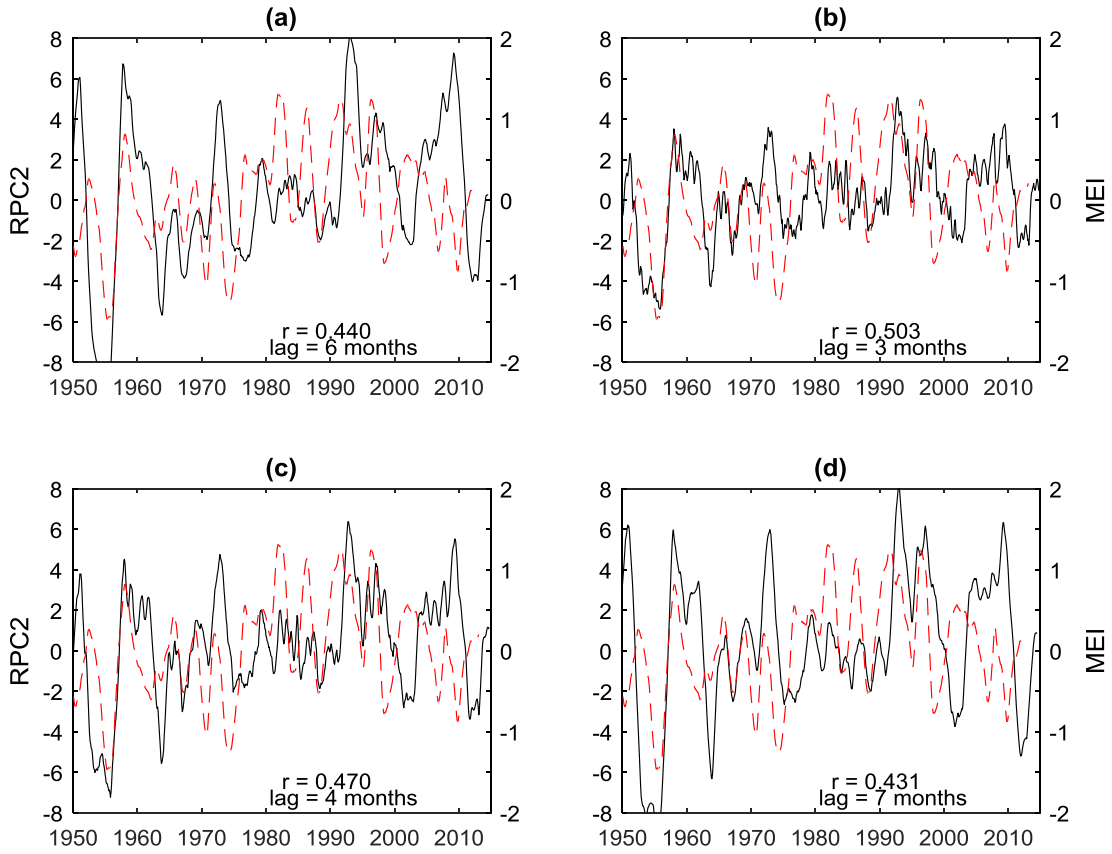

Figure 7. The same as Figure 6 but for monthly RPC2.

4. Discussion

Differences of EOFs spatial and temporal patterns between the PDSI, SPEI, and the SPI are relatively small. The leading principal component of PDSI exhibits higher spatial and temporal variability than all SPEI time steps with the greatest difference of 9% between the PDSI and SPEI-24, which most likely results from the additional complexity of the soil budgeting procedures in the PDSI computation and long-term average of the 24-month time step.

The potential effects of climate change are subtle in this analysis. The overall trend for most of Kansas is towards wetting, especially in the eastern portion of the state. This supports

findings by Logan et al. (2010). The PC3 demonstrates increasing intensity of drought and flooding in parts of northeast and southwest Kansas with the strongest signals in the PDSI and SPEI-24. Drying trends were found in the second principal components of the PDSI and longer time steps of SPEI or SPI although it is overshadowed by a stronger wetting signal in the first component. The strongest, unrotated pattern of drying was exhibited by the SPEI-24.

The Ogallala aquifer in the central high plains of the United States is an important irrigation source for farmers in western Kansas, which receives less than 20 inches of rainfall annually. Changes in aquifer levels are heavily impacted by changes in climate and local irrigation use (Rosenberg et al. 1999). Most of the recharge occurs during the non-growing season (winter) when evapotranspiration is minimal and water can accumulate into the root zone and move downward into the water table. The underlying frequency of hydrologic drought (SPEI-24) is subtly increasing in the southwest Kansas at an approximately half-century cycle, which could slowly diminish the ability of the Ogallala aquifer to effectively recharge over in the 21st and 22nd centuries.

Rotation of EOFs, however, did not emphasize this drying in western Kansas by any drought index. The rotation pushed EOF3 very close to zero correlations in southwest Kansas for the PDSI and SPEI-12 as well as SPEI-24, indicating a weaker correlation to RPC3. The wetting signal for hydrologic drought (longer SPEI time steps) was stronger in southeast Kansas than the drying signal in agricultural drought for southwest Kansas.

The rotated leading components with wetting trends were slightly stronger for the SPI than the SPEI at the 24-month time step (see Appendix D). Although the SPI and SPEI are fundamentally similar drought indices, the SPI only includes precipitation as its primary variable while the SPEI additionally includes potential evapotranspiration. An increase in temperature

over time results in an increase in potential evapotranspiration and larger differences between indices (Vicente-Serrano et al. 2010). Although precipitation is the dominant driver of most drought indices (Ward 2013), an increase in monthly average temperature would dampen the effects of an increase in precipitation due to losses from evapotranspiration. This effect is most notable at longer time steps.

The fundamental period of the strongest signal for all types of drought (agricultural, meteorological, and hydrologic) in the leading mode of EOFs is 14 years. Underlying signals oscillated at periods greater than forty years for the second leading mode (PC2) of drought, and one and eight years for meteorological (SPEI-3) and hydrologic drought (SPEI-24), representing higher frequency but lower energy drought fluctuations.

Positive cycles of El Nino are associated with wetting across the state. The second rotated components for all drought indices showed the highest cross-correlation with El Nino in western Kansas. When the eastern equatorial Pacific Ocean warms, wetter conditions generally dominate the Kansas climate with its strongest relationship between 3 and 7months lag (see Figs. 6 and 7) according to EOF1 and REOF2 temporal and spatial patterns. Thus, strong El Nino winters generally correspond to a wet spring and vice versa for La Nina. During La Nina the subtropical jets weaken and move poleward, altering the meridional and vertical propagation of transient eddies and resulting in an anomalous eddy-driven mean meridional (MMC) circulation that causes descent and drying at mid latitudes (Seager et al. 2005). Previous literature showed inconclusive evidence of an ENSO relationship with precipitation and temperature in the high plains (Ropelewski and Halpert 1986), which would include western Kansas. EOF methods are able to demonstrate the multidecadal relationship of drought and ENSO in the state.

5. Conclusion

In this study, decadal drought variability was investigated in Kansas using the instrumental records from 1900-2014. The drought indices used were the PDSI, SPEI, and SPI, and the -3,-6,-12, and -24 month time steps were individually assessed. Empirical Orthogonal Functions (EOFs) techniques and Varimax rotation were applied to the drought datasets. Differences between drought types were relatively small for both unrotated and rotated spatial and temporal patterns. Large-scale synoptic patterns primarily dominate the Kansas drought structures, especially during long-term wet and drought periods in central and eastern Kansas. The first principal components explained approximately 70% of the drought variability across the state and demonstrated a statistically significant wetting trend for the state over the last century, oscillating at a dominant period of about 14 years for all drought indices in this study.

The strongest evidence of drying was shown in the second unrotated principal components for western Kansas especially for long-term hydrologic droughts. This underlying drying signal dampens the dominant wet signals in western Kansas, which might put the Ogallala aquifer at risk of losing its ability to recharge in the long-term in Kansas. An increase in temperature will increase evapotranspiration and exacerbate the water scarcity in western Kansas. The third principal component, which explains less than 10% drought variability, shows increasing intensity of drought and flooding after 1980. Rotation applied to the EOFs emphasized strong wetting patterns in southeast, northeast, and a small subsection of southwest Kansas. The 99°W meridian acted as the dominant transitional line demarcating the areas of Kansas' climate and vegetation (crop, grassland) relationship. The MEI signal as it modulates global and regional climate variabilities provided a potential tool to couple Kansas drought's

leading modes by varying lags of 3 to 7 months depending on the use of drought index and time steps selected.

References

Batisani, N., 2011: Spatio-temporal ephemeral streamflow as influenced by climate variability in Botswana. *Journal of Geographical Sciences*, **21,** 417-428.

Bjornsson, H., and S. A. Venegas, 1997: *A Manual for EOF and SVD Analyses of Climatic Data.*

Bojariu, R., L. F. Velea, R. D. Cica, A. E. Dobrinescu, M. Birsan, and A. Dumitrescu, 2012: Mechanisms of Drought Persistence in Romania in the Climate Change Perspective. *UNIVERSITATEA DIN CRAIOVA*, **17**.

Bonaccorso, B., I. Bordi, A. Cancelliere, G. Rossi, and A. Sutera, 2003: Spatial Variability of Drought: An Analysis of the SPI in Sicily.

Cai, W., Y. Zhang, Q. Chen, and Y. Yao, 2015: Spatial Patterns and Temporal Variability of Drought in Beijing-Tianjin-Hebei Metropolitan Areas in China. *Advances in Meteorology*, **2015,** 1-14.

Cheval, S., A. Busuioc, A. Dumitrescu, and M. V. Birsan, 2014: Spatiotemporal variability of meteorological drought in Romania using the standardized precipitation index (SPI). *Climate Research*, **60,** 235-248.

Cook, E., D. Meko, D. Stahle, and M. Cleavland, 1999: Drought Reconstructions for the Continental United States. *Journal of Climate*, **12,** 1145-1162.

Cook, E. R., R. Seager, M. A. Cane, and D. W. Stahle, 2007: North American drought: reconstructions, causes, and consequences. *Earth-Science Reviews*, **81,** 93-134.

Dai, A., 2011: Characteristics and trends in various forms of the Palmer Drought Severity Index during 1900–2008. *Journal of Geophysical Research*, **116**.

Gallo, K., and E. Wood, 2015: Historical Drought Events of the Great Plains Recorded by Native Americans. *Great Plains Research*, **25,** 151-158.

Hannachi, A., I. T. Jolliffe, and D. B. Stephenson, 2007: Empirical orthogonal functions and related techniques in atmospheric science: A review. *International Journal of Climatology*, **27,** 1119-1152.

Hartmann, D. L., 2014: Matrix Methods for Analysis of Structure in Data Sets.

Hayes, M. J., O. V. Wilhelmi, and C. L. Knutson, 2004: Reducing Drought Risk: Bridging Theory and Practice. *Natural Hazards Review*, **5,** 106-113.

Heim, R. R., 2002: A Review of Twentieth-Century Drought Indices Used in the United States. *Bulletin of the American Meteorological Society*, **83,** 1149-1165.

Kaiser, H. F., 1958: The varimax criterion for analytic rotation in factor analysis. *Psychometrika*, **23,** 187-200.

Layzell, A., 2012: A thousand years of drought and climatic variability in Kansas: Implications for water resources management. *Kansas Geological Survey*.

Logan, K. E., N. A. Brunsell, A. R. Jones, and J. J. Feddema, 2010: Assessing spatiotemporal variability of drought in the U.S. central plains. *Journal of Arid Environments*, **74,** 247-255.

Lorenz, E. N., and M. I. o. T. S. F. Project, 1956: *Empirical Orthogonal Functions and Statistical Weather Prediction.* Massachusetts Institute of Technology, Department of Meteorology.

Martins, D. S., T. Raziei, A. A. Paulo, and L. S. Pereira, 2012: Spatial and temporal variability of precipitation and drought in Portugal. *Natural Hazards and Earth System Science*, **12,** 1493-1501.

Metzger, S., 2013: Kansas Water Plan Update.

North, G., T. Bell, R. Cahalan, and F. Moeng, 1982: Sampling Errors in the Estimation of Empirical Orthgonal Functions.

Preisendorfer, R. W., and C. D. Mobley, 1988: *Principal component analysis in meteorology and oceanography*. Elsevier.

Prism, 2016: PRISM Climate Group. O. S. University, Ed.

Raziei, T., I. Bordi, L. S. Pereira, and A. Sutera, 2010: Space-time variability of hydrological drought and wetness in Iran using NCEP/NCAR and GPCC datasets. *Hydrology and Earth System Sciences*, **14,** 1919-1930.

Richman, M. B., 1986: Rotation of principal components. *Journal of Climatology*, **6,** 293-335.

Ropelewski, C. F., and M. S. Halpert, 1986: North American Precipitation and Temperature Patterns Associated with the El Niño/Southern Oscillation (ENSO). *Monthly Weather Review*, **114,** 2352-2362.

Rosenberg, N., D. Epstein, D. Wang, L. Vail, R. Srinivasan, and J. Arnold, 1999: Possible Impacts of Global Warming on the Hydrology of the Ogallala Aquifer Region. *Climatic Change*, **42,** 677-692.

Seager, R., N. Harnik, W. A. Robinson, Y. Kushnir, M. Ting, H. P. Huang, and J. Velez, 2005: Mechanisms of ENSO-forcing of hemispherically symmetric precipitation variability. *Quarterly Journal of the Royal Meteorological Society*, **131,** 1501-1527.

Soil Survey Staff, 2014: Gridded Soil Survey Geographic (SSURGO) Database for KS, CO, OK, NE, and MO. N. R. C. S. United States Department of Agriculture, Ed.

Solow, A. R., and Coauthors, 1998: The Value of Improved ENSO Prediction to U.S. Agriculture. *Climatic Change*, **39,** 47-60.

Tatli, H., and M. Türkeş, 2011: Empirical Orthogonal Function analysis of the palmer drought indices. *Agricultural and Forest Meteorology*, **151,** 981-991.

Tomanek, G. W., 1995: Prairies of Kansas. *Rangelands*, **17,** 151-153.

Torrence, C., and P. J. Webster, 1998: The annual cycle of persistence in the El Niño/Southern Oscillation. *Quarterly Journal of the Royal Meteorological Society*, **124,** 1985-2004.

Vicente-Serrano, S. M., S. Beguer á, and J. I. L ópez-Moreno, 2010: A Multiscalar Drought Index Sensitive to Global Warming: The Standardized Precipitation Evapotranspiration Index. *Journal of Climate*, **23,** 1696-1718.

Weaver, J. E., and F. W. Albertson, 1936: Effects on the great drought on the prairies of Iowa, Nebraska, and Kansas. *Ecology*, **17,** 567-639.

Wolter, K., and M. S. Timlin, 1998: Measuring the strength of ENSO events: How does 1997/98 rank? *Weather*, **53,** 315-324.

——, 2011: El Niño/Southern Oscillation behaviour since 1871 as diagnosed in an extended multivariate ENSO index (MEI.ext). *International Journal of Climatology*, **31,** 1074-1087.

Woodhouse, C., and J. Overpeck, 1998: 2000 Years of Drought Variability in the Central United States. *Bulletin of the American Meteorological Society*.

Chapter 3 - Seasonal Climate Prediction Downscaled in the U.S. Central Plains

Abstract

Large-scale predictors of surface temperature and precipitation are evaluated from the monthly forecasts in Climate Forecast System version 2.0 (CFSv2) over the states from North Dakota down through central Texas (32.6 - 47.7 ℃N and 92.8 - 104.1 ℃W). By using singular value decomposition (SVD), the CFSv2 monthly forecasts of precipitation and 2-m temperature were statistically downscaled using ensemble mean predictions of reforecasts from 1982-2010. Precipitation skill was considerably less than temperature, and the highest skill occurred during the wintertime for 1-month lead time. Only the central and northern plains had statistically significant correlations between observed and modeled precipitation for 1-month lead time. Beyond a 1-month lead time, prediction skill was regionally and seasonally dependent. For the 3-month lead time, only central plains demonstrated statistically significant mean anomaly correlation. After three-month lead times, the ensemble means of forecasts have shown limited reliable predictions which could make the forecast skill too low to be useful in practice for precipitation. However, temperature forecasts at lead times greater than five months showed some skill in predicting wintertime temperatures.

1. Introduction

Drought results in billions of dollars of agricultural losses in the central United States (Svoboda et al. 2002). Agriculture is highly dependent on climate, and crop yield variability is affected by year-to-year climatic variability with regards to extreme events and changes in historical regional climate (Hoogenboom 2000). Drought warning systems can be utilized to help local, state, and federal governments relocate resources to mitigate impacts (Hayes et al. 2004). Monthly to seasonal climate prediction offers considerable opportunities for decision makers to improve the drought, reservoir, urban power management systems (Anderson et al. 2000; Bracken et al. 2010; Chiew et al. 2000; Hammer et al. 2001). Climate forecasts for the central United States, three to six months ahead of harvest, could enable farmers to take decisions to decrease unwanted impacts and to take advantage of favorable conditions (Cantelaube and Terres 2005). Solow et al. (1998) found that an increase in forecast accuracy based on El Nino Southern Oscillation (ENSO) has substantial value to the United States agriculture through the use of more advanced computer models. Since last decade the seasonal climate forecasts has been developed (Luo and Wood 2006) and dynamical atmosphere-ocean coupled global circulation models (AOGCMs) have been successfully used for seasonal climate prediction (Feddersen and Andersen 2005; Saha et al. 2006). These dynamical AOGCMs are able to predict to some degree the chaotic internal components that have slow variations on time scales from months to seasons (Kim et al. 2012). Unlike pure atmospheric models, which have errors that grow quickly with lead time on the order of days to weeks, coupled models add skills for several months (Song and Mapes 2012).

The Climate Forecast System version 2.0 (CFSv2) was developed as a daily real-time seasonal forecast system by the Environmental Modeling Center at the National Centers for

Environmental Prediction (NCEP) and became operational in March 2011. It is an extension to NCEP's first model, CFSv1, developed in 2004 and has improvements that include but are not limited to: upgraded four-layer soil model, interactive three layer sea-ice model, and improved consistency between the model and initial states produced by the data assimilation system (Saha et al. 2012). On average for a global scale, the CFSv2 increased the predictive skill for month-1 land surface air temperature and precipitation by 37% and 29%, respectively, compared to predictions from CFSv1 (Yuan et al. 2015; Yuan et al. 2013). It is an AOGCM that incorporates several new physical packages for cloud-aerosol-radiation, land surface, ocean and sea ice processes, as well as a new atmosphere-ocean-land data assimilation system (Regonda et al. 2016; Saha et al. 2012).

Saha et al. (2012) discussed the poor global skill for raw precipitation forecasts (1982-2010). This skill for precipitation rate over the Northern Hemispheric land is low for CFSv1, CFSv2, GCM models from National Aeronautics and Space Administration (NASA) and the Geophysical Fluid Dynamics Laboratory (GFDL), climate models at National Center for Atmospheric Research (NCAR), and two International Research Institute climate models with anomaly correlations between 0.04 and 0.12, highlighting consistent poor precipitation predictions from models (Saha et al. 2012). Yuan et al. (2011) found in a separate study that the global mean correlation between the observed and forecast ensemble mean series at a 1-month lead time for four months is 0.27. Only 9% of global grid cells had statistically significant correlation for the month-2 precipitation (a lead time of 2 months) forecast, and most of them were located within the Amazon basin. One drawback of CFSv2 as compared with other models is that it under-predicts the interannual variability of precipitation by about 30% globally (Yuan et al. 2011). During evaluating reforecast skill, one of critical issues is the choice of the observation datasets or

reanalysis datasets as validation datasets, which can contribute to uncertainty in skill prediction due to inconsistencies between them (Kim et al. 2012).

Recent applications of drought prediction using the CFSv2 have met with some success, especially over tropical regions due to higher skills over tropics compared to extra tropics. The CFSv2 successfully identified severe drought using the soil moisture parameter during the 1982/1983 El Nino event in Western Australia up to 7 months lead time using retrospective forecasts due to stronger El Nino's teleconnections (Yuan et al. 2011). However, it had difficulties predicting the 1988 drought across the United States beyond a 1-month lead time (Yuan et al. 2011). Yoon et al. (2012) found that seasonal prediction of the Standardized Precipitation Index (SPIs) over the contiguous United States using multiple statistical downscaling techniques resulted in reasonable skill for month-3 or 4for the SPI-6 and 1- and 2-month lead forecasts for the SPI-3. Beyond these leads, drought prediction became unskillful for all statistical downscale techniques applied. Improvements of downscaled precipitation prediction skill in CFSv2 over CFSv1 were limited to the first lead month due to the improvement in the initial conditions in CFSv2 (Yoon et al. 2012). Mean anomaly correlations greater than 0.1 across the contiguous United States occurred only at a 1-month lead time for four months (Nov, Feb, May, and Aug) (Yoon et al. 2012). Prediction skill for temperature has produced much better results than precipitation at lead times longer than one month (Feddersen and Andersen 2005; Kim et al. 2012).

The ability of CFS to reproduce the local observed climate across the Great Plains is one of the most important indicators of its utility for seasonal prediction applications (Wilson et al., 1987). Due to the coarse grid size in raw CFS forecasts, Feddersen and Andersen (2005) examined that downscaling raw multi-model ensemble mean predictions generally adds more skill for

precipitation than temperature but these precipitation and temperature prediction skills were spatially varied across the contiguous U.S.(Yuan et al. 2015) Therefore, in this study the objectives are to 1) downscale the CFSv2 forecasts for surface temperature (2-m temperature) and precipitation, and 2) to assess surface temperature and precipitation skill across the U.S. Central Plains. In following sections, the data sources used and downscaling techniques as well as forecasting evaluation metrics are described in section 2. The evaluation results of downscaled seasonal precipitation and temperature are presented and cross-validated in section 3. Discussion and conclusions are given in section 4.

2. Data and Methods

2.1 Study Area

The area coverage in this study is bounded by 32.598 - 47.716 ºN and 92.812 - 104.062 ºW, which includes a total of 234 CFSv2 grid points (18 in latitude by 13 in longitude) in a T126 projection (384 × 190 Gaussian, 0.9375 ° × 0.9449 °, roughly about 100 km × 100 km) (Fig. 1). This region encompasses most of the US Great Plains from North Dakota down through North Central Texas and is the highest agriculturally productive region in the United States. The study region was vertically and equally divided into three distinct regions (northern, central, and southern plains) to capture the regional variations and facilitate the regional analysis in AOGCM simulations (Fig. 1).

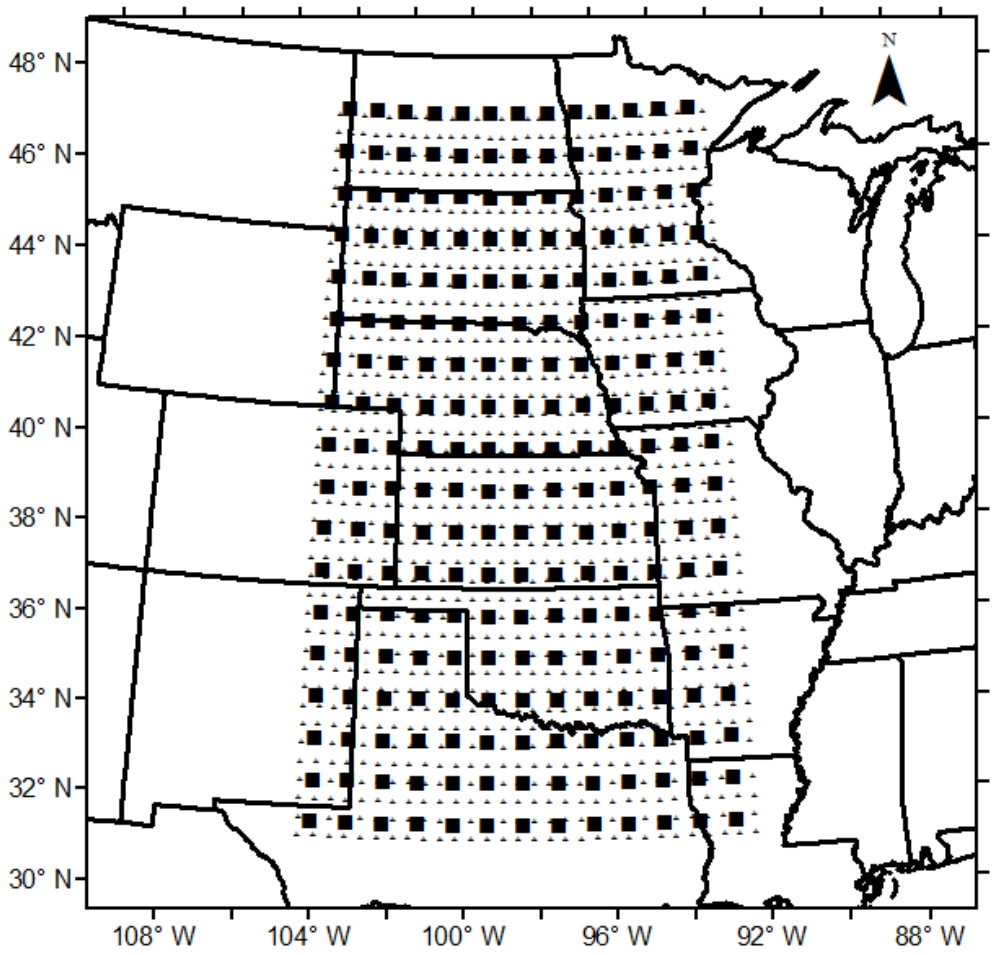

Figure 1. Resolution of CFSv2 (square) and the downscaling grid (triangle) used in this study.

2.2 Forecasted data from NCEP CFSv2

The monthly flux variables pertinent to this study are precipitation rate [kg m^{-2} s^{-1}] and average temperature at 2 meters [K]. Precipitation rate [kg m^{-2} s^{-1} or mm s^{-1}] was converted to obtain inches per month. The retrospective forecasts have initial conditions for the 0, 6, 12, and 18Z cycles for every 5th day, starting January 1 0Z every year for the period 1982-2010 (Fig. 2).

For each model run, there are forecasts for leads from 1 to 9 months. The monthly ensemble mean includes all the members from each month.

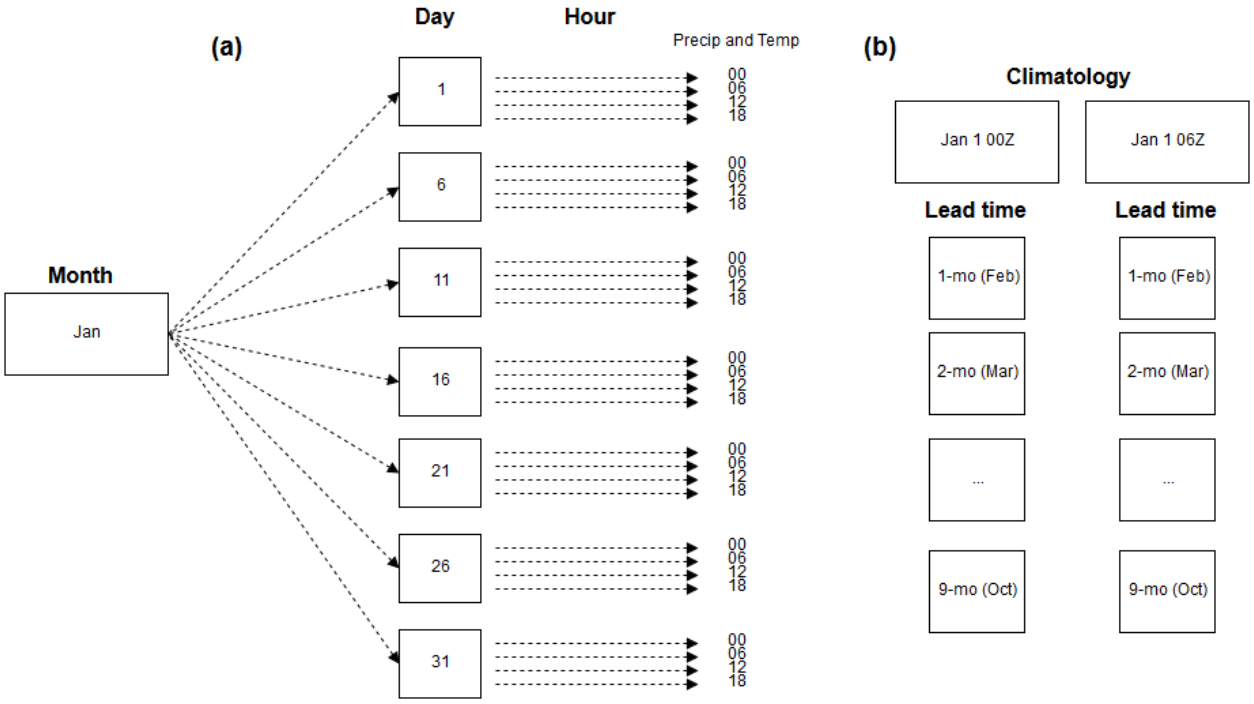

Figure 2. (a) CFSv2 reforecast model run configuration and (b) reforecast climatology configuration.

The initial state conditions for retrospective forecasts were obtained from the NCEP Reanalysis (R2) dataset. Calibration model's climatologies for this reforecast dataset are provided by the National Center of Environmental Information (NCEI) for each forecast lead time (1-9 months). Thus, for each model run at the four six-hourly cycles, there is a corresponding calibration climatology file at one to nine months lead time that must be accessed (Saha et al., 2011) (Fig. 2). For example, there are 1464 (total model runs per year, including leap year runs) calibration climatologies for each lead time (*i.e.*, the first being a climatology of

all January 1st 00Z model runs). CFSv2 anomalies were defined as the departure from the model climatology for the same lead time from the training period (Yoon et al. 2012).

2.3 Observed data from PRISM

Observed precipitation and temperature datasets from the Parameter-elevation Regressions on Independent Slopes Model (Prism 2016) developed at Oregon State University were used as a surrogate for long-term observations for forecast verification and downscaling. Monthly total precipitation (P) and surface average temperature (T) from PRISM (original resolution of 4 km) were aggregated to 40 km resolution for a total of 348 observations (12 months per year and 29 years) at 1200 grid points (Fig. 1).

Monthly precipitation climatology files for 30 year normals (1981-2010) were also obtained from PRISM and re-gridded similarly. Monthly observed precipitation and temperature were transformed into anomalies by subtracting the climatological value from the monthly observation (Maraun et al. 2010; Tian et al. 2014; Yoon et al. 2012). Precipitation from the CFSv2 reforecast files between 1982 and 2010 was evaluated deterministically against the PRISM verification datasets.

2.4 Statistical Downscaling by Singular Value Decomposition (SVD)

A variable that is often predicted on a local scale by dynamic seasonal climate prediction models is precipitation. Statistical downscaling is one methodology for improving predictions by specifying a local field (predictand) from a large scale field (predictor), which is accurately predicted by the dynamic model (Eden and Widmann 2014; Maraun et al. 2010). Statistical downscaling is an important procedure to be conducted before data from GCMs can be

pragmatically applied to regional impact studies across the Great Plains (Yoon et al. 2012). Raw GCM data might lead to erroneous conclusions due to its poor performance (Saha et al., 2012). Downscaling techniques are based on the assumption that atmospheric variability on small spatial scales is conditioned, though not determined, by larger scales in atmospheric general circulation models (Starr 1942; Storch et al. 1995; Wilks 2011). The major theoretical weakness of statistical downscaling is that the basic assumption is not verifiable, i.e., that the statistical relationships developed for the present day climate also hold under the different forcing conditions of possible future climates (Wilby et al. 2004). One generalized technique, Model Output Statistics (MOS), chooses the model field as the training predictor to account for model systematic errors in the predictions (Feddersen and Andersen 2005). MOS techniques apply a correction and a downscaling step and can only be applied to the model for which it was developed. A major drawback of MOS is the need for long series of hindcasts. Most MOS approaches are not designed for corrections in spatial correlations since the predictand inherits much of the spatial correlation structure of the simulated precipitation (Boé et al. 2007; Feddersen and Andersen 2005).

Singular value decomposition (SVD) is an MOS downscaling approach, and it decomposes the cross-covariance matrix between observed (predictand) and reforecast (predictor) precipitation anomalies, which can be used to find coupled regional patterns between the predictand and predictors (Widmann et al. 2003) (Fig. 3). SVD identifies linear transformations of the cross-covariance matrix that concentrate as much of the mean-squared temporal variance into a smaller number of variables (Bretherton et al. 1992). The observed field anomalies are linearly regressed on the leading SVD modes derived from the ensemble mean of the model predictions (Fig. 3). The choice for the predictor region should not only include the

corresponding observations but also be large enough to resolve relevant large scale patterns. The purpose of SVD is to capture the spatial correlation structure of the predictor (forecasted) and predictand (observed).

The predictor (X) and predictand (Y) are both standardized by removing grid point means and dividing by their standard deviations for a specific month and a specific lead time (for example, all Januaries; a lead of 1 month). The two original data matrices (e.g., temperature fields from observation and modeling over 29 years at a different domain) are permuted and reshaped into a matrix for X (29x234) and Y (29x1200). The SVD is performed on the cross-covariance matrix (C),

$$C=X'Y \tag{1}$$

$$[U, L, V] = SVD(C) \tag{2}$$

where U are the patterns (eigenvectors) associated with X (left field), V are the patterns associated with Y (right field), and L are the eigenvalues used to explain the variance of each mode.

The time series or expansion coefficients are given by the projection of the standardized fields on their respective patterns,

$$A_m=X\cdot U \text{ (29 x 234)} \tag{3}$$

$$B_m=Y\cdot V \text{ (29 x 1200)} \tag{4}$$

Because U and V are singular vectors of the cross-covariance matrix of X and Y, the covariance between A_1 and B_1 to A_m and B_m are maximized under the condition that each mode is orthogonal to the mode proceeding it.

Multiple regression is performed on the leading modes ($x = A_1, A_2, \ldots A_m$) and the observed anomalies (Y) at each downscaled grid point.

$$\hat{Y} = \beta_0 + \beta_1 A_1 + \beta_2 A_2 + \beta_3 A_3 \ldots \beta_m A_m \quad (5)$$

The beta coefficients for each associated mode are calculated to minimize the expected root-mean-square difference between modeled $\hat{Y}$ and observed Y. North's rule of thumb was used to determine which leading modes (A_m) were significant (North et al. 1982). These significant modes were the modes included in equation (5). Cross-validation was conducted by dividing the reforecast period 1982 to 2010 into training and validation sets. The training period was 28 years and one year, a validation set, was withheld from the predictor dataset, and a prediction is made for the withheld year. For example, SVD procedures are applied to a training dataset of predictors and predictands, and the observed field is linearly regressed on the leading SVD modes. Then the leading modes are projected onto the validation year, and the regression equation (5) is used to produce a prediction. This is repeated for every year resulting in 29 years predictions (Feddersen and Andersen 2005). Leave-one-out cross-validation procedures are sufficient given that over the United States precipitation lag correlation is non-significant at 1-month lag (Yoon et al. 2012). Feddersen and Andersen (2005) found statistically significant mean precipitation anomaly correlations (0.23) for the contiguous United States only during the January, February, and March season at a 2-month lead time for a multi-model ensemble (Meteo-France, ECMWF, UK Office) using the SVD methodology.

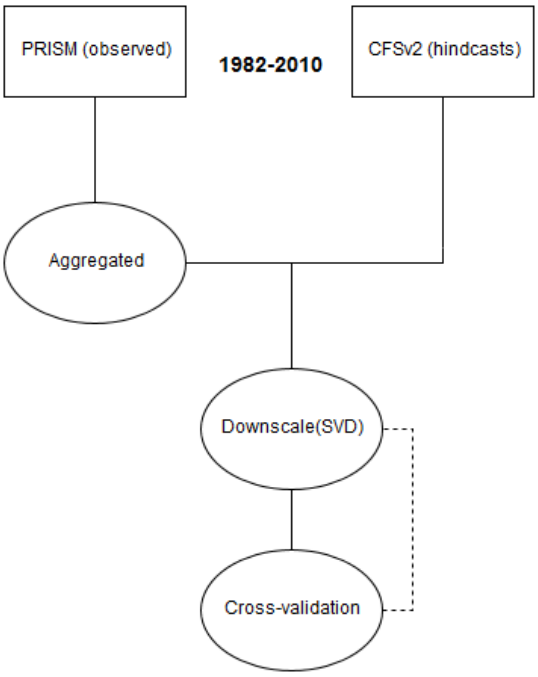

Figure 3. Flow chart outlining the downscale procedures used in this study. Dashed line represents repeated cycles.

2.5 Forecast Skill

Three measures of forecast skill were used in this study: anomaly correlation, root-mean-square error (RMSE), and skill score. Anomaly correlation is the correlation between the observed anomaly and the downscaled anomaly. The anomaly correlation depends on the climatology used and is not sensitive to the magnitude of the hindcast anomalies; thus, higher correlated anomalies could potentially have larger errors. Given that there are 29 years (*N*) or 27 degrees of freedom (N-2), correlations have to be greater than 0.367 at the 95% confidence level (Yoon et al. 2012). The skill score (SS) was defined as

$$SS=1-\frac{MSE_{forecast}}{MSE_{climatology}} \quad (6)$$

Equation (6) was used to assess if forecast error ($MSE_{forecast}$) is smaller or larger than the error predicted by climatology ($MSE_{climatology}$) (Wilks 2006). Positive SS values indicate that the

model predicts better than climatology, which suggests the forecasts add valuable information to users. Climatology anomalies in this study are zeros for temperature and precipitation.

3. Results

3.1 Precipitation

The statistical downscaling procedure was applied to model hindcasts for the entire study area. Figure 4 shows the cross-validated anomaly correlation for precipitation of 1-month lead for all calendar months. Each plot is for the month when the forecasts were initialized, e.g., the January plot is the forecast for February. The predictive skill varied both spatially and temporally. The highest geographically uniform anomaly correlations occur for forecasts initialized in June for July. Seasonally, cross-validated anomaly correlations through time for December, January, and February (DFJ) and June, July, and August (JJA) lead-one forecasts are shown in Figure 5. Both seasons showed large variability. During the summer the dominant amount of rainfall occurs from convective processes over the central United States. These mesoscale processes are difficult to be modeled accurately (Yoon et al. 2012). At longer lead times, high positive anomaly correlations were found in fewer months and isolated to particular regions. For example, at a lead time of 3 months, only September forecasts for December in western Kansas, the Oklahoma panhandle, and eastern Colorado are robust with a mean skill score 0.23, respectively (not shown). Regionally, the entire study area had statistically significant correlations between observed and modeled precipitation anomalies at a lead time of one month (Table 1). As the lead time increased, the correlations became less significant as expected. However, for three- and four-month lead times, the mean anomaly correlations were statistically significant in the central plains and southern plains, respectively (Table 1).

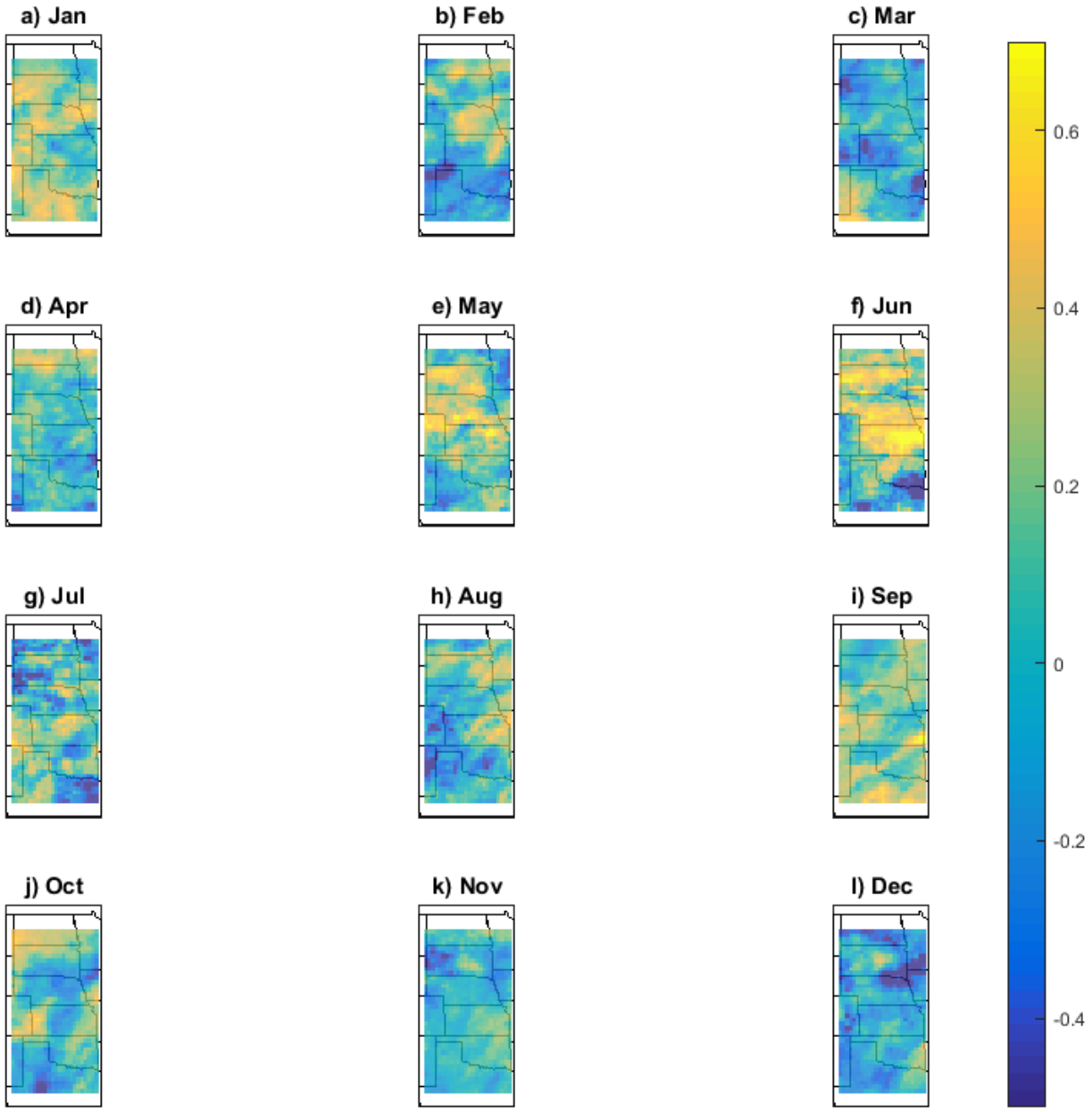

Figure 4. Cross-validated precipitation anomaly correlations 1-month lead across the study area for Jan-Dec (a-l).

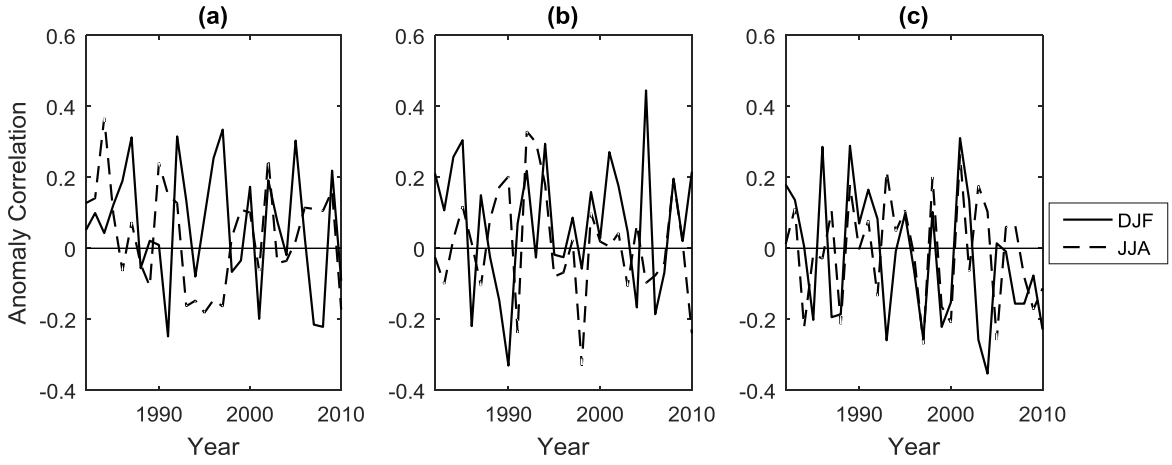

Figure 5. Cross-validated mean anomaly correlation for precipitation predictions for north (a), central (b), and southern (c) plains in DJF (-) and JJA (--) between 1982 and 2010. Lead time is one month.

November initialized forecasts for month-4 lead times are promising for the southern plains (Fig. 6 and Table 1). Spring precipitation anomalies can be reasonably forecasted during by early fall. June forecasts for western Kansas in the central plains are also skillful. Early fall is an important time for farmers in these regions who begin to sow winter crops such as red winter wheat, one of the most lucrative crops in the United States. The results for precipitation forecasts with lead times greater than six months are qualitatively more difficult to describe with some skill occurring in isolated locations throughout the study area.

Table 1. Mean precipitation anomaly correlations for northern, central, and southern plains by lead time (*, **, * significant at the 0.01, 0.05, and 0.10 levels, respectively).**

	1-month lead	2-month lead	3-month lead	4-month lead
North	0.14***	0.09*	-0.06	-0.01
Central	0.24***	0.01	0.09*	0.07
South	0.10*	0.01	-0.02	0.13***

The mean anomaly correlation for the northern, central, and southern Plains for June initialized forecasts was 0.25, 0.38, and -0.09, respectively (Fig. 6). January forecasts for the northern and southern plains were also high ($r > 0.2$) (Figs. 4 and 6). There were grid points that had statistically significant correlations ($r > 0.37$) in all months, and the lowest percentage of statistically significant correlations occurred in the central Plains in November (5.1%). It is important to note that there were statistically significant negative correlations, indicating that climate behaved in direct contrast to CFSv2 forecasts, which is not ideal because this is not a systematic feature of forecasts (Yoon et al. 2012).

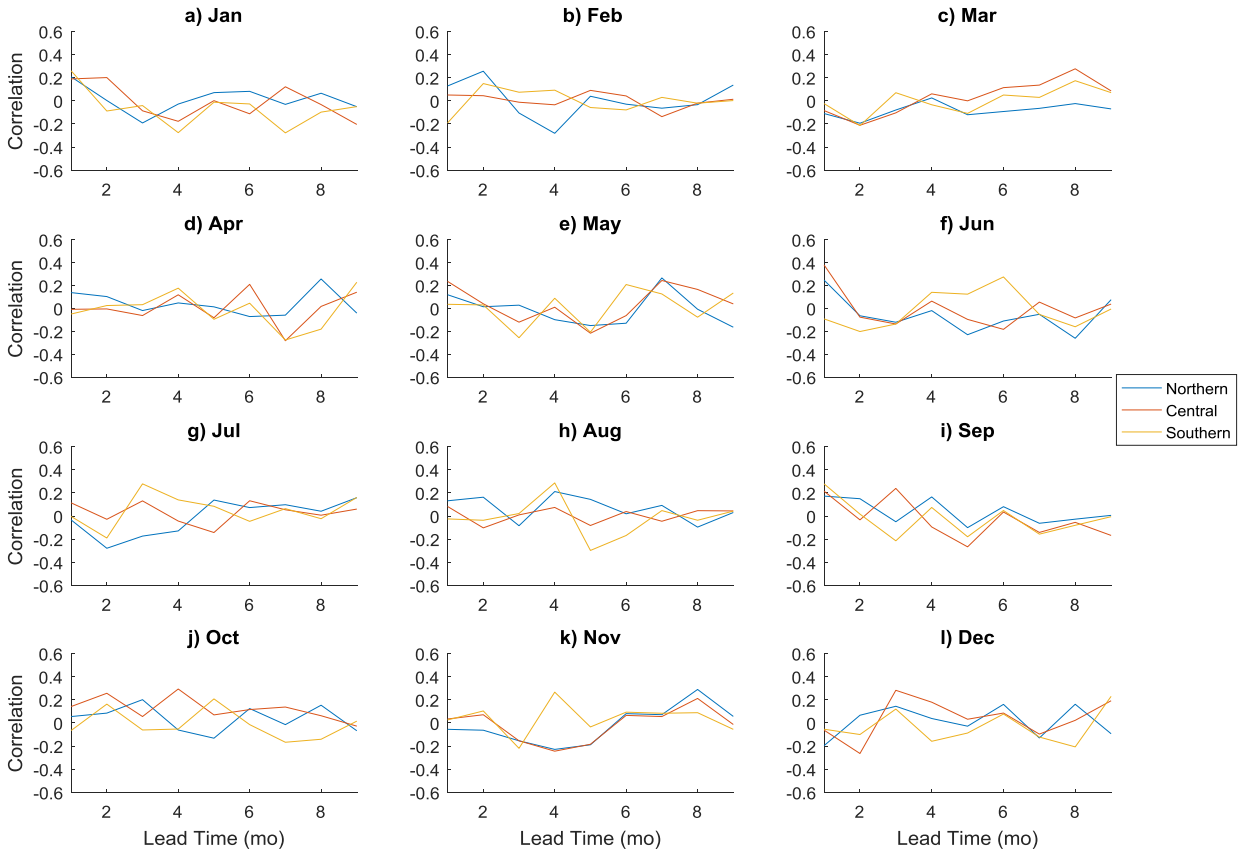

Figure 6. Precipitation anomaly correlations by lead time for Jan-Dec (a-l). Each line represents one of three regions in the study area.

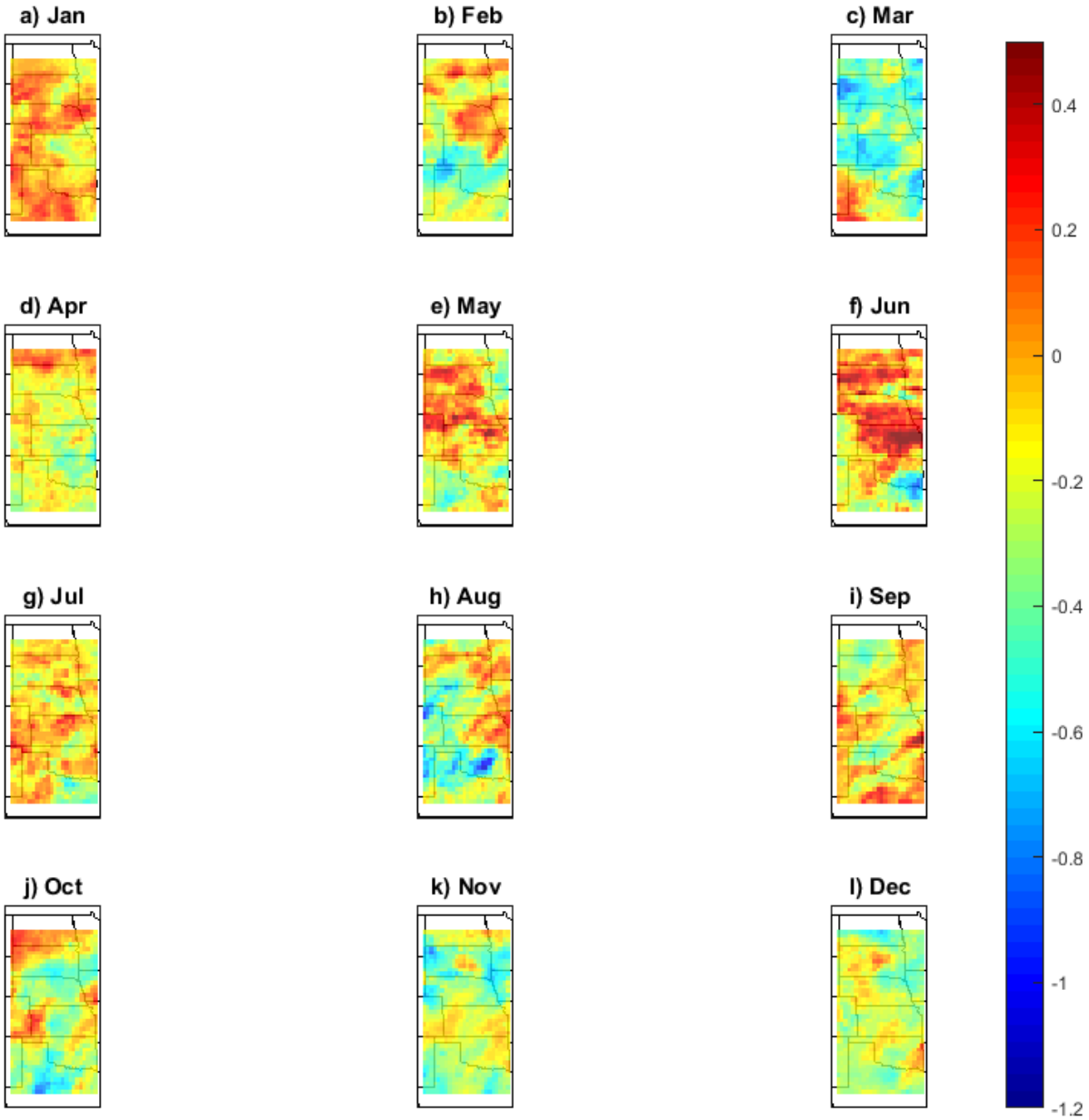

Figure 7. Skill scores for 1-month lead precipitation anomalies.

The utility of these forecasts for practical application can be tested using the skill score, which assesses whether the CFSv2 prediction is more robust than predicting climatology based on the mean square error between observed and forecast variables. The spatial patterns of lead 1-

month skill score closely resemble the patterns of the anomaly correlations (Fig. 7). Thirty-one percent of all grid points in the study area have positive skill score in January, 44% in June, 30 % in September, and the remaining had less than 25%.

3.2 Two-Meter Temperature

Predictive skill for 2-m air temperature was much higher than surface precipitation at both short and long lead times. The months with the highest mean anomaly correlations at a 1-month lead time across the entire region were August (0.46), January (0.41), and October (0.41) (Fig. 8). The worst predictive months were December, June, September with mean anomaly correlations of -0.08, 0.001, and 0.03, respectively (Fig. 8). Eighty-two percent of grid points in August had positive skill score, and nine months had over 35% of downscaled grid points with positive skill score (Figs. 8 and 11). Mean monthly anomaly time series for a 1-month lead time were statistically correlated for all three regions at 99% confidence levels (Table 2). Only the northern plains at the 2-month lead time had a statistically significant correlation between observed and modeled temperature anomalies (Table 2). For the 3-month lead time, every region in the study area had statistically significant positive correlations, followed directly by statistically negative correlations at a 4-month lead time, which is not ideal behavior for CFSv2 temperature forecasts (Yoon et al. 2012) (Table 2).

The 1-month seasonal winter (DJF) temperature skill showed higher variability between positive and negative correlations through time than summer (JJA) temperature skill, particularly for the central and southern plains (Fig. 9). The southern plains winter forecasts displayed both the highest and lowest mean anomaly correlations through time across the study area, occurring in 2003 and 2005, respectively (Fig. 9). The average anomaly correlation for July forecasts at 2-month lead time in the northern Plains was 0.33 (Fig. 10). April 3-month lead time forecast skill

was greater than April 1- or 2- month lead time prediction skill, demonstrating a mean anomaly correlation of 0.53 as compared to 0.31 and -0.18 for 1- and 2- month lead times, respectively. At a 4-month lead time, July showed the highest skill among all months for the northern plains (Fig. 10).

The northern plains had the highest overall skill through time during the winter and summer. Higher summertime prediction reliability is favorable for management systems sensitive to heat stress and extreme temperature. August in particular showed high skill across the entire region; however, skill was isolated towards the central and northern plains in June and July (Fig. 11).By a lead of two months, skillful forecasts were limited to one or two months out of the year. July forecasts for September in Nebraska and South Dakota had modest predictive skills (not shown).

At longer lead times, forecast skill generally degraded (Fig. 10). However, forecasts initialized in the springtime for winter exhibited moderate to strong skill. For example, June 6-month lead time predictions for December had statistically significant skill for the central and northern plains (Fig. 10). The mean anomaly correlation for June 6-mo lead time predictions in the northern, central, and southern plains were 0.54, 0.45, and 0.33, respectively. The correlation for the northern plains is only slightly less than the highest correlation in the entire study, which was the 1-month lead time correlation in January (0.57) (Fig. 10). In addition, May initialized forecasts for 7- and 8- month lead times demonstrated high anomaly correlations ($r > 0.35$) exclusively for the northern and central plains (Fig. 10). These long-term predictions of seasonal wintertime temperatures can be utilized by agricultural, municipal, and energy sectors for many applications, including but not limited to food production, early freeze detection, and energy consumption. By a lead time of nine months, April, May, and June initialized forecasts displayed

mean anomaly correlations between 0.25 and 0.30 (averaged across the study area) with 43% of downscaled grid points in April demonstrating skill better than climatology (not shown). Southern plains forecast skill at a 9-month lead time was higher than the other regions, excluding June which showed the largest skill ($r > 0.50$) in southwest North Dakota (not shown). November temperature forecast skill in the southern plains was also unusually high ($\bar{r} = 0.32$) with a bulls-eye of anomaly correlations greater than 0.50 in north central Texas (not shown). While wintertime temperatures can be predicted with some skill at lead times greater than six months (depending on the lead time and month chosen), summer temperature predictions displayed consistently reliable skill at lead times of three months or less.

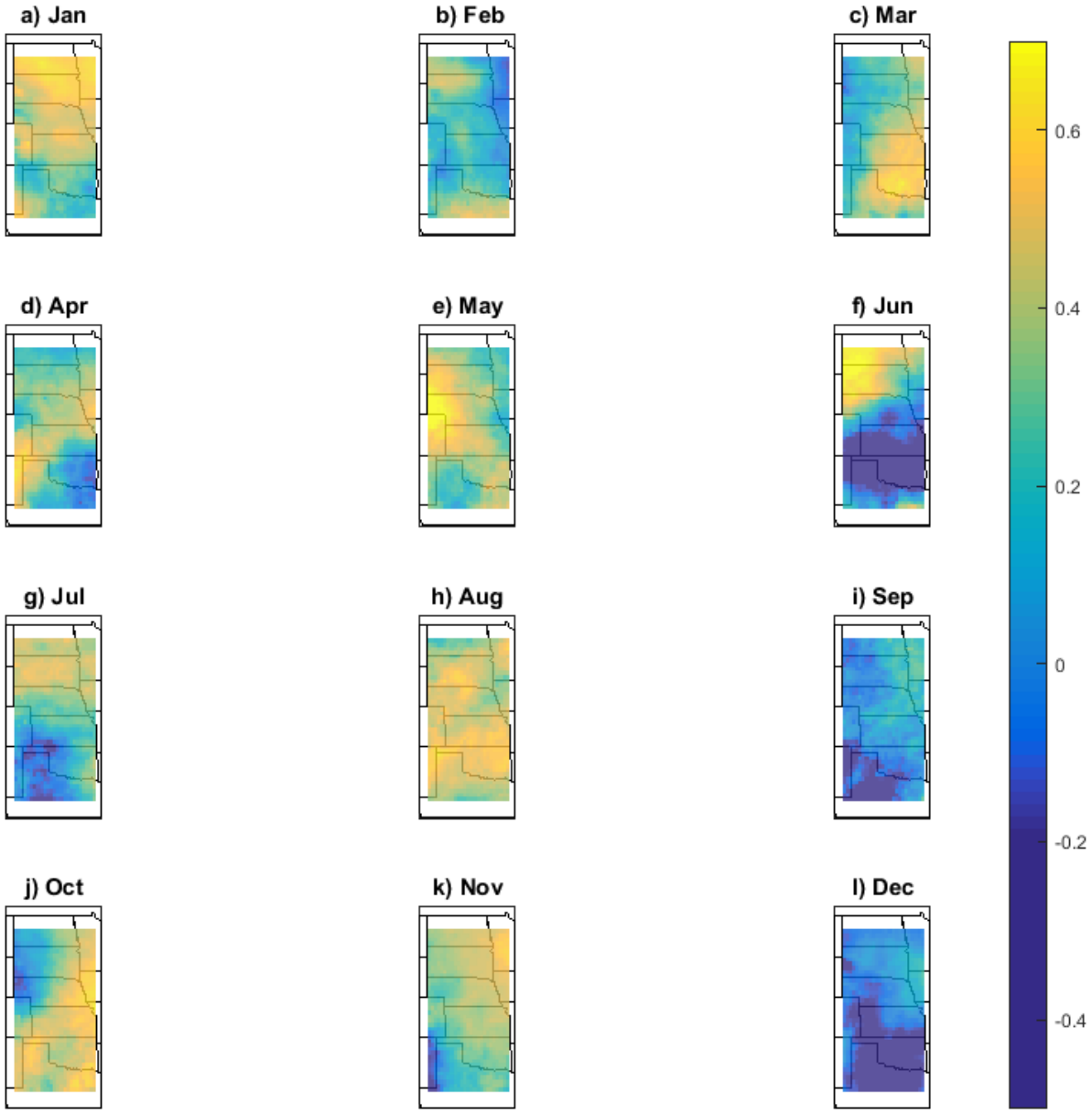

Figure 8. Two-meter temperature anomaly correlations Jan-Dec (a-l) for a lead time of one month.

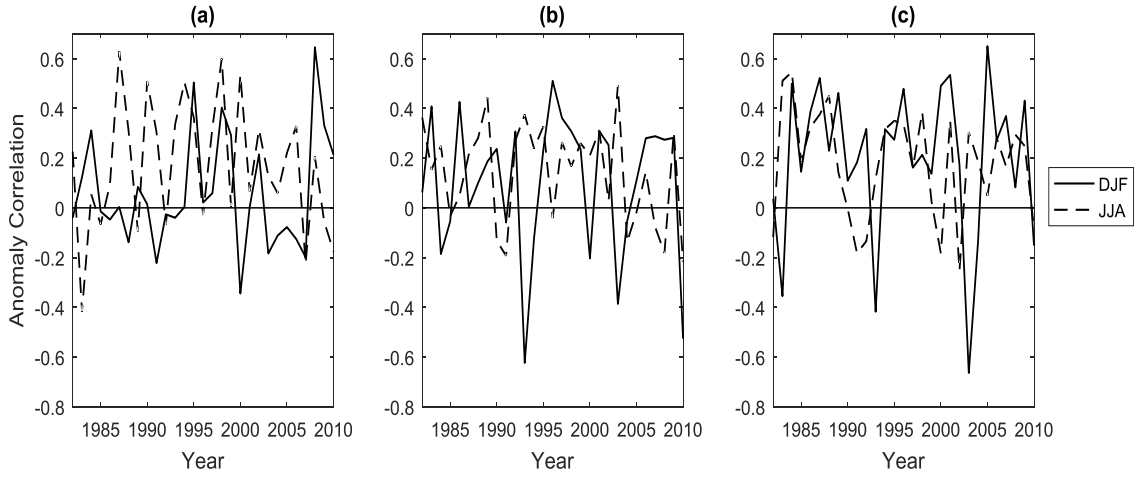

Figure 9. Cross-validated mean anomaly correlation between observed and predicted temperatures for north (a), central (b), and southern (c) plains in DJF(-) and JJA (--) between 1982-2010. Lead time is one month.

Table 2. Mean temperature anomaly correlations for northern, central, and southern plains by lead time (*, **, * significant at the 0.01, 0.05, and 0.10 levels, respectively).**

	1-month lead	2-month lead	3-month lead	4-month lead
North	0.34***	0.13**	0.16***	-0.09*
Central	0.28***	0.04	0.11*	-0.09*
South	0.19***	-0.04	0.13**	0.02

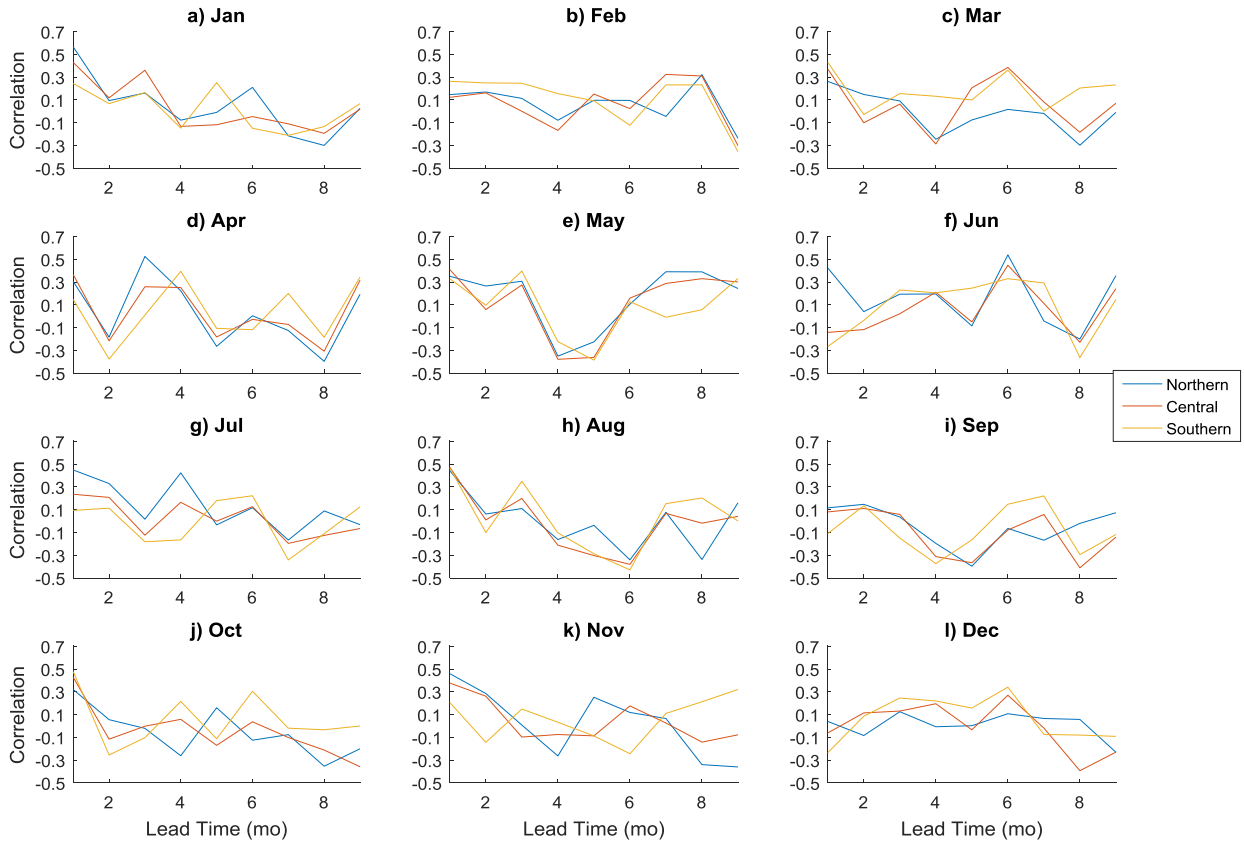

Figure 10. Two-meter temperature anomaly correlations by lead time for Jan-Dec (a-l). Each line represents one of three regions in the study area.

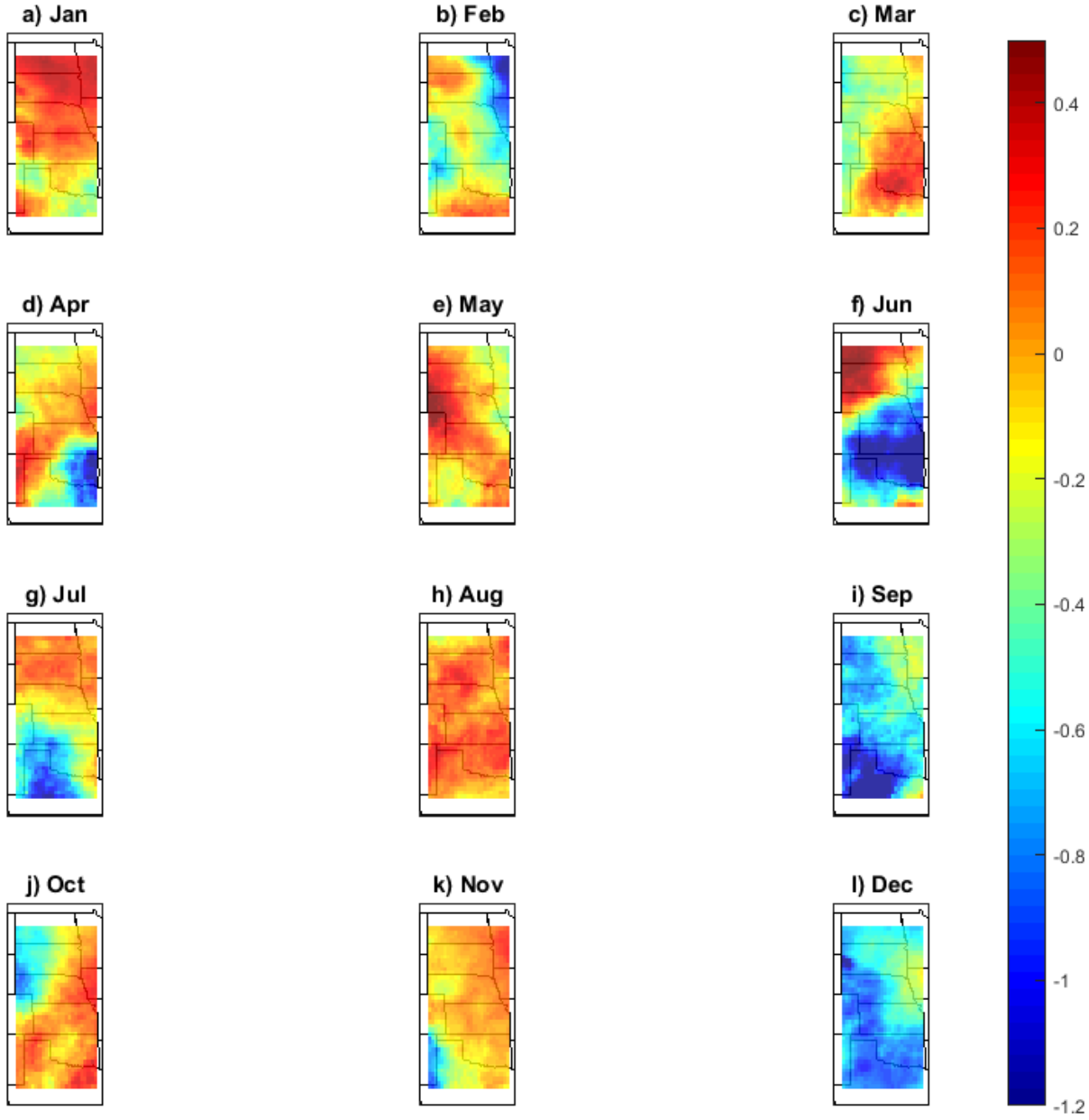

Figure 11. Skill scores for 1-month lead temperature anomalies.

4. Conclusions

CFSv2 monthly forecasts of precipitation and 2-m temperature have been statistically downscaled using ensemble mean predictions and reforecasts between 1982 and 2010. The

motivation of this work was to utilize climatic variables for drought and flooding applications in the central plains of the United States, a highly productive agricultural region.

The results indicated that overall from 1982 to 2010 the downscaled predictions of precipitation and temperature were more skillful in month-1 and some of month-2. Temperature prediction skill was better than precipitation at both short and long lead times. Only month-1 predictions for both precipitation and temperatures showed statistically significant correlations for northern, central, and southern plains. As the lead time increased, the predictions became unskillful especially for southern plains. For example, seasonal predictions showed some skill for specific months for specific locations but not statistically significant for all month-3 forecasts. Regionally, the northern plains had better prediction scores than southern plains for both precipitation and temperature. Central plains' prediction performance was better than southern plains, which is critical for agricultural producers in Kansas, Nebraska, and northern Oklahoma. After three-month lead times, the ensemble mean of forecasts showed limited reliable predictions, which could make forecast skill too low to be useful in practice. Although efforts have been made in realistically initializing land surface conditions and hydrological ensemble predictions, further improvements in CFSv2 need to be completed to be useful for long term forecasting applications in the central United States.

Operational seasonal precipitation and temperature forecasts using the downscaling procedures can be provided to farmers and decision makers for a variety of applications. Masks for each month and lead time can be applied to operational forecasts to only show forecasts for grids that had statistically significant positive anomaly correlations during the training period. Each month and lead time will differ on the forecast coverage for the study area. Thus, some lead times and months will have more utility than others, which should be effectively communicated

to those who wish to use CFsv2 downscaled forecasts.

References

Anderson, L. M., D. M. Mierzwa, and L. M. Kavvas, 2000: Probabilistic seasonal forecasts of droughts with a simplified coupled hydrologic-atmospheric model for water resources planning. *Stochastic Environmental Research and Risk Assessment*, **14,** 263-274.

Boé, J., L. Terray, F. Habets, and E. Martin, 2007: Statistical and dynamical downscaling of the Seine basin climate for hydro-meteorological studies. *International Journal of Climatology*, **27,** 1643-1655.

Bracken, C., B. Rajagopalan, and J. Prairie, 2010: A multisite seasonal ensemble streamflow forecasting technique. *Water Resources Research*, **46,** n/a-n/a.

Bretherton, C. S., C. Smith, and J. M. Wallace, 1992: An Intercomparison of Methods for Finding Coupled Patterns in Climate Data. *Journal of Climate*, **5,** 541-560.

Cantelaube, P., and J.-M. Terres, 2005: Seasonal weather forecasts for crop yield modelling in Europe. *Tellus A*, **57,** 476-487.

Chiew, F., T. McMahon, S.-L. Zhou, and T. Piechota, 2000: Streamflow Variability, Seasonal Forecasting and Water Resources Systems. *Applications of Seasonal Climate Forecasting in Agricultural and Natural Ecosystems*, G. L. Hammer, N. Nicholls, and C. Mitchell, Eds., Springer Netherlands, 409-428.

Eden, J. M., and M. Widmann, 2014: Downscaling of GCM-Simulated Precipitation Using Model Output Statistics. *Journal of Climate*, **27,** 312-324.

Feddersen, H., and U. Andersen, 2005: A method for statistical downscaling of seasonal ensemble predictions. *Tellus A*, **57,** 398-408.

Hammer, G. L., J. W. Hansen, J. G. Phillips, J. W. Mjelde, H. Hill, A. Love, and A. Potgieter, 2001: Advances in application of climate prediction in agriculture. *Agricultural Systems*, **70,** 515-553.

Hayes, M. J., O. V. Wilhelmi, and C. L. Knutson, 2004: Reducing Drought Risk: Bridging Theory and Practice. *Natural Hazards Review*, **5,** 106-113.

Hoogenboom, G., 2000: Contribution of agrometeorology to the simulation of crop production and its applications. *Agricultural and Forest Meteorology*, **103,** 137-157.

Kim, H.-M., P. J. Webster, and J. A. Curry, 2012: Seasonal prediction skill of ECMWF System 4 and NCEP CFSv2 retrospective forecast for the Northern Hemisphere Winter. *Climate Dynamics*, **39,** 2957-2973.

Luo, L., and E. F. Wood, 2006: Assessing the idealized predictability of precipitation and temperature in the NCEP Climate Forecast System. *Geophysical Research Letters*, **33,** n/a-n/a.

Maraun, D., and Coauthors, 2010: Precipitation downscaling under climate change: Recent developments to bridge the gap between dynamical models and the end user. *Reviews of Geophysics*, **48**.

North, G., T. Bell, R. Cahalan, and F. Moeng, 1982: Sampling Errors in the Estimation of Empirical Orthgonal Functions.

Prism, 2016: PRISM Climate Group. O. S. University, Ed.

Regonda, S. K., B. F. Zaitchik, H. S. Badr, and M. Rodell, 2016: Using climate regionalization to understand Climate Forecast System Version 2 (CFSv2) precipitation performance for the Conterminous United States (CONUS). *Geophysical Research Letters*, **43,** 6485-6492.

Saha, S., and Coauthors, 2006: The NCEP Climate Forecast System. *Journal of Climate*, **19,** 3483-3517.

Saha, S., and Coauthors, 2012: NCEP Climate Forecast System Version 2 (CFSv2) Monthly Products. Research Data Archive at the National Center for Atmospheric Research, Computational and Information Systems Laboratory.

Solow, A. R., and Coauthors, 1998: The Value of Improved ENSO Prediction to U.S. Agriculture. *Climatic Change*, **39,** 47-60.

Song, S., and B. Mapes, 2012: Interpretations of systematic errors in the NCEP Climate Forecast System at lead times of 2, 4, 8, ..., 256 days. *Journal of Advances in Modeling Earth Systems*, **4,** n/a-n/a.

Starr, V. P., 1942: *Basic Principles of Weather Forecasting.* Harper & Brothers.

Storch, H. v., G. Bürger, R. Schnur, and J.-S. v. Storch, 1995: Principal Oscillation Patterns: A Review. *Journal of Climate*, **8,** 377-400.

Svoboda, M., and Coauthors, 2002: The Drought Monitor. *Bulletin of the American Meteorological Society*, **83,** 1181-1190.

Tian, D., C. J. Martinez, W. D. Graham, and S. Hwang, 2014: Statistical Downscaling Multimodel Forecasts for Seasonal Precipitation and Surface Temperature over the Southeastern United States. *Journal of Climate*, **27,** 8384-8411.

Widmann, M., C. S. Bretherton, and E. P. S. Jr., 2003: Statistical Precipitation Downscaling over the Northwestern United States Using Numerically Simulated Precipitation as a Predictor. *Journal of Climate*, **16,** 799-816.

Wilby, R. L., S. P. Charles, E. Zorita, B. Timbal, P. Whetton, and L. O. Mearns, 2004: Guidelines for use of climate scenarios developed from statistical downscaling methods.

Wilks, D. S., 2006: *Statistical Methods in the Atmospheric Sciences.* Academic Press.

——, 2011: *Statistical Methods in the Atmospheric Sciences.* Academic Press.

Yoon, J.-H., K. Mo, and E. F. Wood, 2012: Dynamic-Model-Based Seasonal Prediction of Meteorological Drought over the Contiguous United States. *Journal of Hydrometeorology*, **13,** 463-482.

Yuan, X., E. F. Wood, and Z. Ma, 2015: A review on climate-model-based seasonal hydrologic forecasting: physical understanding and system development. *Wiley Interdisciplinary Reviews: Water*, **2,** 523-536.

Yuan, X., E. F. Wood, L. Luo, and M. Pan, 2011: A first look at Climate Forecast System version 2 (CFSv2) for hydrological seasonal prediction. *Geophysical Research Letters*, **38**.

Yuan, X., E. F. Wood, J. K. Roundy, and M. Pan, 2013: CFSv2-Based Seasonal Hydroclimatic Forecasts over the Conterminous United States. *Journal of Climate*, **26,** 4828-4847.

Appendices

Appendix A - Available Water Capacity in Kansas Soils

Strong associations between total available water capacity (AWC) and mild, moderate, and severe drought frequency were present in the original Kansas data (Fig. A1). Increasing water capacities resulted in lower mild, moderate, and severe drought frequencies. PDSI was recalculated for a manually set range of AWCs (76 to 305 mm) for each station to assess changes in drought characteristics. Total drought frequency decreased and stabilized after 150 mm of AWC for stations in western Kansas (Fig. A2). Total drought frequency in western Kansas by using AWC from 76 and 150 mm is 15-20% higher in western Kansas than eastern Kansas, which does not get above 45% for any station (not shown). When AWC was increased, the peak drought index decreased for stations in eastern and central Kansas but increased for stations in western Kansas. For most of the state, extreme relative frequency of drought increases with higher AWC with changes most notable when the available water is higher than 150 mm. However, stations in far western Kansas (Saint Francis, Lakin, and Liberal) saw a peak in extreme drought relative frequency at 76 mm and a minimum at approximately 150 mm of water (Fig. A3). The farther east stations are in western KS (Norton or Ashland), the more steadily the extreme drought relative frequency rises until AWC reaches 150 mm when it begins to resemble the rest of the state (Fig. A4). Areas at the largest risk of severe and extreme drought based on low available water capacity (less than 150 mm) are dominantly in southwest Kansas near the Arkansas and Cimarron Rivers (Fig. A5).

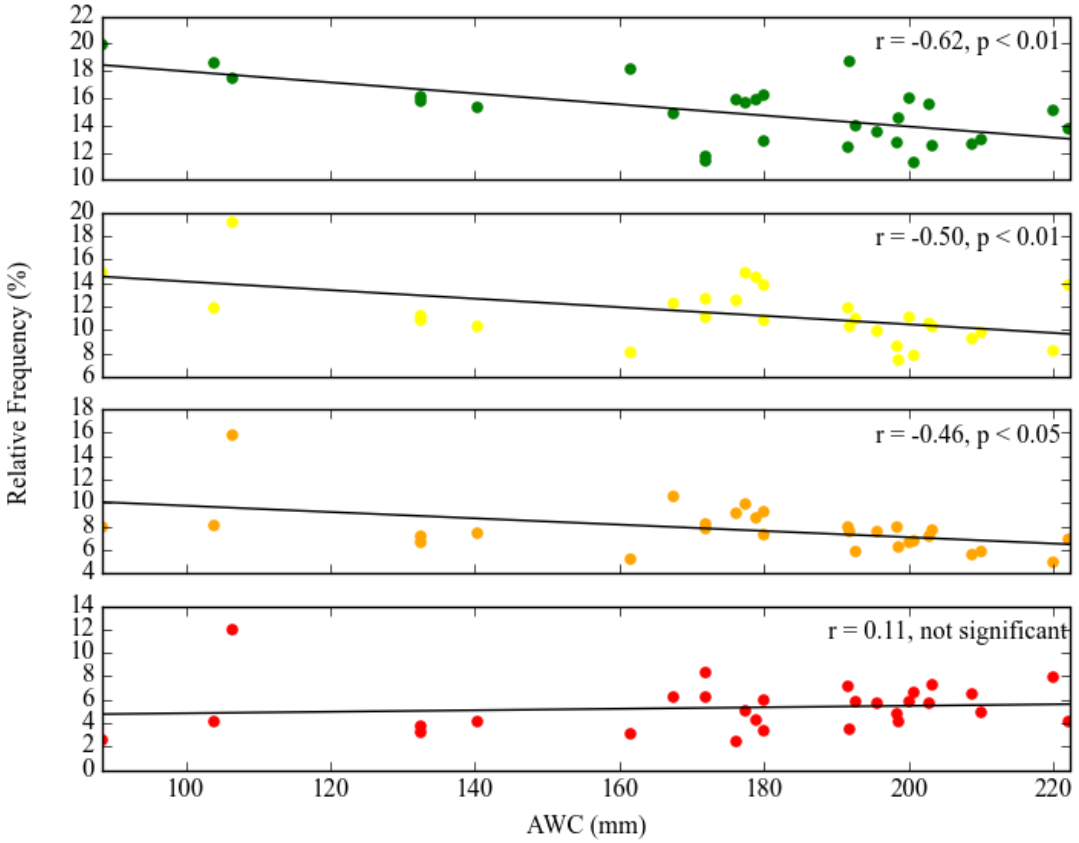

Figure A1 PDSI relative frequencies of mild, moderate, severe, and extreme drought (top to bottom) for all stations and their available water capacity.

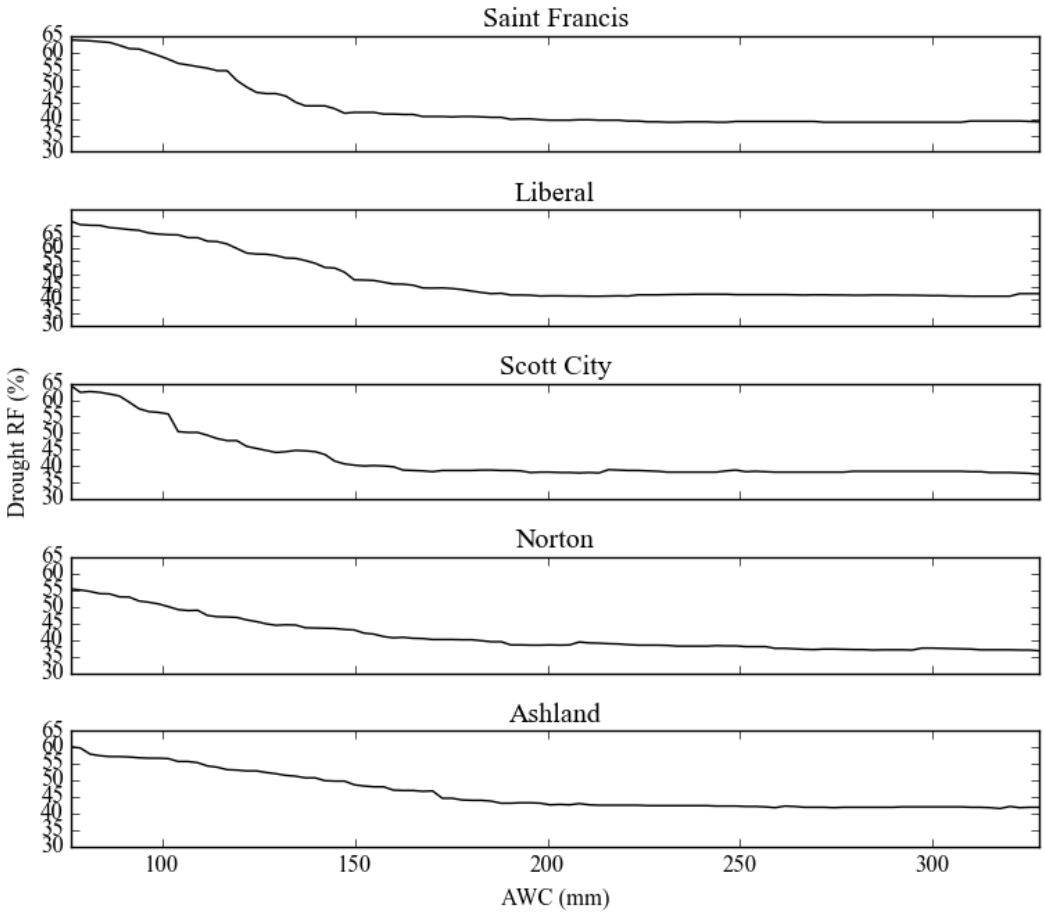

Figure A2. Relationship between total drought relative frequency (RF) (PDSI) and available water capacity (AWC) in western Kansas.

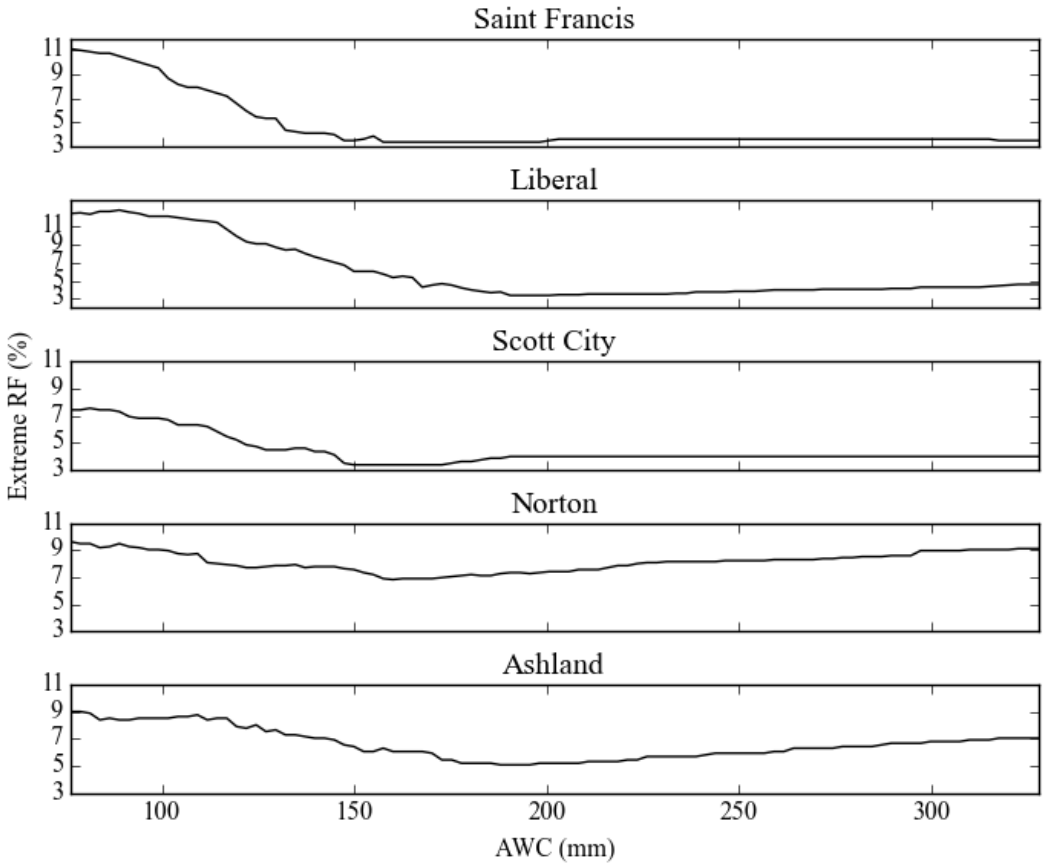

Figure A3. The same as Figure B2 except for extreme drought relative frequency.

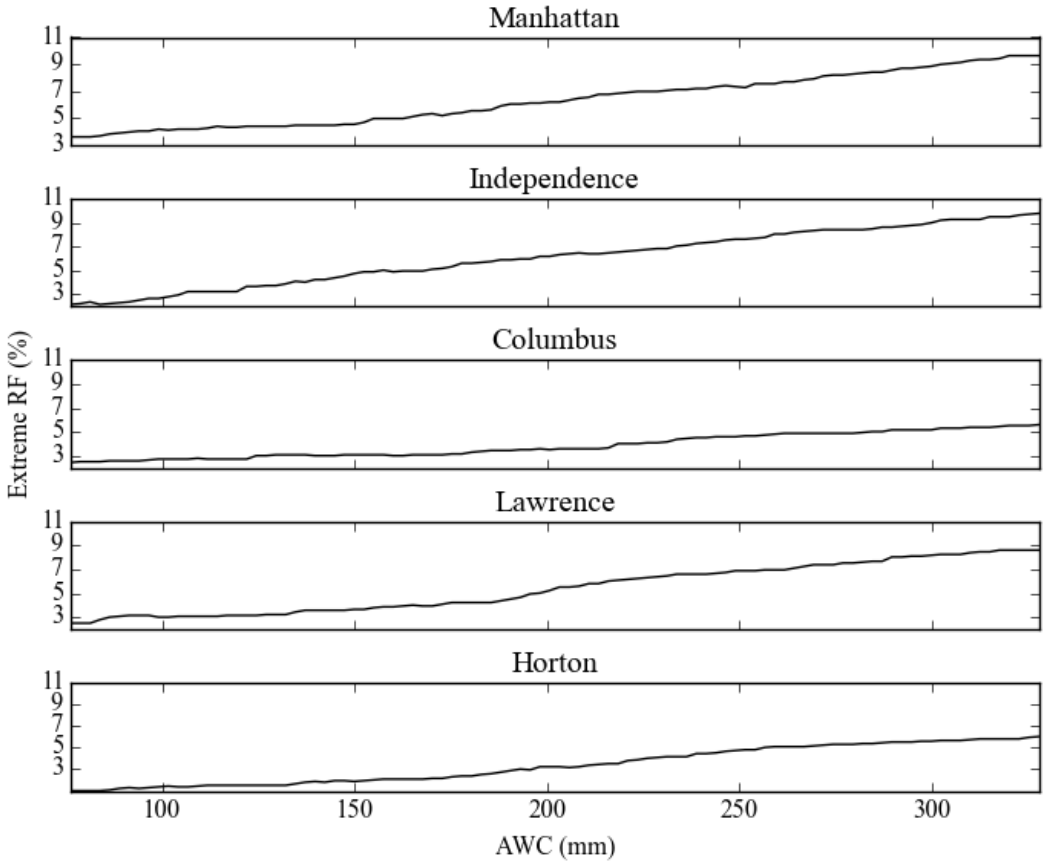

Figure A4. Relationship between extreme drought relative frequency (RF) (PDSI) and available water capacity (AWC) for selected stations in eastern Kansas.

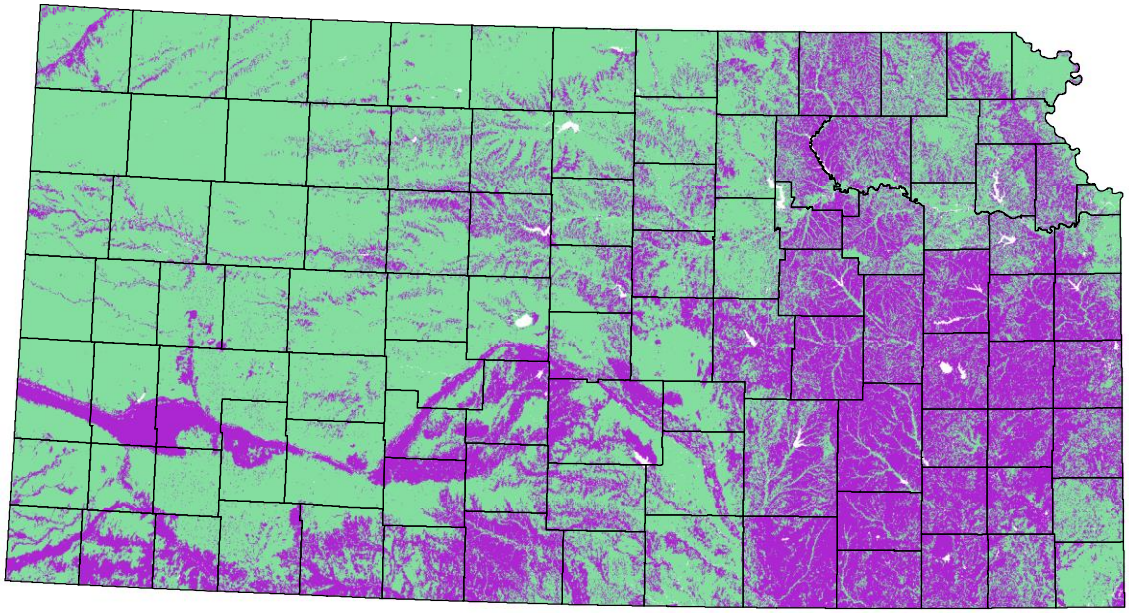

Figure A5. Available water capacity (AWC) less than 150 mm in Kansas (in purple).

Appendix B - Drought Tool Verification

The python tools developed at Kansas State University had excellent agreement with available drought tools in other programming languages. To compare our PDSI results against other methods, we used the MATLAB tool developed by Jacobi et al. (2013) at Vanderbilt University (Fig. B1) using the full record calibration setting. Here we compared Manhattan PDSI time series from 1900 to 2014 between two tools. The correlation coefficient is greater than 0.999. There are minor differences between two tools, which are caused by computation rounding and different AWC assumption used. The difference between two tools is the assumption of AWC in the surface layer of soil. In our code it is not equal to 1 inch but the amount of water in the top 15 cm of soil obtained from the 10m x 10m gSSURGO dataset. The effects of this change are relatively negligible in Manhattan time series.

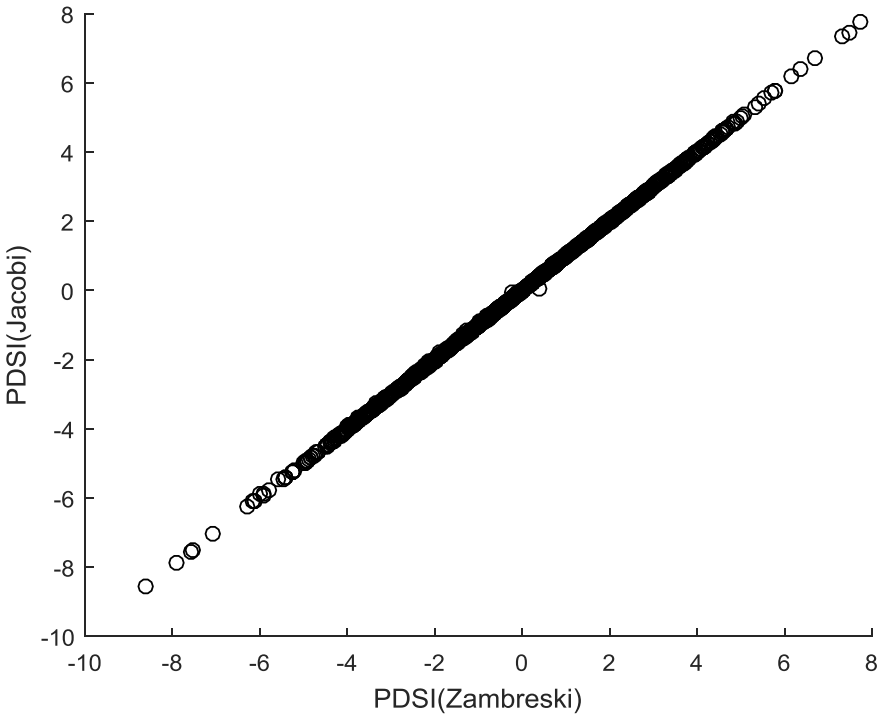

Figure B1.One-to-one plot of Manhattan, KS PDSI calculated using Jacobi's tool and the tool developed at Kansas State University (Zambreski).

The tools for calculating SPI and SPEI were compared to results from the National Drought Mitigation Center's Drought Atlas. Agreement for both tools was also extremely high ($r>0.999$).

Appendix C - Drought Characteristics by SPEI and SPI

The 29 station's SPEI- and SPI-3, -12, and -24 drought characteristics are summarized in Tables C1 to C4. The Figure C1 shows the drought intensity time series for eastern Kansas by SPEI- and SPI-3, -12, and -24.

Table C1. Station SPEI-3 drought characteristics, including minimum peak SPEI-3 and station's longest drought.

Station	Peak SPEI- 3 Intensity			Longest Duration (SPEI-3≤0)			
	SPEI-3	Year	Mo	Duration (mo)	Years	Severity	Intensity
Atchison	-2.44	1910	4	20	1955-1956	-24.06	-1.2
Columbus	-2.78	1956	4	26	1900-1902	-32.57	-1.25
Council Grove	-3.01	1910	4	23	1955-1957	-21.39	-0.93
El Dorado	-2.43	1936	8	26	1932-1934	-24.08	-0.93
Ft Scott	-2.32	2012	7	26	2010-2013	-36.69	-1.41
Horton	-2.83	1910	4	23	1932-1934	-16.94	-0.74
Independence	-2.26	1980	7	23	1938-1940	-16.25	-0.71
Lawrence	-2.66	1930	4	24	1955-1957	-26.24	-1.09
Leavenworth	-2.64	1953	10	15	1937-1938	-12.95	-0.86
Manhattan	-2.87	1910	4	20	1953-1955	-15.98	-0.8
Olathe 3E	-2.59	1936	4	22	1955-1957	-22.46	-1.02
Ottawa	-3.51	1910	4	20	1938-1940	-21.7	-1.08
Sedan	-2.44	1939	11	22	1962-1964	-21.42	-0.97
Anthony	-2.43	1947	10	37	1952-1955	-38.84	-1.05
Coldwater	-2.46	1956	10	24	1932-1934	-26.59	-1.11
Ellsworth	-2.51	1936	8	20	1987-1989	-18.11	-0.91
Hays 1 S	-2.58	2012	7	17	1988-1989	-16.96	-1
Larned	-2.55	1983	9	21	1987-1989	-20.19	-0.96
McPherson	-2.53	1910	4	24	1955-1957	-29.69	-1.24
Minneapolis	-2.82	1947	10	26	1916-1918	-22.65	-0.87
Smith Center	-2.64	2012	7	18	1939-1940	-23.98	-1.33
Ashland	-2.65	2011	7	19	1955-1957	-19.36	-1.02
Lakin	-2.57	1963	4	26	1962-1964	-27.21	-1.05
Liberal	-2.83	2012	8	23	2012-2014	-17.58	-0.76
Norton 9SSE	-2.71	1910	4	21	1939-1940	-24.2	-1.15
Oberlin	-3.63	1937	2	24	1955-1957	-20.36	-0.85
Saint Francis	-3	1910	4	14	1934-1935	-16.37	-1.17
Scott City	-3.82	2012	7	18	1952-1953	-13.65	-0.76
Wakeeney	-3.62	2012	6	18	2010-2011	-12.03	-0.67

Table C2. Station SPEI-12 drought characteristics, including minimum peak SPEI-12 and station's longest drought.

Station	Peak SPEI- 12 Intensity			Longest Duration (SPEI-12≤0)			
	SPEI-12	Year	Mo	Duration (mo)	Years	Severity	Intensity
Atchison	-2.56	1988	12	33	1935-1938	-32.92	-1
Columbus	-2.58	1902	4	37	1952-1955	-57.61	-1.56
Council Grove	-2.16	1988	12	63	1936-1941	-84.4	-1.34
El Dorado	-2.16	1956	10	66	1929-1935	-62.99	-0.95
Ft Scott	-2.71	2012	6	46	1929-1933	-48.97	-1.06
Horton	-2.55	1934	8	69	1919-1925	-53.14	-0.77
Independence	-2.26	1956	10	64	1962-1967	-73.72	-1.15
Lawrence	-2.37	1934	8	63	1952-1957	-88.74	-1.41
Leavenworth	-2.51	1902	4	61	1952-1957	-75	-1.23
Manhattan	-2.74	1934	8	64	1936-1941	-68.78	-1.07
Olathe 3E	-2.31	1936	11	68	1952-1958	-81.31	-1.2
Ottawa	-2.17	2012	7	50	2000-2004	-45.24	-0.9
Sedan	-2.28	1911	6	60	1952-1957	-73.74	-1.23
Anthony	-2.21	1954	12	68	1932-1938	-74.49	-1.1
Coldwater	-2.38	1956	6	59	1952-1957	-76.68	-1.3
Ellsworth	-2.58	1935	3	59	1952-1957	-61.01	-1.03
Hays 1 S	-2.52	1957	2	44	2010-2014	-50.13	-1.14
Larned	-2.18	2012	6	57	1952-1957	-68.22	-1.2
McPherson	-2.37	1955	6	118	1930-1940	-127.19	-1.08
Minneapolis	-2.6	1934	8	87	1931-1938	-102.15	-1.17
Smith Center	-2.36	1935	3	103	1932-1941	-143	-1.39
Ashland	-2.44	1935	3	128	1930-1941	-126.99	-0.99
Lakin	-2.45	1935	4	89	1933-1940	-113.36	-1.27
Liberal	-2.37	2011	8	60	1952-1957	-77.36	-1.29
Norton 9SSE	-2.4	2002	9	116	1931-1941	-154.72	-1.33
Oberlin	-2.47	1940	4	79	1931-1938	-89.66	-1.13
Saint Francis	-2.47	1935	3	57	1952-1957	-90.13	-1.58
Scott City	-2.53	1956	6	83	1934-1941	-97.16	-1.17
Wakeeney	-2.6	2012	12	53	2010-2014	-71.55	-1.35

Table C3. Station SPEI-24 drought characteristics, including minimum peak SPEI-24 and station's longest drought.

Station	Peak SPEI- 24 Intensity			Longest Duration (SPEI-24≤0)			
	SPEI-24	Year	Mo	Duration (mo)	Years	Severity	Intensity
Atchison	-2.36	1957	2	96	1933-1941	-113.68	-1.18
Columbus	-2.58	1902	5	88	1931-1938	-72.8	-0.83
Council Grove	-2.22	1940	7	99	1933-1942	-135.81	-1.37
El Dorado	-2.1	1955	5	135	1930-1941	-145.64	-1.08
Ft Scott	-2.82	2012	12	64	1930-1935	-70.29	-1.1
Horton	-2.44	1934	8	146	1930-1942	-171.19	-1.17
Independence	-2.15	1954	4	86	1931-1938	-81.11	-0.94
Lawrence	-2.26	1937	11	139	1930-1941	-147.68	-1.06
Leavenworth	-2.21	1954	7	97	1933-1941	-116.64	-1.2
Manhattan	-2.49	1934	10	122	1932-1942	-154.97	-1.27
Olathe 3E	-2.38	1937	11	127	1930-1940	-147.99	-1.17
Ottawa	-2.28	1937	11	135	1930-1941	-141.7	-1.05
Sedan	-2.52	1911	6	71	1963-1969	-82.51	-1.16
Anthony	-2.3	1955	4	74	1932-1938	-93.17	-1.26
Coldwater	-2.4	1934	8	103	1933-1941	-137.6	-1.34
Ellsworth	-2.57	1940	6	120	1931-1941	-181.33	-1.51
Hays 1 S	-2.52	1940	6	90	1934-1941	-126.16	-1.4
Larned	-2.43	2012	7	120	1931-1941	-129.31	-1.08
McPherson	-2.44	1956	6	132	1931-1942	-167.52	-1.27
Minneapolis	-2.57	1935	4	127	1931-1941	-172.94	-1.36
Smith Center	-2.62	1940	7	103	1933-1941	-171.77	-1.67
Ashland	-2.37	1934	8	133	1930-1941	-156.18	-1.17
Lakin	-2.01	1964	7	104	1932-1941	-140.09	-1.35
Liberal	-2.44	2012	8	121	1931-1941	-137.77	-1.14
Norton 9SSE	-2.17	1940	6	119	1932-1942	-179.08	-1.5
Oberlin	-2.38	1940	6	111	1932-1941	-167.98	-1.51
Saint Francis	-2.32	1956	6	117	1997-2007	-101.11	-0.86
Scott City	-2.27	2012	7	88	1934-1941	-120.65	-1.37
Wakeeney	-2.35	2013	8	99	1933-1941	-130.48	-1.32

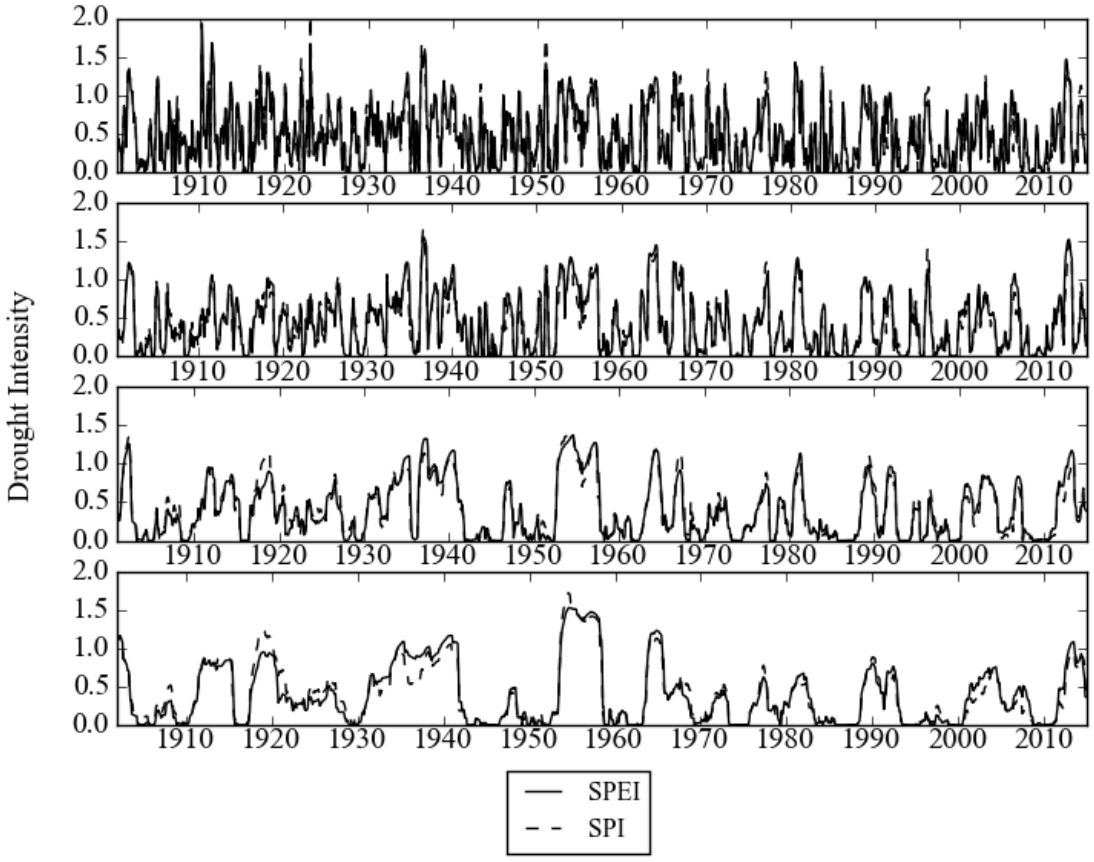

Figure C1. Drought intensity across time for the SPEI and SPI -3,-6,-12,-24 (top to bottom) for eastern Kansas

Appendix D - SPEI-n EOF, REOF, and Spectral Analysis of PCs

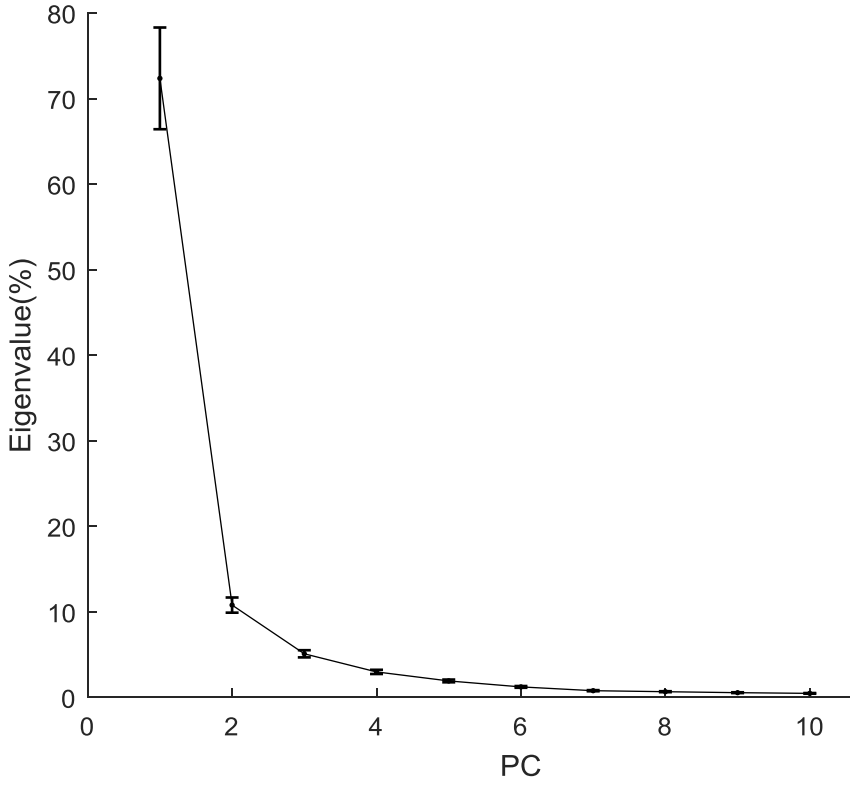

Figure D1. Spectrum of the variance explained by each eigenvalue (%) of the first 10 principal components for the SPEI-3.

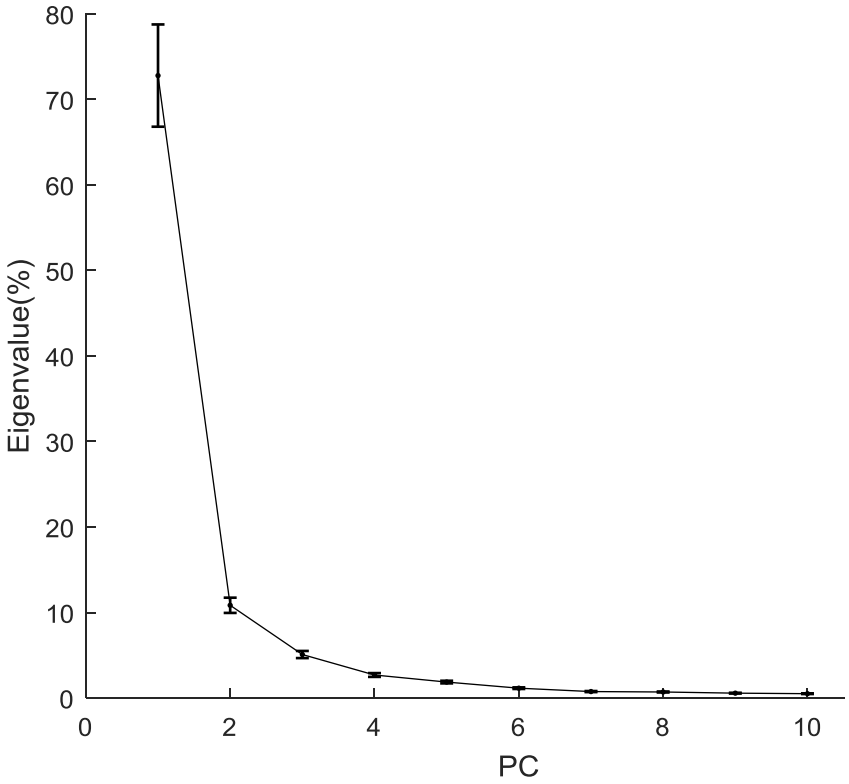

Figure D2. The same as Fig. D1 but for the SPEI-6.

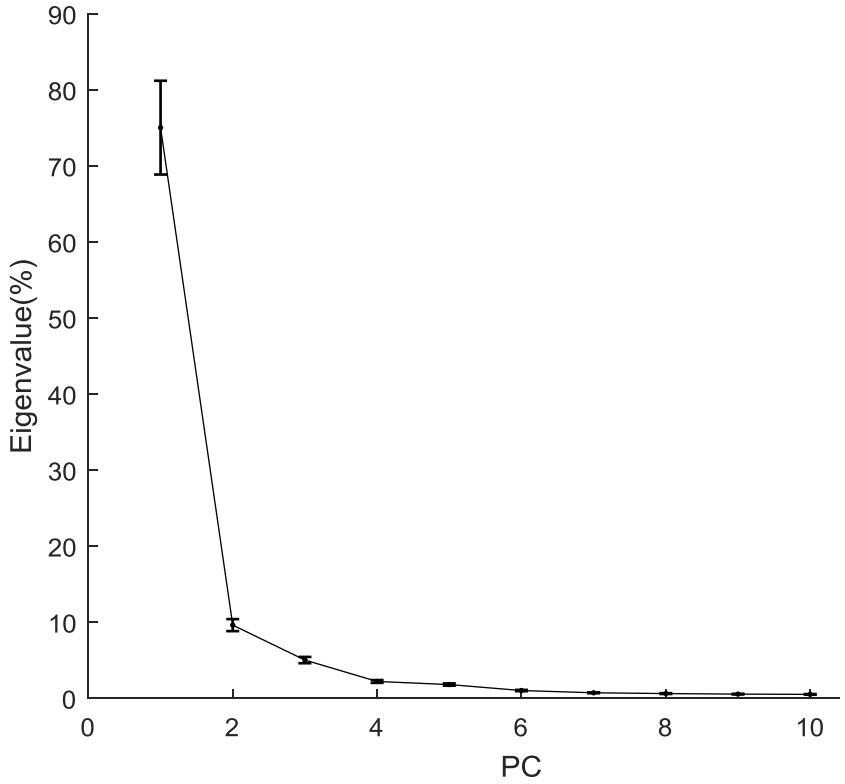

Figure D3. The same as Fig. D1 but for the SPEI-12.

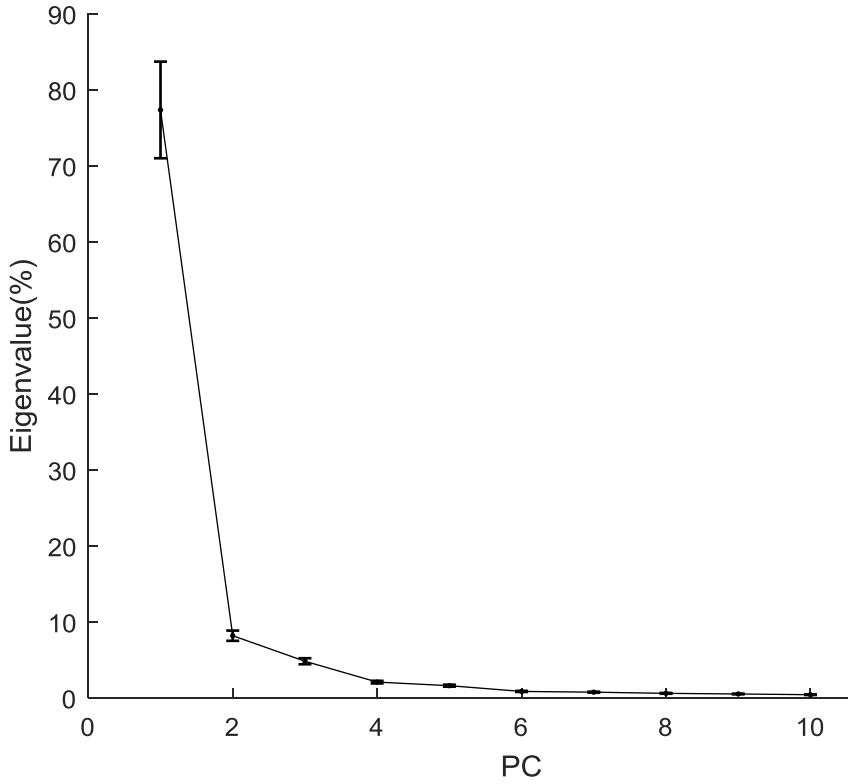

Figure D4. The same as Fig. D1 but for the SPEI-24.

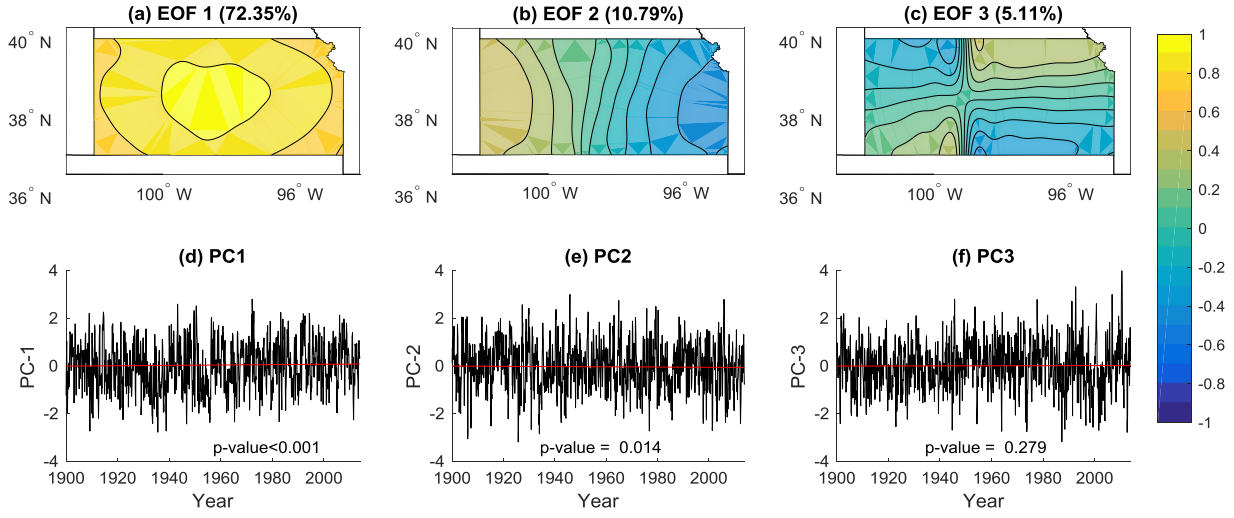

Figure D5. EOFs and PCs by using SPEI-3.

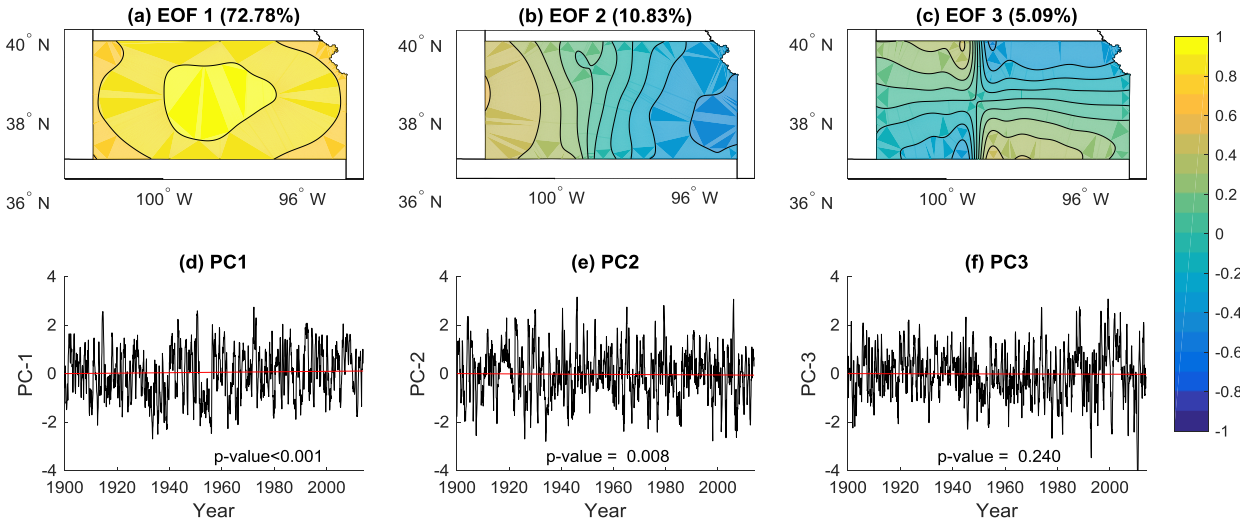

Figure D6. EOFs and PCs by using SPEI-6.

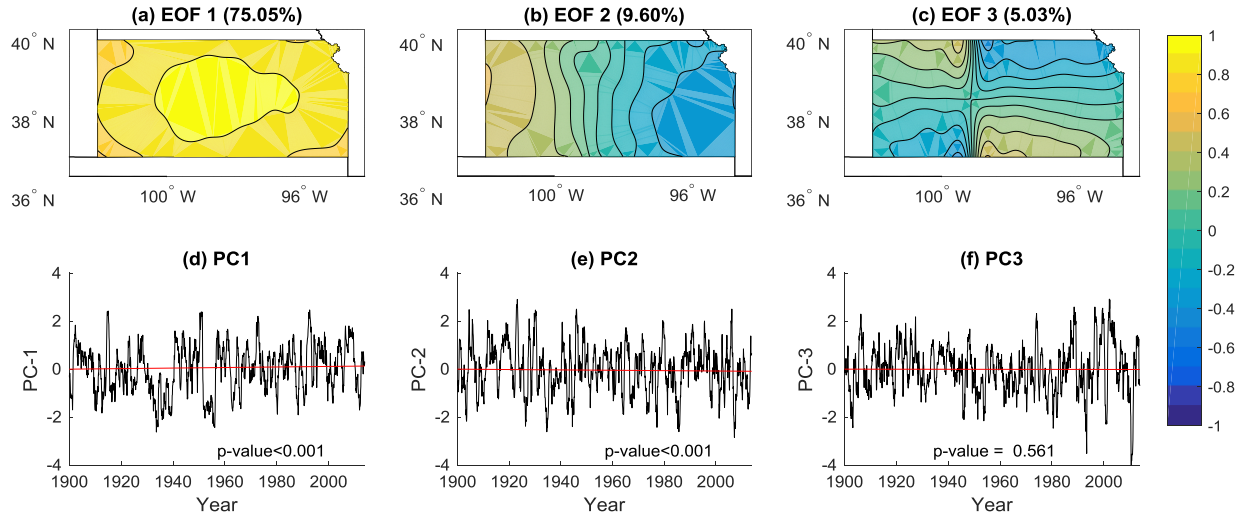

Figure D7. EOFs and PCs by using SPEI-12.

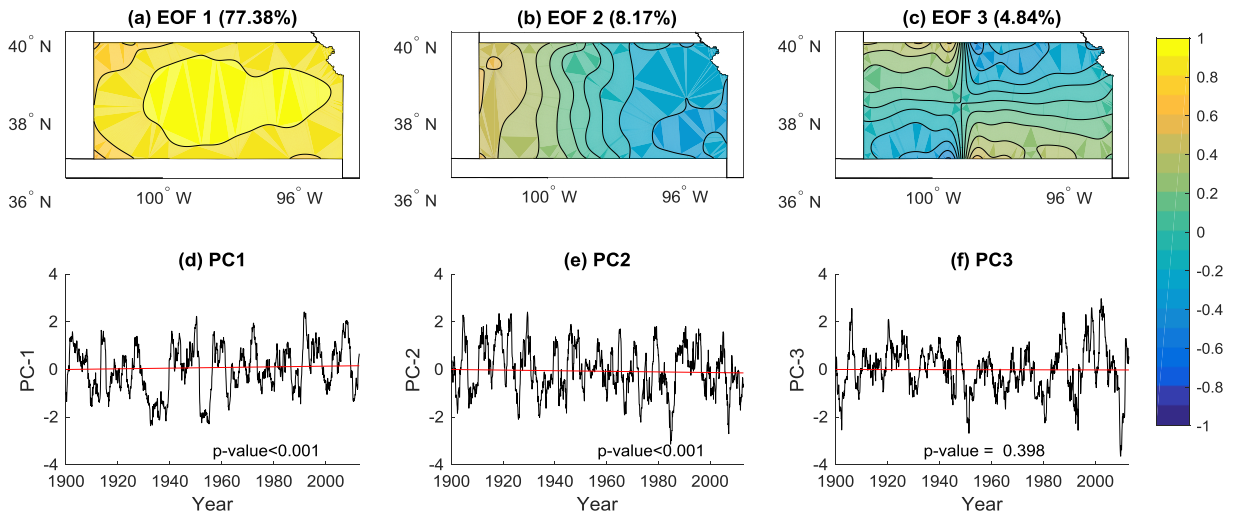

Figure D8. EOFs and PCs by using SPEI-24.

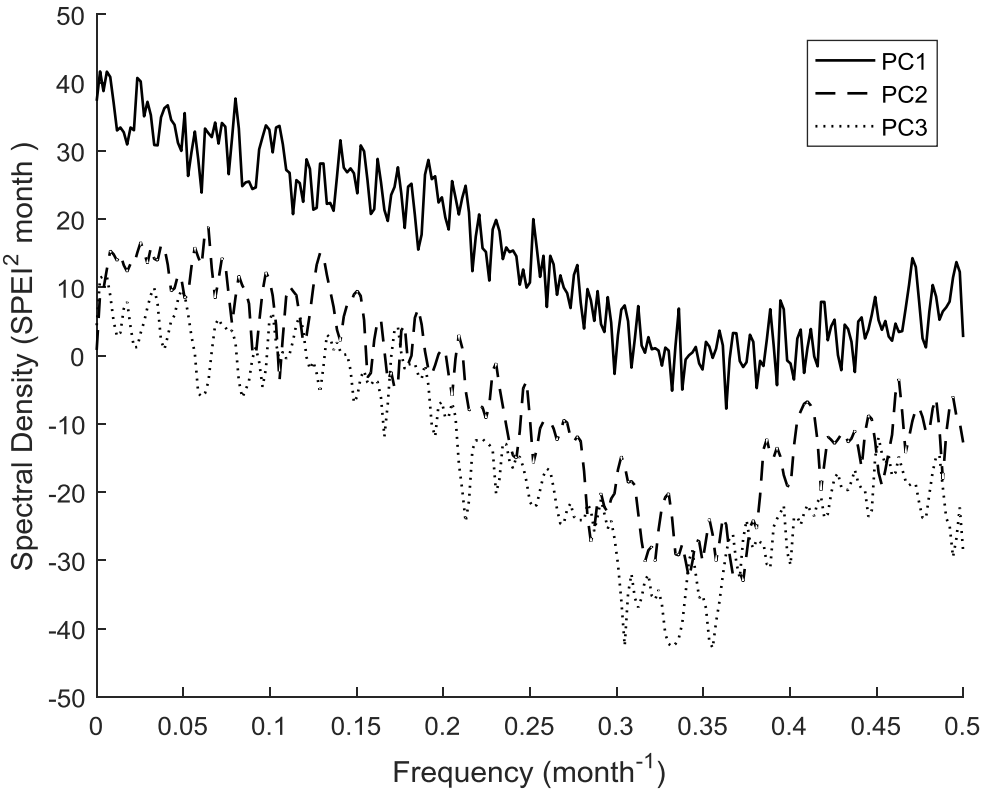

Figure D9. Power spectral density of the PCs for the SPEI-3. Maximum peaks occur at periods of 14.22, 1.29, and 21.33 years for the PC1, 2, 3, respectively.

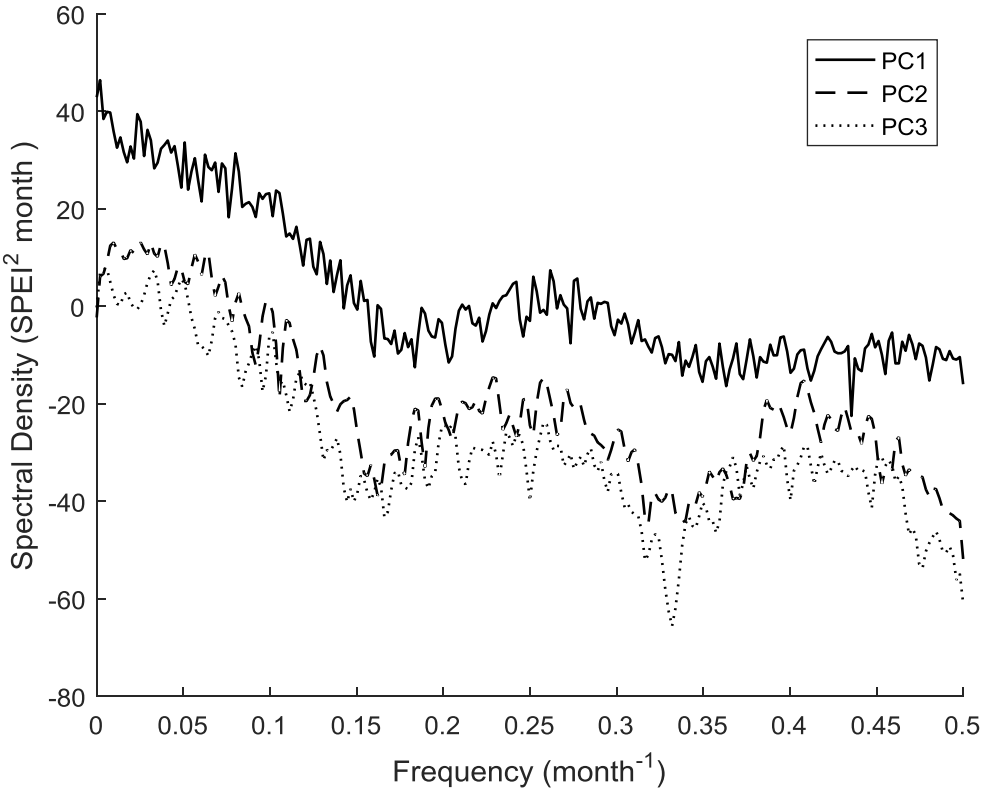

Figure D10. Power spectral density of the unrotated PCs for the SPEI-6. Maximum peaks occur at periods of 14.22, 8.53, and 14.22 years for the PC1, 2, 3, respectively.

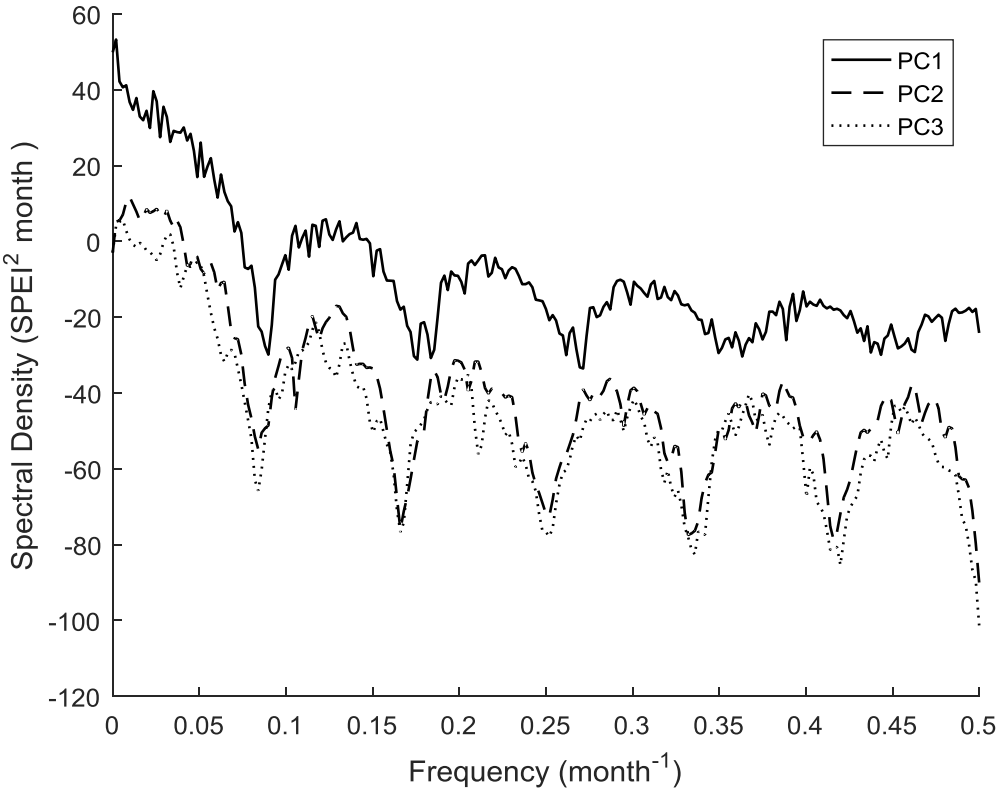

Figure D11. Power spectral density of the unrotated PCs for the SPEI-12. Maximum peaks occur at periods of 14.22, 8.53, and 14.22 years for the PC1, 2, 3, respectively.

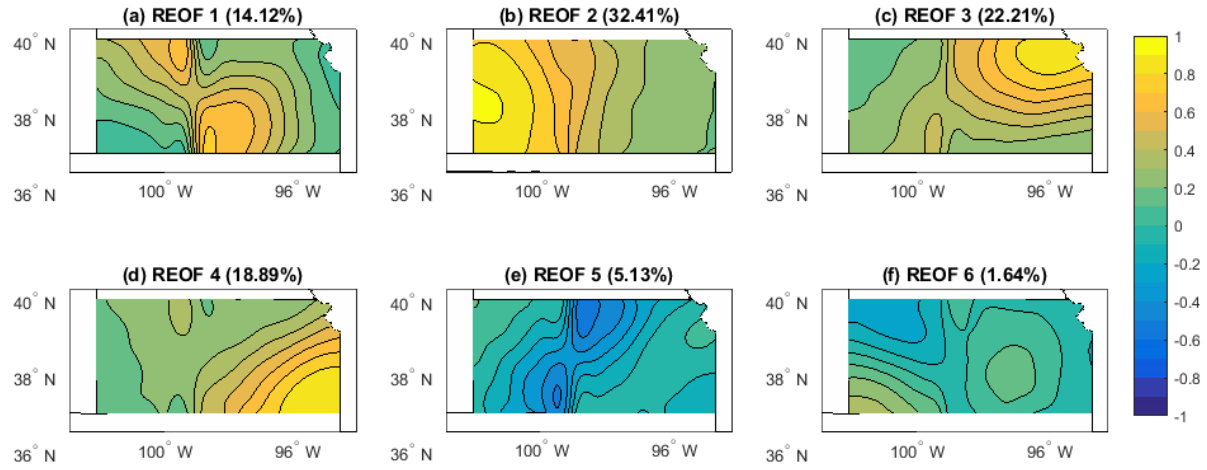

Figure D12. Six REOFs of the SPEI-3.

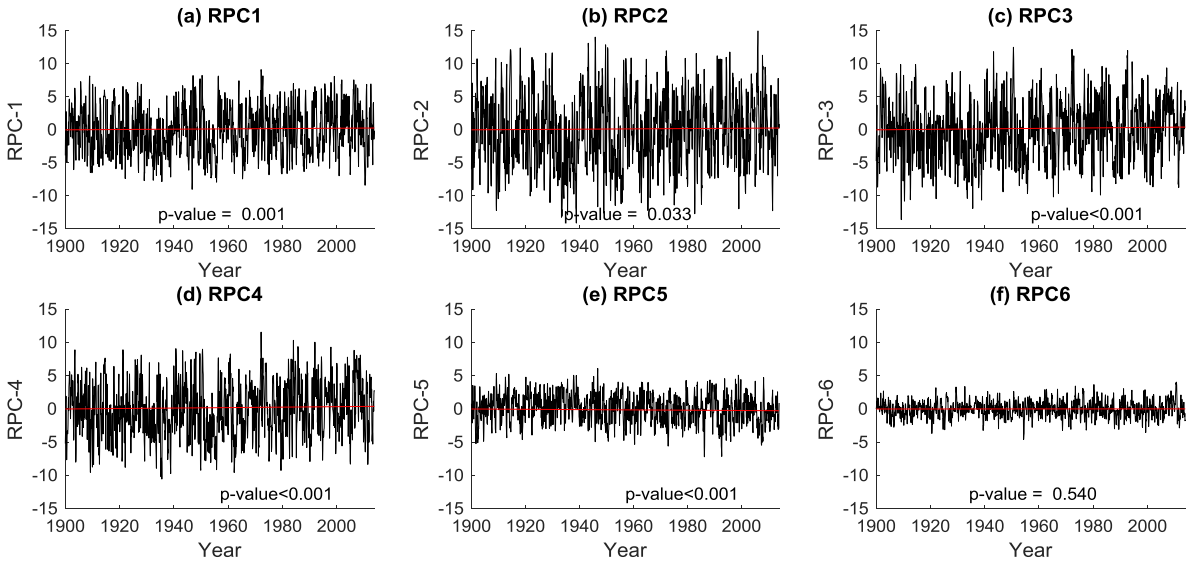

Figure D13. Six RPCs of the SPEI-3.

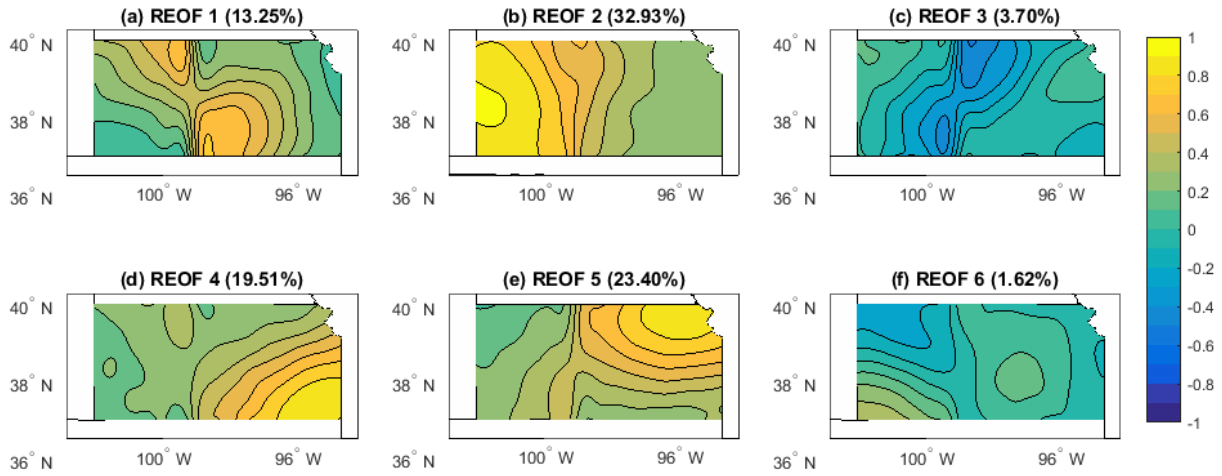

Figure D14. The same as Fig. D12 but for the SPEI-6.

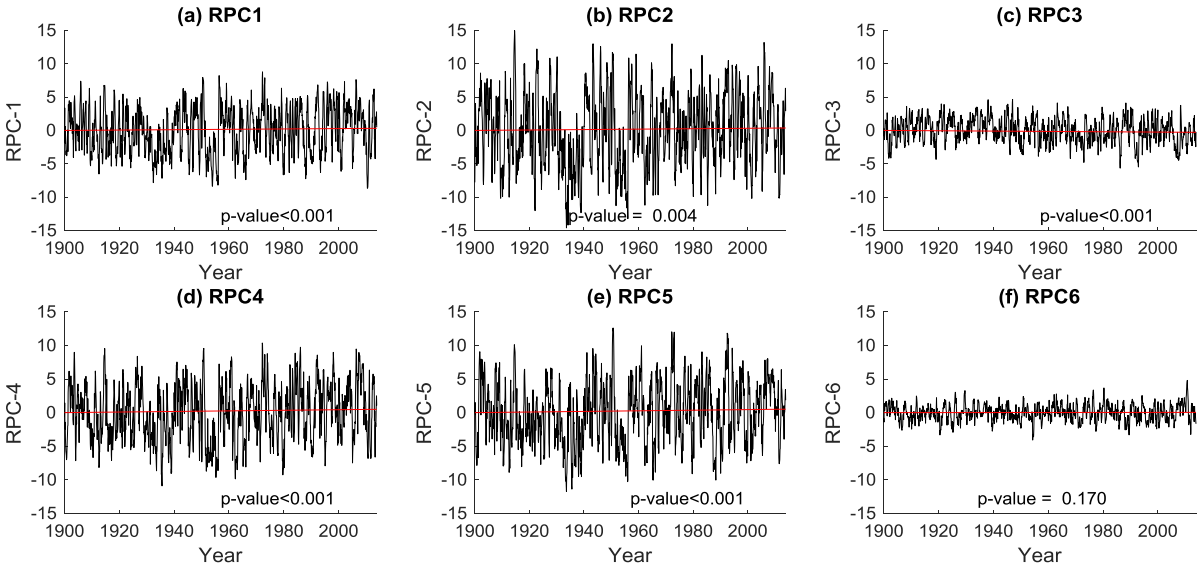

Figure D15. The same as Fig. D13 but for SPEI-6.

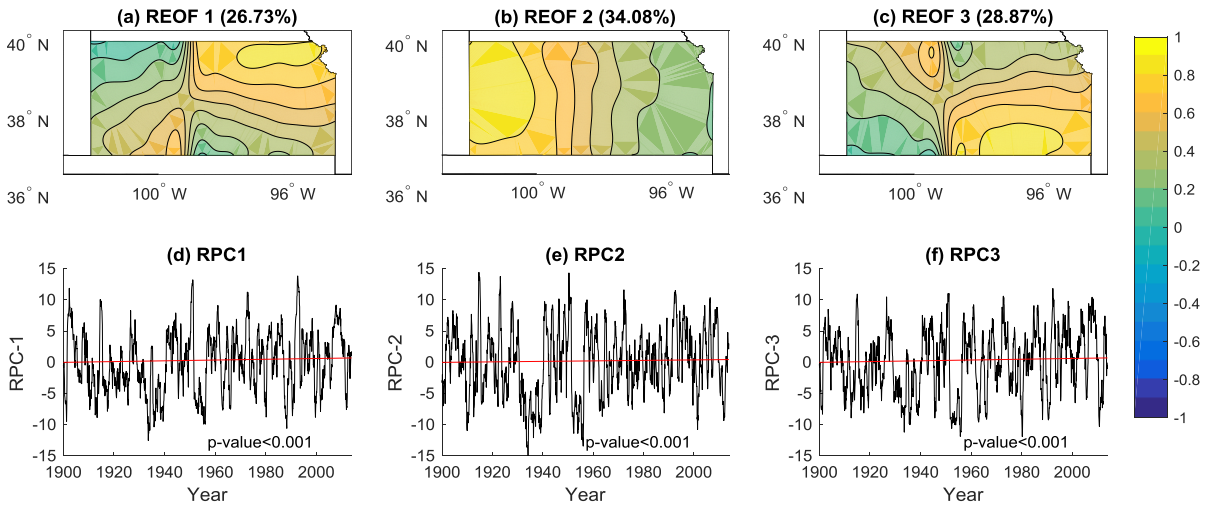

Figure D16. Three Varimax REOFs and RPCs of the SPEI-12. All rotated components have statistically significant positive trends.

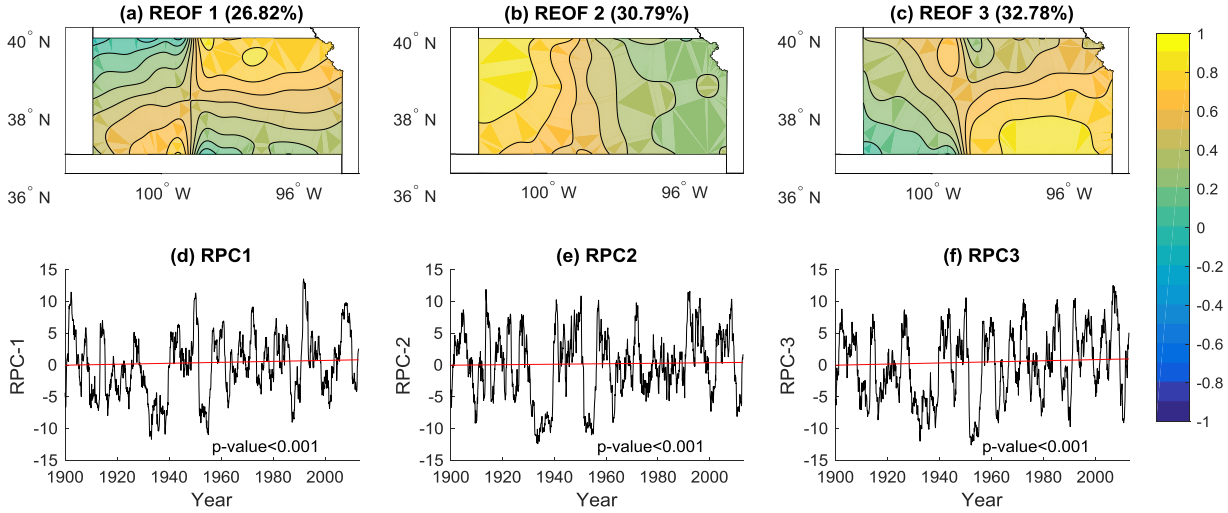

Figure D17. The same as Fig D16 but for the SPEI-24. All rotated components have statistically significant positive trends.

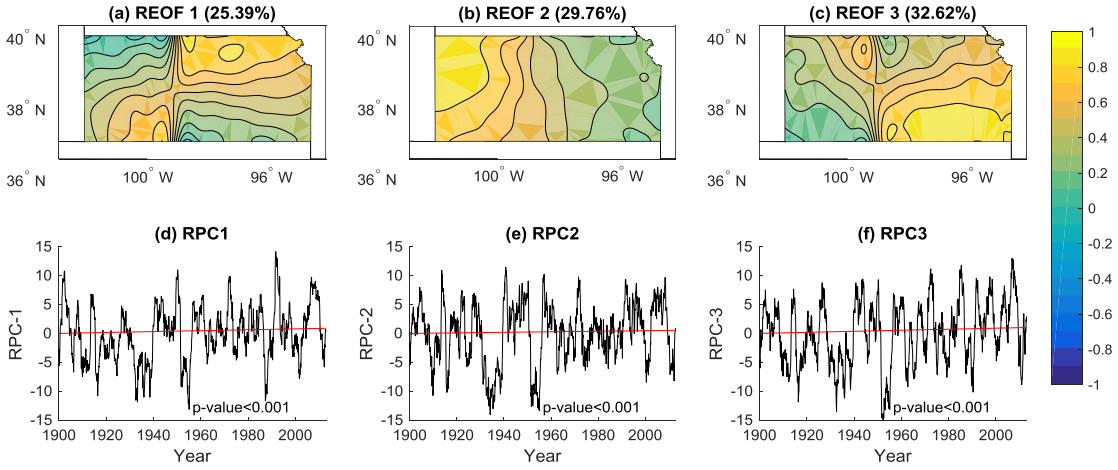

Figure D18. The same as Fig. D16 but for the SPI-24. All rotated components have statistically significant positive trends.